

## Co-evolution of elliptical galaxies and their central black holes

### Clues from their scaling laws

L. CIOTTI<sup>(1)</sup>

<sup>(1)</sup> *Dept. of Astronomy, University of Bologna, via Ranzani 1, 40127 Bologna, ITALY*

#### **Summary.** —

After the discovery that supermassive black holes (SMBHs) are ubiquitous at the center of stellar spheroids and that their mass  $M_{\text{BH}}$ , in the range  $10^6 M_{\odot} - 10^9 M_{\odot}$ , is tightly related to global properties of the host stellar system, the idea of the co-evolution of elliptical galaxies and of their SMBHs has become a central topic of modern astrophysics. Here, I summarize some consequences that can be derived from the galaxy scaling laws and present a coherent scenario for the formation and evolution of elliptical galaxies and their central SMBHs, focusing in particular on the establishment and maintenance of their scaling laws. In particular, after a first observationally based part, the discussion focuses on the physical interpretation of the Fundamental Plane. Then, two important processes in principle able to destroy the galaxy and SMBH scaling laws, namely galaxy merging and cooling flows, are analyzed. Arguments supporting the necessity to clearly distinguish between the origin and maintenance of the different Scaling Laws, and the unavoidable occurrence of SMBH feedback on the galaxy Interstellar Medium in the late stages of galaxy evolution (when elliptical galaxies are sometimes considered as “dead, red objects”), are then presented. At the end of the paper I will discuss some implications of the recent discovery of super-dense ellipticals in the distant Universe. In particular, I will argue that, if confirmed, these new observations would lead to the conclusion that at early epochs a relation between the stellar mass of the galaxy and the mass of the central SMBH should hold, consistent with the present day Magorrian relation, while the proportionality coefficient between  $M_{\text{BH}}$  and the scale of velocity dispersion of the hosting spheroids should be significantly smaller than that at the present epoch.

PACS 98.10 – Stellar dynamics and kinematics.

PACS 98.52 – Normal galaxies.

PACS 98.54 – Quasars.

PACS 98.58 – Interstellar Medium (ISM).

## 1. – Introduction

The mutual interplay between supermassive black holes (hereafter SMBHs) at the center of stellar spheroids<sup>(1)</sup> and their host systems is now established beyond any reasonable doubt, as indicated by the remarkable correlations found between host galaxy properties and the masses of their SMBHs (e.g. [3]-[10]). More specifically, it is now believed that all early-type galaxies with  $M_B \lesssim -18$  mag ([11]) host a central SMBH (e.g. [12]-[14]), whose mass  $M_{\text{BH}}$  scales *linearly* with the spheroid stellar mass  $M_*$ ; the correlation of  $M_{\text{BH}}$  with the central stellar velocity dispersion  $\sigma_*$  of the host galaxy is even tighter. It is then natural to argue (e.g. [15]-[27]) that the central SMBHs have played an important role in the processes of galaxy formation and evolution, the imprint of which is represented by the Scaling Laws (hereafter SLs) mentioned above. As an additional supporting argument, several groups have noted the link between the cosmological evolution of QSOs and the formation history of galaxies (e.g. [28]-[32], see also [33]-[37]).

In addition to the SLs of their central SMBHs, early-type galaxies are also known to follow well defined empirical SLs relating their global observational properties, such as total luminosity  $L$ , effective radius  $R_e$ , and central velocity dispersion  $\sigma_*$ . Among others we recall the Faber & Jackson ([38], hereafter FJ), the Kormendy ([39]), the Fundamental Plane ([40, 41], hereafter FP), the color- $\sigma_*$  ([42]), and the  $\text{Mg}_2$ - $\sigma_*$  (e.g. [44]-[46]) relations.

Clearly, all together these scaling relations reveal the *remarkable homogeneity* of early-type galaxies, provide invaluable information about their formation and evolution, and set stringent requirements that must be taken into account by any proposed galaxy-SMBH formation scenario. We recall that two alternative scenarios for the formation of Es have been proposed. In the *monolithic collapse* picture, ellipticals are formed at early times by dissipative processes (e.g., [47]-[49]; see also [50, 51]), while in the *hierarchical merging scenario* spheroidal systems are the end-products of several merging processes of smaller galaxies, the last major merger taking place in relatively recent times, i.e. at  $z \lesssim 1$  (e.g. [52]-[56]). Each of the two scenarios scores observational and theoretical successes and drawbacks (e.g. [57, 58]). For example, the merging picture (in its *dry* flavor, i.e. neglecting the role of the dissipative gas), could be supported by some observational data suggesting that a fraction of red galaxies in clusters at intermediate redshift are undergoing merging processes: these galaxies could be the progenitors of present-day early-type galaxies (e.g. [59]). At the same time, it is not clear how repeated merging events can produce a class of objects following striking scaling laws involving their global structure, dynamics, and stellar population properties, while theoretical investigations showed that the dynamical processes expected to follow the strongly dissipative phases of monolithic collapse apparently lead to systems surprisingly similar to real Es (e.g., see [60, 61]).

In this paper I will summarize some selected topics of research in this field and present a possible coherent scenario for the co-evolution of SMBHs and their host spheroids. Because of the enormous body of dedicated literature now available, I will focus my attention on a few selected topics. Very important arguments, such as the dynamics of binary SMBHs and their effects on the central regions of galaxies (e.g. [62]-[65]) and

---

<sup>(1)</sup> The term *early-type galaxies* is generically used for galaxies belonging to the family of *elliptical* galaxies (Es), *S0* galaxies, *dwarf ellipticals* (dE), and *dwarf spheroidals* (dSph); the class of *stellar spheroids* is made of early-type galaxies and *bulges* of spiral galaxies. For a detailed account of the observational properties of these classes see, e.g., [1, 2].

references therein), or the growth of SMBHs via accretion of stars (e.g. [66] and references therein) are just mentioned here but not discussed. The paper is organized as follows. After a first, observationally based part (Sect. 2), where the main SLs followed by early-type galaxies and by their central SMBHs are described, in Sect. 3 I will focus on the physical interpretation of the FP: this phenomenological part is a prerequisite to the construction of a possible formation scenario. Then (Sect. 4) I discuss two important physical mechanisms in principle able to destroy the galaxy and SMBH SLs, namely *galaxy merging* and *cooling flows*. In this context, I present some arguments that require that we distinguish between the *origin* and *maintenance* of the SLs and the unavoidable occurrence of SMBH *feedback* on the galaxy Interstellar Medium in the late stages (when Es are sometimes considered as “dead, red objects”). This last point is strictly related to the solution of the long-standing problem of cooling flows in Es (and clusters), and to the quiescence of Active Galactic Nuclei (AGN) in low-redshift systems. Section 5 addresses the problem of the *origin* of the SLs, while Sect. 6 provides a summary of the main results, with a short discussion of some very recent observational findings, i.e. the surprisingly high stellar density of Es at high redshift.

## 2. – Basic observational facts

In this Section I review some of the most important SLs of early-type galaxies (Sect. 2.1), of their central SMBHs (Sect. 2.2), and the counterpart of the FP, FJ, and Kormendy relations followed by galaxy clusters (Sect. 2.3). Finally, the AGN underluminosity problem is presented (Sect. 2.4).

### 2.1. *Scaling Laws of early-type galaxies* . –

2.1.1. The Fundamental Plane. Early-type galaxies can be characterized by three main observable global scales: the circularized effective radius  $R_e \equiv \sqrt{a_e b_e}$  (where  $a_e$  and  $b_e$  are the major and minor semi-axis of the effective isophotal ellipse, i.e., the ellipse containing half of the projected system luminosity), the central projected velocity dispersion  $\sigma_o$  (often referred to an aperture radius of  $R_e/8$ , e.g. [67]), and the mean effective surface brightness within  $R_e$ ,  $SB_e = -2.5 \log \langle I \rangle_e$  (where  $\langle I \rangle_e \equiv L_B / 2\pi R_e^2$ , and  $L_B$  is the luminosity of the galaxy, for example in the Johnson B-band). It is well known that Es (with  $\sigma_o \simeq 100 \text{ km s}^{-1}$ ) do not populate uniformly this three-dimensional parameter space; rather, they are confined to the vicinity of a narrow logarithmic plane ([40, 41])

$$(1) \quad \log R_e = \alpha \log \sigma_o + \beta SB_e + \gamma$$

thus called the *Fundamental Plane* (FP). The coefficients  $\alpha$ ,  $\beta$ , and  $\gamma$  depend slightly on the photometric band considered. By measuring  $R_e$  in kpc,  $\sigma_o$  in  $\text{km s}^{-1}$ , and  $SB_e = 42.0521 - 2.5 \log(L_B / 2\pi R_e^2)$  in  $\text{mag/arcsec}^2$ , where  $L_B$  is expressed in units of the solar Blue luminosity, reported values are  $\alpha = 1.25 \pm 0.1$ ,  $\beta = 0.32 \pm 0.03$ ,  $\gamma = -8.895$  (e.g [68]-[74]). An alternative expression for the FP has been obtained by [75], with the introduction of the  $k$  coordinate system, in which the new variables are a linear combination of the observables:

$$(2) \quad k_1 \equiv \frac{\log(\sigma_o^2 R_e)}{\sqrt{2}}, \quad k_2 \equiv \frac{\log(\sigma_o^2 \langle I \rangle_e^2 R_e^{-1})}{\sqrt{6}}, \quad k_3 \equiv \frac{\log(\sigma_o^2 \langle I \rangle_e^{-1} R_e^{-1})}{\sqrt{3}}.$$

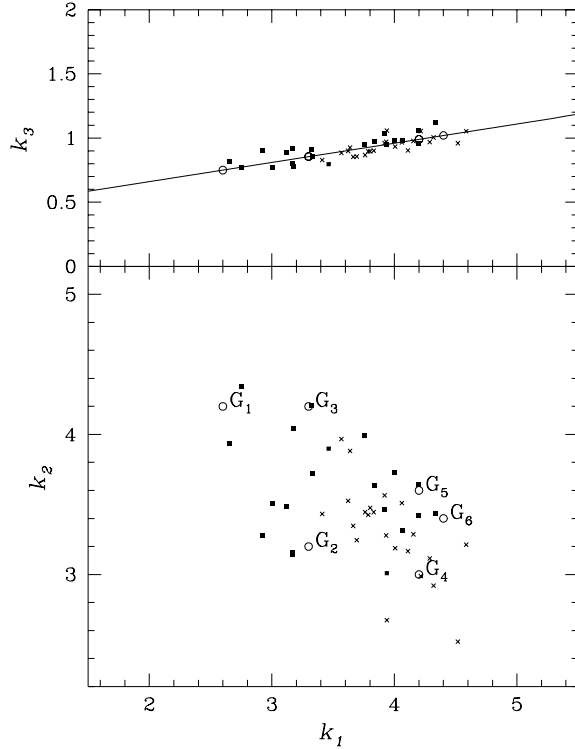


Fig. 1. – The distribution of Virgo (closed boxes) and Coma (crosses) ellipticals in the  $(k_1, k_2, k_3)$  space. The upper panel shows the FP edge-on; in the lower panel the FP is seen nearly face-on (from [94]).

In particular, when projected on the  $(k_1, k_3)$  plane, the FP is seen almost edge-on and it is considerably thin, while the distribution of galaxies in the  $(k_1, k_2)$  plane is considerably broader. For example, Virgo ellipticals are distributed on the  $(k_1, k_3)$  plane according to the best-fit relation

$$(3) \quad k_3 = 0.15k_1 + 0.36$$

(when adopting respectively, kpc,  $\text{km s}^{-1}$  and  $L_{B\odot} \text{ pc}^{-2}$  as length, velocity and surface brightness units, based on a Virgo distance of 20.7 Mpc, see Fig. [1]). The systematic increase of  $k_3$  along the FP described by eq. (3) and the nearly constant and very small dispersion of  $k_3$  at every location on the FP (for example with  $\sigma[k_3] \simeq 0.05$  for Virgo ellipticals) are usually referred to as *tilt* and *thickness* of the FP.

**2.1.2.** The Faber-Jackson and the Kormendy relations. Connected with the FP are the less tight FJ and Kormendy relations. These scaling relations have often been considered just as projections of the FP with no additional information, and, for this reason, their constraining power on galaxy formation scenarios has been underestimated. However, this is not fully correct, because these two relations describe *where* Es are distributed on the FP and so, even if characterized by a larger scatter than the edge-on view of the FP, they contain important information on the galactic properties. The proposed original

form of the FJ relation was  $L_B \propto \sigma_o^n$ , with  $n \approx 4$ , while [76] found that the double-slope fit

$$(4) \quad \frac{L_B}{10^{11} L_{B\odot}} \simeq 0.23 \left( \frac{\sigma_o}{300 \text{ km s}^{-1}} \right)^{2.4} + 0.62 \left( \frac{\sigma_o}{300 \text{ km s}^{-1}} \right)^{4.2}$$

provides a better description of the data. Note that for small galaxies and bulges ( $\sigma_o \lesssim 170 \text{ km s}^{-1}$ ) the single power-law fit would give  $n \simeq 2.4$ , considerably smaller than 4 (see also [77, 78] for the case of the galaxies of the Virgo and Coma clusters). Recent measurements, based on the large data set obtained from the Sloan Survey SSDS ([79]), converge to an exponent 4 in the K band; thus, this value is currently adopted in applications of the FJ relation to high-luminosity galaxies.

The total luminosity of bright spheroidal systems also correlates with their length scale as measured by  $R_e$ : in fact, such Kormendy relation can be written in the form

$$(5) \quad R_e \propto L_B^a,$$

where the exponent  $a$  is strongly dependent on the galaxy sample used, and is found in the range  $0.88 \lesssim a \lesssim 1.62$  (e.g. [80]). The latest estimates appear to converge to a value  $a \sim 0.7$  or less, as a function of waveband ([79]).

**2.1.3. Structural weak homology.** The empirical  $R^{1/4}$  luminosity “law” ([81], see eq. [6] below with  $m = 4$ ), has long been recognized to fit the surface brightness profiles  $I(R)$  of Es successfully, to the point that Es are routinely identified by means of this characteristic photometric signature. It has no *free parameters* and depends on two well defined *physical scales*, the effective radius  $R_e$  and the central surface brightness  $I_0$ . In practice the overall  $R^{1/4}$  fit is characterized by residuals typically of the order of  $0.1 - 0.2 \text{ mag/arcsec}^2$  (e.g. [82]-[86]). These deviations from the  $R^{1/4}$  law, although small, are often larger than the typical observational errors involved. In fact, the surface brightness distribution of ellipticals is better described by the Sersic ([87])  $R^{1/m}$ -law

$$(6) \quad I(R) = I_0 \exp \left[ -b(m) \left( \frac{R}{R_e} \right)^{1/m} \right], \quad I_0 = \frac{L}{R_e^2} \frac{b^{2m}}{2\pi m \Gamma(2m)}$$

(e.g. [88]-[100]). In the above equation  $\Gamma$  is the complete Gamma function. An extremely accurate analytical representation of the factor  $b(m)$  for  $m \geq 1$  is given by its truncated asymptotic expansion  $b(m) \sim 2m - 1/3 + 4/405m$  ([101]). For a dynamical analysis of models with  $R^{1/m}$  projected density profile see, e.g. [102]-[105]; see also [106]).

It has soon become clear that the shape parameter  $m$  of the  $R^{1/m}$  law correlates with global quantities such as total luminosity and effective radius (e.g. [90, 97], [107]-[111]), with  $m$  increasing with luminosity from  $\sim 1/2$  up to  $\sim 15$ . For example [112, 113] report the following relations

$$(7) \quad \log m \simeq 0.28 + 0.52 \log R_e; \quad m \simeq -19.082 + 3.0275 \log L.$$

This remarkable luminosity dependence of the surface brightness profile has been called *weak homology*.

In addition to the global trends described above, also *local* relations - relevant in the present context - have been found. For example, ground based observations ([114]) and

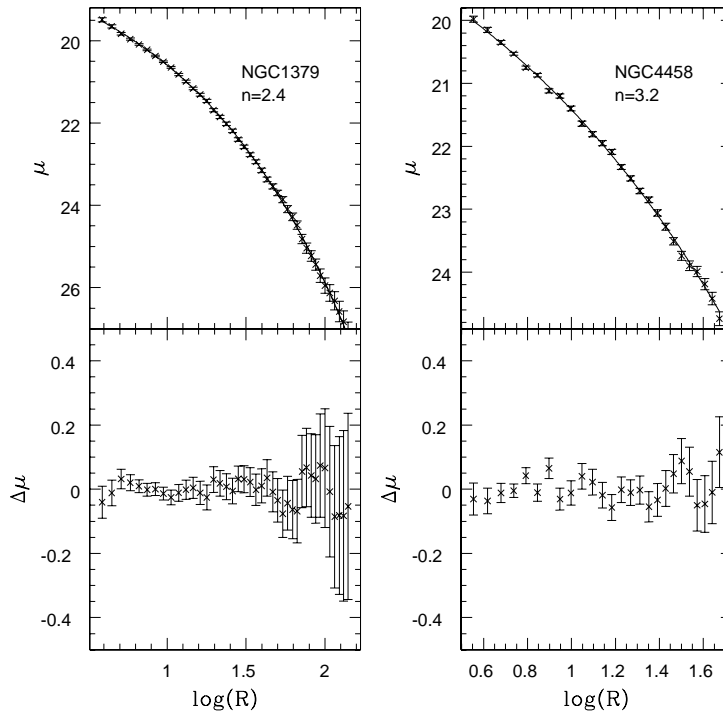


Fig. 2. –  $R^{1/m}$  fit.  $R$  is in arcsec,  $\mu$  in mag/arcsec<sup>2</sup>. The data points are in the Blue band, taken from [112, 113]. Note the limiting surface brightness reached for each galaxy (from [100]).

Hubble Space Telescope data show that the volume luminosity profiles of Es approaches the power-law form  $\rho(r) \propto r^{-\gamma}$  at small radii, with  $0 \leq \gamma \leq 2.5$  ([115]-[121]). In particular, HST observations reveal that at small radii some profiles are rather flat (core galaxies) while others are characterized by steep cusps (power-law galaxies). In general, core profiles are common among bright Es, but fainter systems tend to have power-law cusps; remarkably, other galaxy global properties are related to the presence of the core ([122, 123]). In the context of surface brightness profiles, it has also been found that while the surface brightness profiles of power-law galaxies are well fitted by the  $R^{1/m}$  law all the way into the center, within a break radius  $R_b$  the surface brightness profile of core galaxies stays well below their global best-fit Sersic model; in addition, intermediate and low-luminosity galaxies often present additional star clusters at their center (e.g. [111, 124]-[128]). From these central-to-global relations, very interesting consequences can be derived (see Sects. 5 and 6).

**2.2. Scaling laws of the central SMBHs.** – The masses  $M_{\text{BH}}$  of central SMBHs lie in the range  $10^6 - 10^9 M_{\odot}$  and correlate surprisingly well with several *global* and *local* properties of the host systems (e.g. [10, 129, 130]). Because of the rapidly increasing number of papers on the subject, it is almost impossible to list all the contributions to the subject. Therefore, I will just recall the most famous SLs. For example, it has been

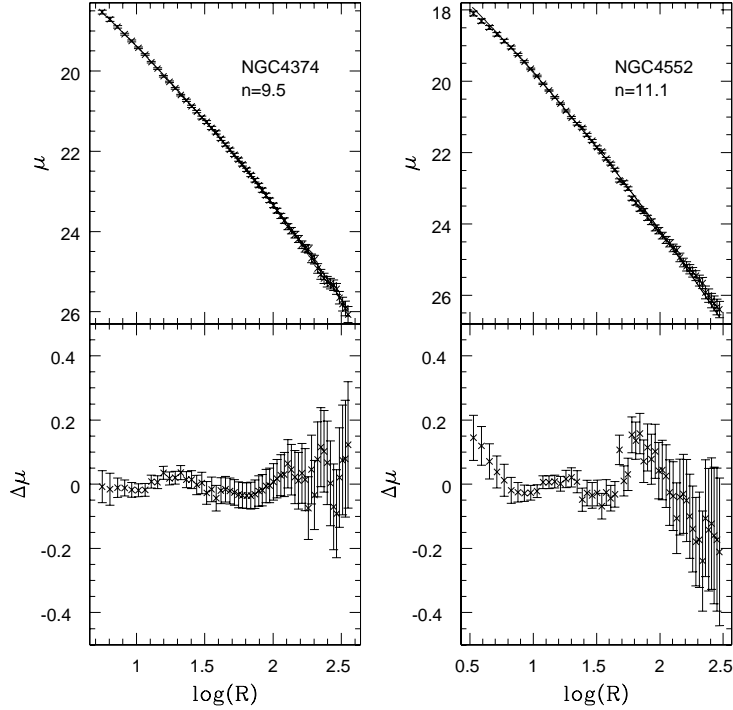


Fig. 3. –  $R^{1/m}$  fit.  $R$  is in arcsec,  $\mu$  in  $\text{mag}/\text{arcsec}^2$  (from [100]).

found that

$$(8) \quad M_{\text{BH}} \propto \sigma_{\circ}^{\alpha},$$

where  $\sigma_{\circ}$  is the projected central (or within  $R_{\text{e}}$ ) velocity dispersion of the hosting galaxy; after some debate, the currently accepted value of  $\alpha$  is very near to 4 (e.g., see [4, 5, 7, 131]). An important characteristic of this relation (known as the  $M_{\text{BH}}\text{-}\sigma_{\circ}$  relation) is its extremely small scatter, consistent with measurements errors only, so that eq. (8) is often considered a “perfect” relation.

Thus, to a good accuracy, both the  $M_{\text{BH}}\text{-}\sigma_{\circ}$  and the FJ relations indicate a proportionality to the fourth power of  $\sigma_{\circ}$ , implying the following linear relation between the mass of the central SMBH and the total mass in stars  $M_{\ast}$  of the host galaxy

$$(9) \quad M_{\text{BH}} \simeq 1.4 \times 10^{-3} M_{\ast}.$$

The latter relation is called the *Magorrian* relation, after its presentation in [3], and has undergone several successive refinements (e.g., see [9, 132, 133]). Note that versions of the above correlation are also provided in terms of the spheroid luminosity instead of the spheroid stellar mass  $M_{\ast}$  [9]. Quite naturally, the possibility of the existence of a FP analogous to that of galaxies, but involving  $M_{\text{BH}}$  instead of galaxy luminosity, has also

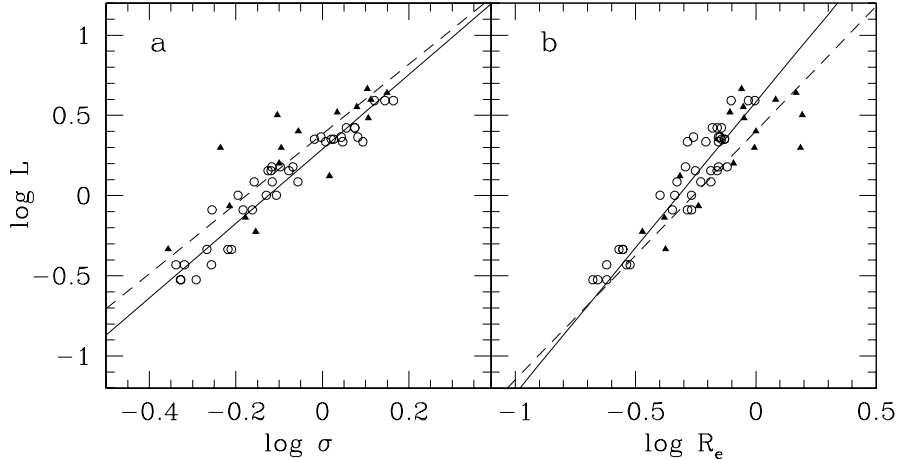


Fig. 4. – *Panel a*: FJ relation for the observed clusters (filled triangles, dashed line) and the dark matter halos obtained from cosmological simulations when eq. (84) is used for the mass-to-light ratio (empty circles, solid line).  $L$  is given in  $10^{12}L_{\odot}/h^2$ ,  $\sigma$  in 1000 km/s,  $R_e$  in Mpc/ $h$ , for an Hubble constant value of  $H_0 = 100h \text{ km s}^{-1} \text{ Mpc}^{-1}$ , with  $h = 0.7$  (see Sect. 5.3). *Panel b*: with the same symbols, the Kormendy relation for the same data as in Panel a. Each dark matter halo is represented by 3 empty circles corresponding to the 3 line-of-sight projections. (from [143]).

been explored, in search of a relation possibly tighter than eqs. (8)-(9). However, so far no definite answer has been reached yet (e.g., see [9, 130, 134]-[137]).

Finally, I wish to mention there is another family of interesting SLs relating the SMBH mass to the galaxy Sersic index [138, 139]. For example, [6, 140] found that

$$(10) \quad \log M_{\text{BH}} \simeq 2.69 \log(m/3) + 7.81,$$

with scatter as small as that of the  $M_{\text{BH}}\text{-}\sigma_0$  relation.

**2.3. The scaling relations of clusters of galaxies.** – The FP is not an exclusive property of early type galaxies. For example, clusters of galaxies (within the limitations of a poorer statistics) also define their own FP (e.g., see [141]-[143]). In addition, other SLs exist for clusters, such as those based on the luminosity and temperature of the Intracluster Medium (e.g., see [144]-[147]), but they will not be discussed here. The existence of a FP for clusters (for example defined in terms of their total luminosity in stars, of the effective radius of the galaxy projected number density, and on some characteristic velocity dispersion of the galaxy population) is interesting because the physics behind cluster formation is expected to be quite different from the (more complex) physics of galaxy formation. Therefore, important clues can be obtained by comparing the SLs of clusters and those of galaxies: this will be one of the main subjects of Sect. 5. In particular, Lanzoni et al. [143] performed a Principal Component Analysis on the Schaeffer sample of Abell clusters, obtaining the following *cluster* FJ and Kormendy



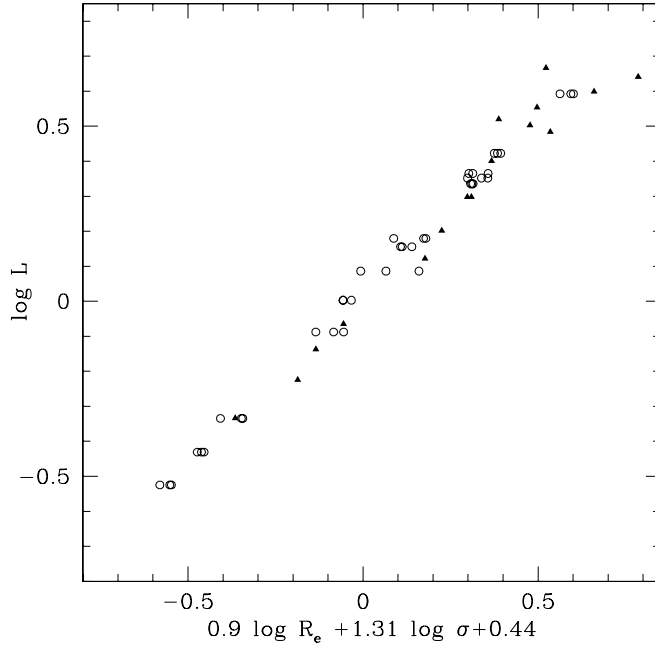


Fig. 5. – The FP of observed clusters (filled triangles) and cosmological dark matter halos when eq. (84) is used for the mass-to-light ratio (empty circles) (from [143]).

relations:

$$(11) \quad L \propto \sigma^{2.18 \pm 0.52}, \quad L \propto R_e^{1.55 \pm 0.19},$$

where the errors on the exponents also include the observational uncertainties (see also [148]). As can be seen from Fig 4, where the relations given in eqs. (11) are plotted together with the Schaeffer data, the two relations above describe scalings among the cluster properties, even if their scatter is quite large (*rms* dispersion 0.19 in both cases). Similarly to what happens for galaxies, a considerable improvement is achieved by combining all the three observables together in a FP relation

$$(12) \quad L \propto R_e^{0.9 \pm 0.15} \sigma^{1.31 \pm 0.22}.$$

This relation is shown (edge-on) in Fig. 5, and is characterized by an *rms* dispersion of  $\sim 0.07$ . Thus, the similarity of the FP for clusters with that for galaxies is remarkable. For example, the FP of Es in the B band can be written as  $L \propto R_e^{\sim 0.8} \sigma^{\sim 1.3}$  (e.g. [41, 68, 74, 149]). The situation is similar for the Kormendy relation: in fact,  $L \propto R_e^{1.7 \pm 0.07}$  has been reported for ellipticals in the B band ([79]). The only apparent difference is that of the FJ: in fact,  $L \propto \sigma^4$  for (luminous) Es ([79]), while for clusters the slope is around 2.

**2.4. Cooling flows and AGN underluminosity.** – Ellipticals present a well-known “cooling flow problem”: the time for a significant fraction of the centrally located gas to cool (*via* the observed radiative output) and to collapse is short (typically  $\sim 10^6 - 10^7$  years)

compared to the age of these systems (e.g. [150]), while in Es the mass return rate from the (passively) evolving stellar population (the main source of Interstellar Medium) is

$$(13) \quad \dot{M}_*(t) \simeq 1.5 \times \frac{L_B}{10^{11} L_{B\odot}} t_{15}^{-1.3} M_{\odot} \text{yr}^{-1},$$

where  $L_B$  is the present galaxy blue luminosity and  $t_{15}$  is time in units of 15 Gyr ([151]). It is then clear that a long-lived cooling flow would accumulate a mass in the galaxy central regions substantially exceeding that currently observed for SMBHs or in the resident diffuse gas. Young stellar populations observed in the body of ellipticals also cannot account for the total mass released and alternative forms of cold mass disposal (such as distributed mass drop-out/star formation) are not viable solutions (e.g. [152]). In addition to this mass disposal problem, *which must be solved in any scenario of SMBH formation and evolution*, the X-ray luminosity  $L_X$  of low-redshift Es is also inconsistent with the standard cooling flow model. In fact, low-redshift Es with optical luminosity  $L_B \gtrsim 3 \times 10^{10} L_{\odot}$  show a significant range in the ratio of gas-to-total mass at fixed  $L_B$ , with values ranging from virtually zero up to few % ([153]); most of the gas is detected in X-rays, with temperatures close to the virial temperatures of the systems ( $\sim 10^{6.7}$  K, e.g. [154]). *The idea of a SMBH feedback<sup>(2)</sup> on the Interstellar Medium is then most natural, as will be introduced and discussed in Sect. 4.2.* Here I just recall that there is increasing evidence in the local Universe of hot gas disturbances on various galactic scales, most likely resulting from recent nuclear activity (e.g. [155]). For example, *Chandra* revealed two symmetric arm-like features across the center of NGC4636 ([156, 157]), accompanied by a temperature increase with respect to the surrounding hot Interstellar Medium. The existence of these features has been related to shock heating of the Interstellar Medium, caused by a recent nuclear outburst. Other pieces of evidence include the observation of: a hot filament in the nuclear regions of NGC821 and NGC3377 ([158]-[160]); a “bar” feature, presumably due to a shock, at the center of NGC4649 ([161]); a nuclear outflow in NGC4438 ([162]); an unusual temperature profile present in NGC 3411 ([163]).

I finally mention another observational riddle that it is almost certainly associated with some kind of feedback, i.e., that of the apparent “underluminosity” of Active Galactic Nuclei in the local Universe, which are observed to emit less than expected, based on standard stationary accretion models applied to the circumnuclear environment (e.g. [164]-[167]). Quite obviously, the cooling flow and underluminosity problems should be interpreted and solved in terms of the co-evolution of SMBHs and of the host spheroids. In fact, *any plausible scenario for the initial formation of the host galaxy and of the central SMBH, should also be accompanied by the identification of the mechanism able to stop the SMBH growth over the entire galaxy life.*

### 3. – The FP and its interpretation

In this Section, following [168], I address the problem of the physical interpretation of the FP (and of the other SLs) followed by early-type galaxies. This because *the galaxy*

---

<sup>(2)</sup> The term *feedback* generally describes the result of the physical phenomena associated with the interaction of the emerging radiation from the accreting material onto the host system, on different spatial and temporal scales.

*SLs*, when considered in the context of galaxy formation, provide important constraints also on the possible evolution of their central SMBHs.

Quite surprisingly, despite the large amount of dedicated work, no definite interpretation of the FP in terms of the intrinsic galaxy properties has been found yet. In general, studies of the FP (e.g. [169]-[179]) are carried out under the guiding principle that the FP reflects the existence of an underlying mass–luminosity relation for such galaxies (e.g. [180, 181]), in a scenario where galaxies are homologous systems in dynamical equilibrium. However, as we will see this is not necessarily the case. Given the importance of this subject, I review here some of the proposed solutions. I start by giving a short discussion about the relation between the FP and the Virial Theorem. Then, I present various possible causes to the origin of the observed systematic departure from *homology* (structural, dynamical) and/or from a constant *stellar* mass-to-light ratio.

The characteristic dynamical time of Es (e.g., within  $R_e$ ) is  $T_{\text{dyn}} \simeq (G < \rho >_e)^{-1/2} \simeq 10^8 \text{yrs}$  and their collisionless relaxation time is of the same order ([182]), i.e., both are short with respect to the age of Es. As a consequence, presumably only very few galaxies currently undergoing strong perturbations are caught in a non-stationary phase, while most Es obey the Virial Theorem which, for a galaxy of total stellar mass  $M_*$  embedded in a dark matter halo of total mass  $M_h$ , can be written as

$$(14) \quad \sigma_V^2 \equiv \frac{2K_*}{M_*} = \frac{|U_{**}| + \mathcal{R}|W_{*h}|}{M_*} = \frac{G\Upsilon_* L_B}{R_e} \times (|\tilde{U}_{**}| + \mathcal{R}|\tilde{W}_{*h}|),$$

where  $\sigma_V$  and  $K_*$  are the so-called (three-dimensional) virial velocity dispersion and total kinetic energy of the stellar component,  $\mathcal{R} \equiv M_h/M_*$  and  $\Upsilon_* = M_*/L_B$  is the *stellar* mass-to-light ratio in the specific band used to measure  $L_B$  and  $R_e$ . The dimensionless functions  $\tilde{U}_{**}$  and  $\tilde{W}_{*h}$  are the stellar gravitational self-energy and the interaction energy between the stars and the dark matter halo, corresponding to

$$(15) \quad U_{**} = - \int \langle \mathbf{x}, \nabla \Phi_* \rangle \rho_* d^3 \mathbf{x}, \quad W_{*h} = - \int \langle \mathbf{x}, \nabla \Phi_h \rangle \rho_* d^3 \mathbf{x};$$

where  $\Phi_*$  and  $\Phi_h$  are the gravitational potentials generated by stars and dark matter, respectively, and  $\langle, \rangle$  is the standard scalar product. Thus, the r.h.s. of eq. (14) depends only on the luminous and dark matter density profiles (with the dimensionless functions of the order of unity, see, e.g. [102, 183, 184]). Obviously, the virial velocity dispersion is a global measure of the total kinetic energy, and does not depend on how such energy is distributed between ordered or disordered motions nor on whether the pressure tensor is isotropic or not.

In turn,  $\sigma_V^2 >$  is related to  $\sigma_o^2$  through a dimensionless function that depends on the galaxy structure, its specific internal dynamics and on projection effects:

$$(16) \quad \sigma_V^2 = C_K [\text{structure, anisotropy, projection}] \times \sigma_o^2.$$

It is important to note that – even in the case when the pressure tensor of the stellar system is isotropic –  $C_K$  is very sensitive to galaxy-to-galaxy structural differences, because it relates a weakly structure dependent quantity ( $\sigma_V$ ) to a local property (the central projected velocity dispersion  $\sigma_o$ ). In fact it can be easily proved that using larger and larger apertures to define the relevant projected velocity dispersion  $\sigma_a$  (see eq. [27]), in

a spherical system without dark matter  $C_K \rightarrow 3$ , independently of the galaxy internal orbital structure ([185]). If we define

$$(17) \quad K_V \equiv \frac{C_K}{|\widetilde{U}_{**}| + \mathcal{R}|\widetilde{W}_{*h}|},$$

from eqs. (14)-(16) we obtain

$$(18) \quad \frac{G\Upsilon_* L_B}{R_e} = K_V \sigma_o^2.$$

From eq. (18) and eqs. (2), we get

$$(19) \quad k_1 = \frac{1}{\sqrt{2}} \log \frac{G\Upsilon_* L_B}{K_V}; \quad k_3 = \frac{1}{\sqrt{3}} \log \frac{2\pi G\Upsilon_*}{K_V},$$

while using eq. (1), we find

$$(20) \quad \frac{\Upsilon_*}{K_V} \propto R_e^{\frac{2-10\beta+\alpha}{\alpha}} L_B^{\frac{5\beta-\alpha}{\alpha}}.$$

*Note that the Virial Theorem does not imply any FP.* In fact, for fixed  $L_B$  different galaxies, all satisfying the Virial Theorem, can in principle have very different  $K_V$  and  $\Upsilon_*$ , and so be scattered everywhere in the  $k$ -space. Equation (20) reveals instead that the FP cannot result from pure *homology*. In practice, in real Es, no matter how complex their structure is, the quantity  $\Upsilon_*/K_V$  is a well-defined (i.e., with little scatter) function of any two of the three observables ( $L, R_e, \sigma_o$ ). This systematic trend is known as the *FP tilt* (see also Sect. 2.1.1). Note the curious fact that while in the B-band all the tilt depends on luminosity (e.g. [72, 100]), in the K-band it is almost due only to  $R_e$ , with  $\Upsilon_*/K_V \propto L_K^{0.02} R_e^{0.28}$ . It is evident that *fine tuning* is required to produce the tilt, and yet preserve the tightness of the FP. The central problem posed by the existence of the FP is to determine what is the specific physical ingredient responsible for the tilt. Of course, *the identification of such ingredient would be of extreme importance for our understanding of galaxy formation.*

A first possibility to interpret the trend in eq. (20) is to assume homology (i.e.,  $K_V$  identical for all galaxies), a variable stellar mass-to-light ratio (e.g. [181, 186]), and the empirically suggested identity  $2 - 10\beta + \alpha = 0$ . Under these assumptions the relation would become

$$(21) \quad \Upsilon_* \propto L_B^\delta, \quad \delta = \frac{2-\alpha}{2\alpha} \simeq 0.30 \pm 0.064.$$

This line of investigation is addressed in Sect. 3.1.

An alternative extreme explanation (Sect. 3.2) can be proposed by assuming a constant stellar mass-to-light ratio  $\Upsilon_*$  and the existence of *weak homology* ([90, 94, 97], [186]-[189]). In this case it is the quantity  $K_V$  that is required to be a well-defined function of  $R_e$  and  $L$ . If we take  $2 - 10\beta + \alpha = 0$ , the required dependence is

$$(22) \quad K_V \propto L_B^{-\delta},$$

with  $\delta$  and its scatter the same as above. Equations (21)-(22) represents what Renzini & Ciotti ([186]) called “orthogonal explorations”.

**3.1. A stellar origin: changing the Initial Mass Function.** – When considering the possibility of a stellar origin for the FP tilt, a first candidate is certainly a systematic increase of stellar metallicity with galaxy mass. In fact, brighter galaxies are more metal rich and then *redder* than fainter galaxies, so that the stellar mass-to-light ratio in the blue band increases systematically with galaxy mass, as requested by eq. (21). However, this effect accounts for only a minor fraction of the observed tilt, because the FP tilt is still present when using observations at longer wavelengths, such as the *K* band (which is a very good proxy for the almost metallicity-independent bolometric luminosity, e.g. [41, 190]).

A second possible explanation of the FP tilt based on the properties of stellar populations is a systematic change of the so-called Initial Mass Function, i.e. the number distribution of stars in a galaxy as a function of their mass; observationally the Initial Mass Function of stars in the Solar neighborhood is fairly well described by a power law of stellar mass (with negative exponent). As is well known from stellar evolution, stellar luminosity increases more than linearly with stellar mass, so that the mass-to-light ratio of low mass stars is much higher than the mass-to-light ratio of massive stars. Therefore, a formal solution for the FP tilt could be a systematic change of slope in the Initial Mass Function (with more negative slopes in high-mass galaxies), or a decrease of the minimum stellar mass with galaxy mass (while maintaining the Initial Mass Function slope similar in all galaxies). These formal solutions were studied in detail in [186]. The main conclusion was that a major change of Initial Mass Function slope in the lower main sequence with galaxy mass is necessary to account for the FP tilt. At the same time, in order to preserve the small and constant thickness of the FP, the galaxy to galaxy dispersion in the Initial Mass Function properties should be extremely small, otherwise the edge-on view of the FP would rather look like a wedge (with the wide side at high luminosity), rather than a strip of constant thickness. Such very small galaxy to galaxy dispersion, coupled to a large systematic variation of the slope of the Initial Mass Function, is a rather demanding constraint, showing that fine tuning is required to produce the observed tilt of the FP, while preserving its constant thickness: the Initial Mass Function should be virtually universal for given galaxy mass, and yet exhibit a significant variation with galaxy mass.

We finally note that, besides of the Initial Mass Function,  $\Upsilon_*$  is also a function of age, because so is the galaxy luminosity. Thus, the small thickness of the FP implies a small dispersion in the age of the bulk stellar content of cluster Es. For example, if galaxies are older than  $\sim 10$  Gyr, one gets a tight constraint on the age dispersion, with an upper limit of only 1.5 Gyr. Such small age dispersion is in agreement with the similarly tight limit that is independently set by the tightness of the color- $\sigma$  relation for Virgo and Coma ellipticals ([42]).

**3.2. A structural/dynamical origin.** – In this case, by assuming  $\Upsilon_* = \text{const.}$ , one would like to explore under which conditions structural/dynamical effects may cause the FP tilt via a systematic decrease of  $K_V$  with luminosity. Most of these explorations refer to spherical, non rotating, two-component galaxy models, where the light profiles resemble the  $R^{1/4}$  law when projected (e.g. [103, 186, 187, 191]-[193]), while very few investigations consider non-spherical models (e.g. [181, 194, 195]). Bertin in [2] presented a lucid discussion of the four main different ways of working on the construction of stellar dynamical models. Here I will focus on the so-called  $\rho - to - f$  or “density priority” approach. In the spherical cases, usually carried out under the assumption of a two-integral phase-space distribution function  $f = f(E, J^2)$  (with  $E$  and  $J$  being the star specific energy and angular momentum; in this case the tangential components of the

velocity dispersion tensor are identical, the only possible difference being between  $\sigma_r^2$  and  $\sigma_\theta^2 = \sigma_\phi^2 = \sigma_v^2/2$ , e.g. [196]), the model spatial and projected velocity dispersion profiles are obtained by solving the associated Jeans equation for assigned density and pressure anisotropy profiles (see, e.g. [197]):

$$(23) \quad \frac{d\rho_*(r)\sigma_r^2(r)}{dr} + \frac{2\beta(r)\rho_*(r)\sigma_r^2(r)}{r} = -\frac{GM(r)}{r^2}\rho_*(r),$$

with the boundary condition  $\rho_*(r)\sigma_r^2(r) \rightarrow 0$  for  $r \rightarrow \infty$ , where  $M(r)$  is the total (dark and visible) mass within  $r$ . Usually the orbital anisotropy is introduced in terms of the Osipkov-Merritt ([198]-[200]) parametrization

$$(24) \quad \beta(r) \equiv 1 - \frac{\sigma_\theta^2(r)}{\sigma_r^2(r)} = \frac{r^2}{r^2 + r_a^2},$$

so that the velocity dispersion tensor is nearly isotropic inside  $r_a$  and radially anisotropic outside. The radial component of the velocity dispersion is then given by

$$(25) \quad \rho_*(r)\sigma_r^2(r) = \frac{G}{r^2 + r_a^2} \int_r^\infty \rho_*(r)M(r) \left(1 + \frac{r_a^2}{r^2}\right) dr,$$

The projected velocity dispersion is given by

$$(26) \quad \sigma_P^2(R) = \frac{2}{\Sigma_*(R)} \int_R^\infty \left[1 - \beta(r)\frac{R^2}{r^2}\right] \frac{\rho_*(r)\sigma_r^2(r)r}{\sqrt{r^2 - R^2}} dr,$$

where  $\Sigma_*(R)$  is the surface stellar mass density. The ‘‘observed’’  $\sigma_o$  does not correspond to  $\sigma_P(0)$ , but rather to the average over the aperture used for the spectrographic observations:

$$(27) \quad \sigma_a^2(R_a) = \frac{2\pi}{M_P^*(R_a)} \int_0^{R_a} \Sigma_*(R)\sigma_P^2(R)R dR,$$

where  $M_P^*(R_a)$  is the projected stellar mass inside  $R_a$ . Usually, one refers to  $R_a = R_e/8$  or  $R_e/10$ .

Examples of density profiles that have been extensively assigned are those obtained by deprojecting the  $R^{1/m}$  profiles (as defined in eq. [6]), and the so-called  $\gamma$ -models ([184, 201])

$$(28) \quad \rho_*(r) = \frac{3 - \gamma}{4\pi} \frac{M_* r_c}{r^\gamma (r_c + r)^{4-\gamma}} \quad (0 \leq \gamma < 3),$$

which for  $\gamma = 1$  ( $R_e \simeq 1.82 r_*$ ) and  $\gamma = 2$  ( $R_e \simeq 0.75 r_*$ ) reduce to the well known Hernquist ([202]) and Jaffe ([203]) profiles, respectively. In order to study the effects of dark matter halos, dark matter can be introduced to contribute to the total integrated mass  $M(r)$  and be represented again by  $\gamma$  models (with different total mass and scale-length [191, 193]), or by the Plummer ([204]) density profile

$$(29) \quad \rho_h(r) = \frac{3M_h}{4\pi} \frac{r_h^2}{(r_h^2 + r^2)^{5/2}},$$

and its variants, such as the quasi-isothermal density profile  $\rho \propto (r_h^2 + r^2)^{-1}$  and the King ([205])  $\rho \propto (r_h^2 + r^2)^{-3/2}$  density profile.

In general, two-component  $\gamma$  models are associated with a density profile in the central regions similar to that expected from cosmological simulations, i.e, with a central cusp (e.g. [206]-[209]). In addition, recently two-component models in which the *total* mass profile decreases as  $r^{-2}$  have been found consistent with combined observations of stellar dynamics and gravitational lensing (e.g. [210, 211]).

It should be remarked that not all the models adopted in the FP investigations have realistic velocity dispersion profiles in the central regions. Many of them (for example, those based on Hernquist or  $R^{1/m}$  density profiles) from the solution of eq. (23) are characterized by a sizable central depression in their  $\sigma_P$  (for a detailed discussion of this point, see [94, 100, 102, 103, 187, 212]), while the observed profiles typically decrease monotonically with radius (e.g. [213]-[217]). Thus, some care is needed in the model selection.

Among models with realistic velocity dispersion profiles are the isotropic Jaffe models and the  $f_\infty$  models ([61, 218], and references therein). In particular, the  $f_\infty$  models have been constructed by following the physical scenario that Es may have formed through collisionless collapse ([60]). In the spherical limit, their anisotropic distribution function is given by

$$(30) \quad f_\infty = \begin{cases} A(-E)^{3/2} \exp(-aE - cJ^2/2) & \text{if } E \leq 0, \\ 0 & \text{if } E > 0, \end{cases}$$

where  $E = v^2/2 + \Phi(r)$  and  $J$  are the star energy and the magnitude of the star angular momentum, per unit mass, respectively; here  $A$ ,  $a$ , and  $c$  are positive constants. The models are a one-parameter family, with structure dependent on the concentration parameter  $\Psi = -a\Phi(0)$ .

**3.2.1. Dark matter content and distribution.** In this line of investigation, in the construction of the galaxy models one usually assumes isotropic velocity dispersion, and ascribes all the FP tilt to a systematic variation with galaxy luminosity of the relative amount of dark matter with respect to the stellar component of the galaxy (parametrized by  $\mathcal{R} = M_h/M_*$ ) or to a systematic variation with galaxy luminosity of the relative concentration of the dark matter (parametrized by  $\beta = r_h/r_*$ , where  $r_h$  is a characteristic radius of the dark matter distribution). In the case of models with fixed  $\beta$ , the larger  $\beta$ , the larger the variations of  $\mathcal{R}$  that are required to produce the tilt (see the top panels in Fig. 6 for two examples). In any case, in this interpretation of the FP tilt massive galaxies should be more dark matter dominated than smaller systems. In the complementary exploration, one can fix the value of the total mass ratio  $\mathcal{R} = M_h/M_*$  and explore the required variations of  $\beta = r_h/r_*$ : in general, it turns out that  $\beta$  should decrease as a function of galaxy mass (bottom panels in Fig. 6).

Overall, as already stressed, the narrow and nearly constant thickness of the galaxies distribution about the FP corresponds to a very small dispersion of  $\Upsilon_*/K_V$ , and if  $\Upsilon_*$  and  $K_V$  are not finely anticorrelated, this implies indeed a very small dispersion, separately for both quantities, at any location on the FP. In the present context ( $\Upsilon_* = \text{const}$ ), this translates into strong constraints on the range that  $\mathcal{R}$  and  $\beta$  can span at any location on the FP. For example, the dotted lines in Fig. 6 represent the band within which galaxy to galaxy variations of the corresponding parameter are allowed, and yet are consistent with the restrictions imposed by the tightness of the FP. It is evident from these figures

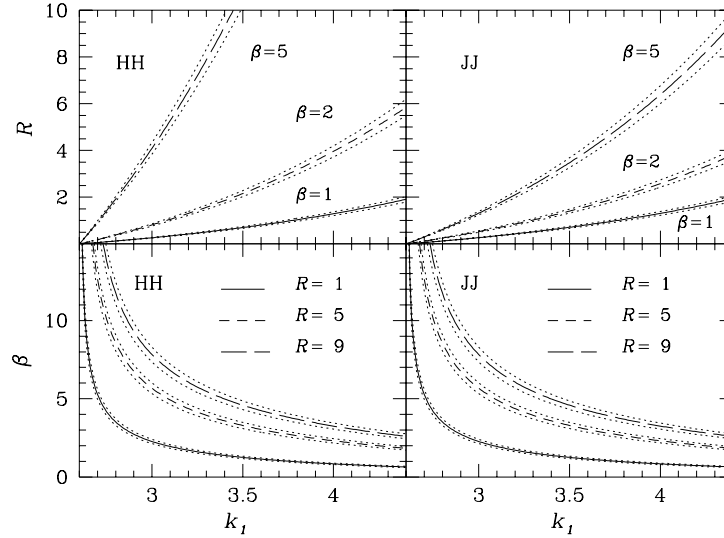


Fig. 6. – The trend along the FP of the dark matter content (upper panels) at constant  $\beta$  and that of the dark matter concentration (lower panels) at constant  $\mathcal{R}$ , required to produce the tilt, in two-component isotropic Hernquist models (HH) and two-component isotropic Jaffe models (JJ) isotropic models. The band within dotted lines marks the boundaries within which  $\mathcal{R}$  and  $\beta$  can vary at each location on the  $k_1$  axis in accordance with the observed FP tightness (from [94]).

that, whatever the structural parameter that is responsible for the tilt of the FP, and whatever the assumed mass distribution, dramatic fine tuning is required to produce the tilt, and yet preserve the tightness of the FP.

**3.2.2. Structural non-homology.** A change of internal structure as systematic way to change  $K_V$  has been proposed and studied by several authors (e.g. [86, 90, 94, 96, 97, 100, 103, 186, 187, 188, 219, 220]). We may call *weak homology* the condition by which the structure and dynamics (density and pressure tensor distributions) of early-type galaxies vary systematically with galaxy luminosity.

An indication that this may be at the origin of the FP tilt is indeed provided by the systematic trends noted above in terms of  $R^{1/m}$  fits (see Sect. 2.1.3). Therefore, this option can be investigated using isotropic  $R^{1/m}$  models without dark matter ([102]), thus ascribing the origin of the tilt to a systematic variation of  $m$ . For example, in the preliminary analysis of [94] it has been shown that in order to produce the tilt  $m$  has to increase from 4 up to  $\sim 10$ . These values are well within the range of values spanned by observations.



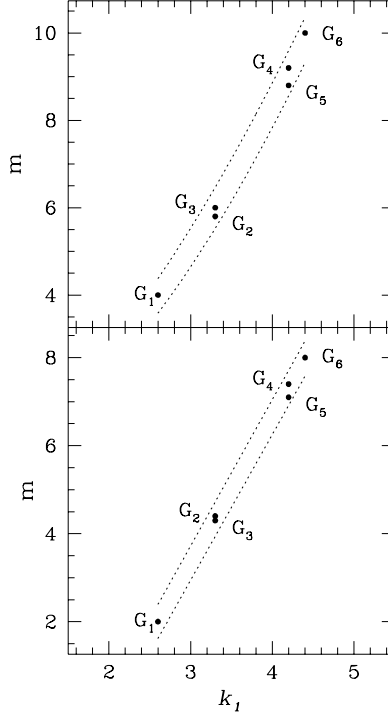


Fig. 7. – The values of  $m$  for the six  $R^{1/m}$  isotropic models required to produce the FP tilt, and the band within which  $m$  can vary at each location on the  $k_1$  axis in accordance with the observed FP tightness. In the upper panels, the faintest model (lowest value of  $k_1$ ) is characterized by  $m = 4$ ; in the lower panel,  $m = 2$  at the faint end of the FP (from [94]).

A much more in-depth analysis of weak homology has been carried out in [100], starting with a very accurate analysis of 4 significant cases of deviations from the  $R^{1/4}$  law, i.e. the surface brightness profiles of NGC 1379, NGC 4374, NGC 4458, and NGC 4552. The analysis (based on the photometric data taken from [112, 113]) confirms that the  $R^{1/m}$  can provide superior fits (the best-fit value of  $m$  can be lower than 2.5 or higher than 10), better than those that can be obtained by a pure  $R^{1/4}$  law, by an  $R^{1/4}$ +exponential model, and by other dynamically justified self-consistent models (such as the  $f_\infty$  models ([218])). Note that according to eq. (22) a factor of 20 in  $L_B$  would require a change in  $K_V$  by a factor of  $\approx 2.45$ . Then, it is of interest to compute the function  $K_V(m)$  for one-component, spherical, non-rotating, isotropic  $R^{1/m}$  models and a simulated spectroscopic aperture of  $R_e/8$  [103, 97]. An accurate and convenient analytical representation in the range  $1 \leq m \leq 10$  (with typical errors on the order of one percent) is given by

$$(31) \quad K_V(m) \simeq \frac{73.32}{10.465 + (m - 0.94)^2} + 0.954 .$$

A similar argument also holds for the  $f_\infty$  models, for which the simple analytical inter-

polation formula

$$(32) \quad K_V(\Psi) \simeq \frac{142.3 - 41.51\Psi + 2.66\Psi^2}{30.61 - 10.7\Psi + \Psi^2}$$

is accurate to around one percent, in the range  $2 \leq \Psi \leq 10$ . Incidentally, this shows again how the determination of the coefficient  $K_V$  is sensitive to the choice of models (e.g., see Fig. 11 in [100]). Note that this leads to significantly different answers with respect to the application of  $R^{1/m}$  models. For example, if we take NGC 4552, the  $R^{1/m}$  modeling would give  $m \simeq 11.14$  and  $K_V \simeq 1.6$ , while the  $f_\infty$  modeling would set  $\Psi \simeq 6.2$  and  $K_V \simeq 2.5$ ; for the galaxy NGC 4458 (closest to the standard  $R^{1/4}$  law in our sample), we find  $m \simeq 3.2$  and  $K_V \simeq 5.7$  based on  $R^{1/m}$  modeling or  $\Psi \simeq 9$ ,  $K_V \simeq 3$  based on  $f_\infty$  modeling. In any case the variations found are consistent with the FP tilt.

A more sophisticated analysis of the problem, based on Monte-Carlo simulations, was also presented in [100]. In practice, the Authors mapped the model space  $(m, \Upsilon_*, L, R_e)$  into the observed space  $(L, R_e, \sigma_e)$  by using the virial coefficients in eqs. (31)-(32), and selecting as acceptable candidates for real galaxies, only those points that turn out to be compatible, in the observed space, with the FP correlation and its observed scatter. For example, Fig. 8 shows, under the assumption of constant  $\Upsilon_*$ , the distribution in the luminosity-Sersic index  $(m)$  plane of galaxies compatible with the FP: in particular, models represented by heavy dots are consistent with a FP of virtually no scatter (what we may call the “backbone” manifold). Of course, by allowing a simultaneous variation of  $\Upsilon_*$  and  $m$ , a much larger number of models becomes compatible with the FP. This case is represented in Fig. 9, where all the points are compatible with the FP with intrinsic scatter artificially reduced. Thus, *these results show that weak homology - both from the observational and from the theoretical point of view - could be a relevant physical ingredient at the origin of the FP.*

**3.2.3. The role of anisotropy.** Among the various galaxy properties in principle able to destroy the FP thinness (as a consequence of a substantial variation at fixed galaxy luminosity), one possibly “effective” might be orbital anisotropy (e.g. [221]). In fact, galaxy models are often believed to be able to sustain a large spread of orbital anisotropies. It is also well known that radial orbital anisotropy can be associated with very high *central* velocity dispersion values, and correspondingly low values of  $K_V$ , thus violating the FP thinness in case of significant scatter among galaxies. Natural questions to be addressed are then 1) if variations in orbital anisotropy can be responsible for the whole FP tilt, and 2) whether empirically, or as a result of some physical reasons, the range of orbital anisotropies present in real galaxies might be limited. In practice, the amount of radial anisotropy in the velocity dispersion tensor should increase with galaxy luminosity (i.e.,  $r_a$  should decrease in the Osipkov-Merritt parameterization), but with values fine-tuned with galaxy luminosity. In other words, in this scenario the FP tilt would be produced by a *dynamical* non-homology due to anisotropy.

The results of a preliminary investigation ([94]) of this problem, based on the behavior of Hernquist and Jaffe density profiles, are shown in Fig. 10. The curves are truncated because of the limits imposed by *dynamical consistency* ([187, 191, 193]): above a certain luminosity, in models constrained to the FP, the phase-space distribution function would run into negative values. A more refined exploration, based on one-component  $R^{1/m}$  models, constructed with different amounts of pressure anisotropy, following the Osipkov-Merritt prescription can be found in ([103]). For these models the self-consistently generated phase-space distribution function has been obtained, and the

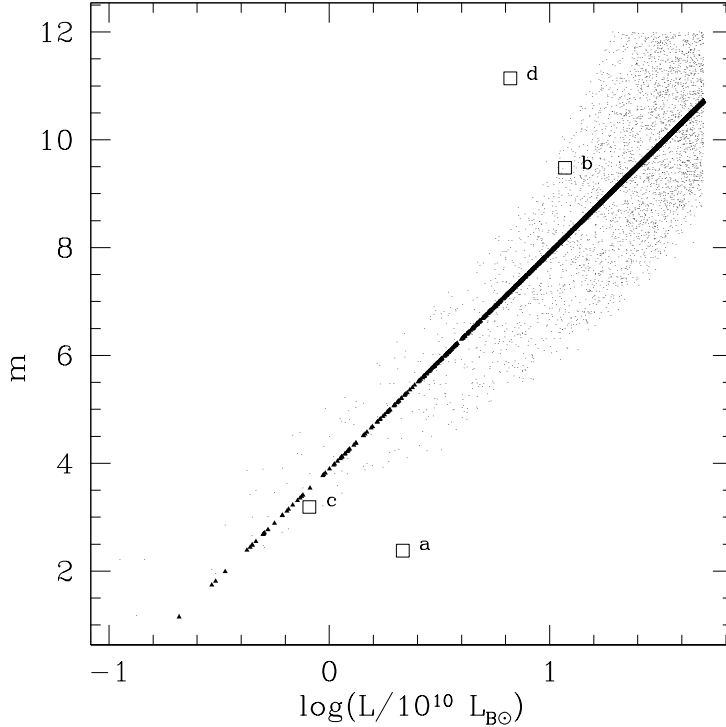


Fig. 8. – Projection on the plane  $(L, m)$  of the manifold in model space identified by  $\Upsilon_* \simeq 3.5$ . The scatter of points reflects the adopted scatter around the FP in the observed space. Solid symbols represent the “backbone” manifold. Open squares represent the four observed galaxies described in this Section (from [100]).

minimum value of the anisotropy radius for the model dynamical consistency has been derived as a function of  $m$ . As for Hernquist and Jaffe models, also for  $R^{1/m}$  models constrained to the FP it is found that above a certain luminosity (dependent on  $m$ ), the phase-space distribution function runs into negative values (as shown in Fig. 11 for the case  $m = 4$ ). Therefore, anisotropy alone cannot be at the origin of the tilt, because the extreme values of  $r_a$  that would be required correspond to dynamically inconsistent models.

The relation between radial anisotropy and FP thickness was also studied in [103] in a semi-quantitative way by considering the radial-orbit instability indicator  $\xi \equiv 2K_r/K_t$  ([222]), where  $K_t = 2\pi \int \rho \sigma_t^2 r^2 dr$  and  $K_r = 2\pi \int \rho \sigma_r^2 r^2 dr$  are the tangential and the radial kinetic energies (see also [223]). In particular, it is empirically known that when  $\xi \gtrsim 1.5 \div 2$  a radially anisotropic spherical system is likely to be unstable<sup>(3)</sup>, and in [103] was argued that  $R^{1/m}$  galaxy models *sufficiently anisotropic to be outside the FP observed*

<sup>(3)</sup> Unfortunately, such indicator is not fully reliable, because indications exist that it can depend significantly on the particular density profile of the model under investigation (e.g. [224]-[229]. See also the recent study [230]).

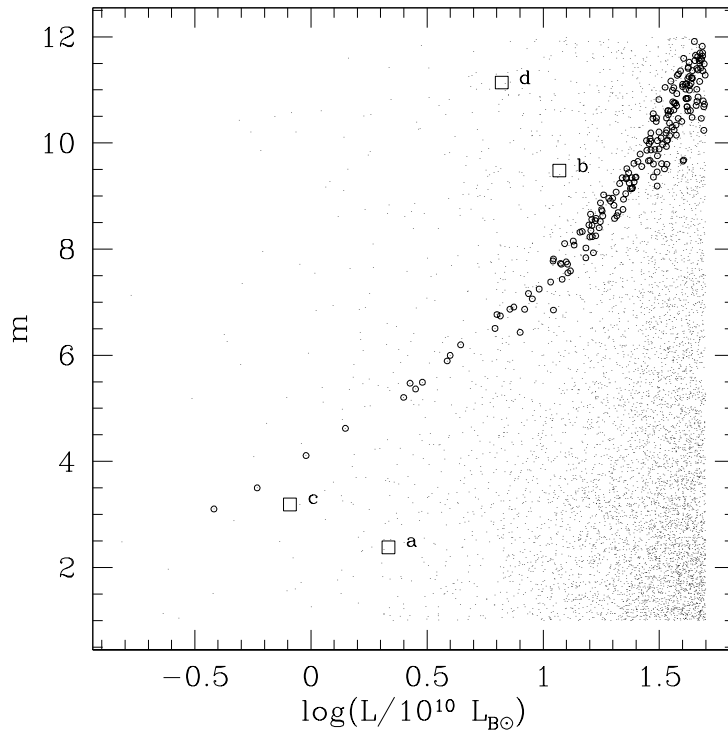


Fig. 9. – Projection on the  $(L, m)$  plane of the entire backbone manifold identified by the FP with scatter artificially reduced to 0.01. Open circles correspond to models with  $3.4 \leq \Upsilon_* \leq 3.6$ , open squares as in Fig. 9 (from [100]).

*thickness (when their parent isotropic model was assumed to lie on the FP) should be unstable.* The relevance of this result in connection with the FP thickness is simple: the effect on the projected velocity dispersion due to the maximum orbital anisotropy allowed by the stability requirement is well within the FP thickness, and so *no fine-tuning for anisotropy is required.*

Of course, those above were qualitative expectations based on necessarily simple analytical models. The entire question was then addressed quantitatively by using high resolution  $N$ -body simulations ([231]) of radially anisotropic one-component and two-component  $\gamma$  models, and exploring the impact of radial orbital anisotropy and instability on the FP properties. The numerical results confirmed the previous studies, and the situation is summarized in Fig. 12. The globally isotropic *parent models* are obtained fixing their structural properties and assuming isotropic pressure, and are placed on the FP by assigning the pair  $(\Upsilon_*, L_B)$ : with the coordinates adopted in the figure, the parent models are placed on the origin. From each of these parent models lying on the FP one then generate a *family* of Osipkov-Merritt radially anisotropic initial conditions by decreasing  $s_a = r_a/R_e$ , while keeping all the other model parameters fixed. The dotted line is the locus of points corresponding to radially anisotropic initial conditions, and for sufficiently small values of  $s_a$  the members of each family are found outside the observed thickness of the FP. The quantity in the vertical axis corresponds to the distance from

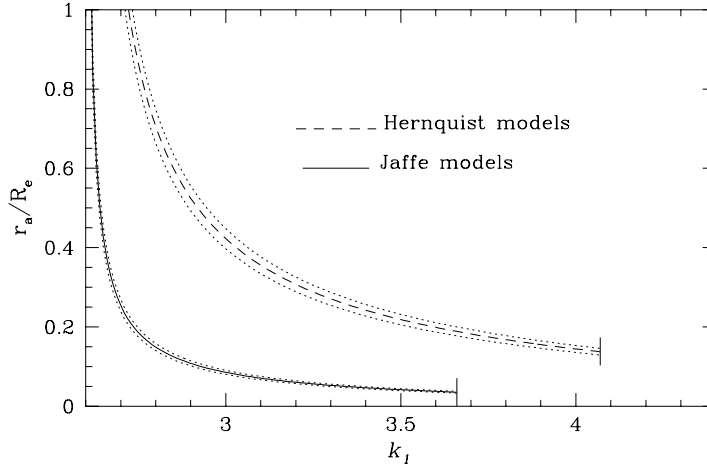


Fig. 10. – The trend of the anisotropy radius in units of  $R_e$  along the FP required to produce its tilt, in Hernquist and Jaffe models. The curves are truncated at the value of  $r_a/R_e$  below which the models become dynamically inconsistent. The band within dotted lines marks the boundaries within which  $r_a$  can vary at each location on the  $k_1$  axis according to the observed FP tightness (from [94]).

the FP of each virialized end-product of the numerical simulations: if  $k_3 = k_3^{\text{iso}}$  then the model has “fallen back” on the FP, so points inside this strip represent models consistent with the observed thickness of the FP. It is apparent how, by increasing the amount of radial anisotropy, the initial conditions move along the dotted line, and when they reach the critical value of the anisotropy radius they become unstable<sup>(4)</sup> and rearrange their density profile and internal dynamics in a new, stable configuration. *It is apparent that all the models, with the exception of two, obey the predictions made in [103]: the restrictions set by the onset of the radial-orbit instability match almost exactly the FP thickness.*

Moving to the strictly related question whether the FP tilt can be due to a systematic variation of  $K_V$  induced by an appropriate underlying correlation  $sa-L_B$  at fixed galaxy

<sup>(4)</sup> In [231] it is found that for one-component  $\gamma$ -models the critical value  $\xi_s$  for the radial-orbit instability is in the range  $1.6 \lesssim \xi_s \lesssim 1.8$ . This range for  $\xi_s$  is compatible with the value 1.7, reported by [222] and used in [103], and with the results of [228], who estimated  $\xi_s \simeq 1.58$  for the family of  $f_\infty$  models; [229] found instead a higher threshold value for stability ( $\xi_s \simeq 2.3$ ).

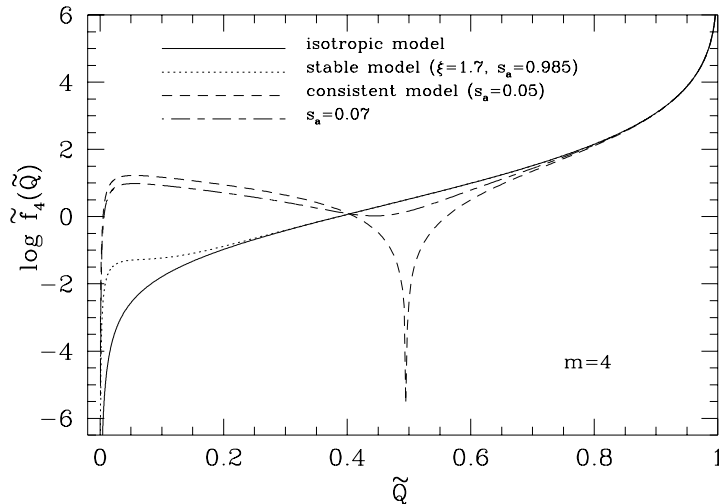


Fig. 11. – The modifications of the (dimensionless)  $R^{1/4}$  distribution function as a function of the Osipkov-Merritt parameter  $Q = E + J^2/(2r_a^2)$  (normalized to the system central potential), moving from the globally isotropic case (solid line) to the critical anisotropy for consistency (dashed line), where  $s_a = r_a/R_e$ . This behaviour is common to the whole family of the  $R^{1/m}$  models, and seems to be more a general property of the adopted anisotropy profile rather than a characteristic of some specific mass model (see also [191, 193]) (from [103]).

structure, in [231] it is also shown that a systematic increase of radial orbit anisotropy with galaxy luminosity is not a viable solution, because the galaxy models become unstable at moderately high luminosities, and the virialized systems originated from unstable initial conditions fall well outside the FP itself. This is illustrated in Fig. 13, where  $k_3^i - k_3^{\text{iso}}$  measures how much a given initial condition is displaced on the FP from its parent isotropic model, and  $k_3 - k_3^i$  measures the position of the corresponding end-product. It is clearly impossible to reproduce the FP tilt over the whole observed range (e.g.,  $\Delta k_1 \simeq 2$  and  $\Delta k_3 \simeq 0.3$  as reported in [75]) by using stable models only. Moreover, Fig. 13 shows also that the end-products of unstable initial conditions fall well outside the FP thickness, and the departure is larger for larger distance from the parent galaxy. Thus, we can safely conclude that *the FP tilt cannot be explained as an effect of a systematic increase of radial anisotropy with galaxy luminosity under the assumption of structural homology.*

**3.3. Summary.** – In this Section the main plausible hypotheses proposed to interpret the properties of the FP have been briefly illustrated. In general, it is shown that,

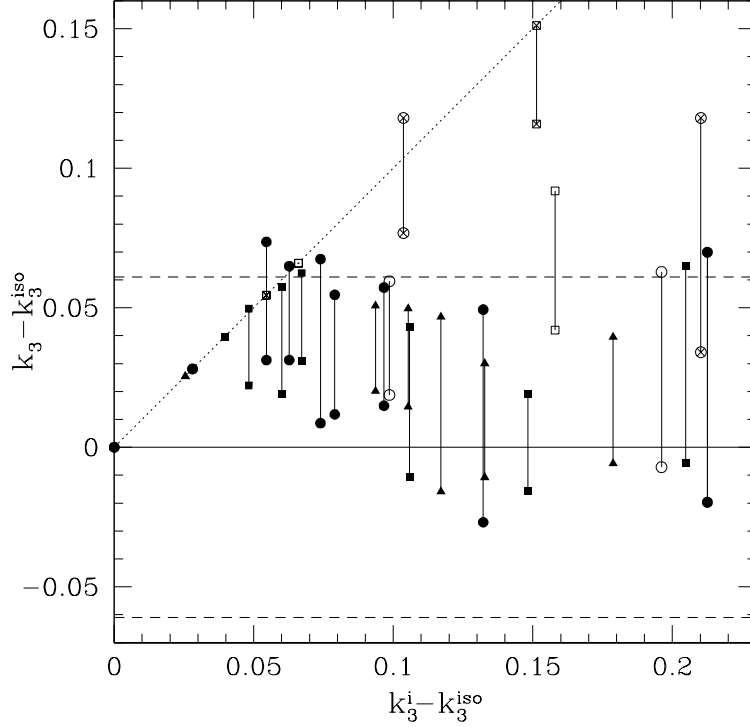


Fig. 12. – Final vs. initial  $k_3$  for one- (solid dots) and two-component (empty dots) galaxy models obtained from  $N$ -body simulations, where  $k_3^{iso}$  is the coordinate of their isotropic parent galaxy. The horizontal dashed lines mark the FP observed thickness  $\sigma(k_3)$ , while the dotted line  $k_3 = k_3^i$  is the locus of the initial conditions. The end-products are asymmetric, and so their representative points span a range of values as a function of the line-of-sight orientation (vertical lines); remarkably, the length of these segments is smaller than the FP thickness (from [231]).

independently of the favoured explanation, a *remarkable fine-tuning* of galaxy structure, dynamics, and properties of stellar population (in particular, of the Initial Mass Function) with galaxy luminosity must exist in order to produce the FP tilt and yet to preserve its thinness. Overall, the most promising explanation of the FP tilt seems to be 1) a synchronized star formation of the bulk of stars; 2) a remarkable regularity in the amount and distribution of dark matter; 3) a systematic dependence of the galaxy stellar density profile on galaxy luminosity (weak homology). This conclusion has been reached also in [232]. Anisotropy seems to be ruled out as a significant contributor to the FP tilt, as well as to its thickness. This latter conclusion is reached both on *theoretical* grounds (i.e., stability arguments) and from powerful *empirical* evidence, i.e., the very existence of the  $M_{BH}-\sigma_0$  relation. In fact, no significant scatter in the anisotropy can be present in real Es, otherwise the thin  $M_{BH}-\sigma_0$  relation would be destroyed (by the way, the thinness of this latter relation also shows that *projection effects*, due to non sphericity of galaxies, cannot affect significantly the observed  $\sigma_0$ , see also [194]).

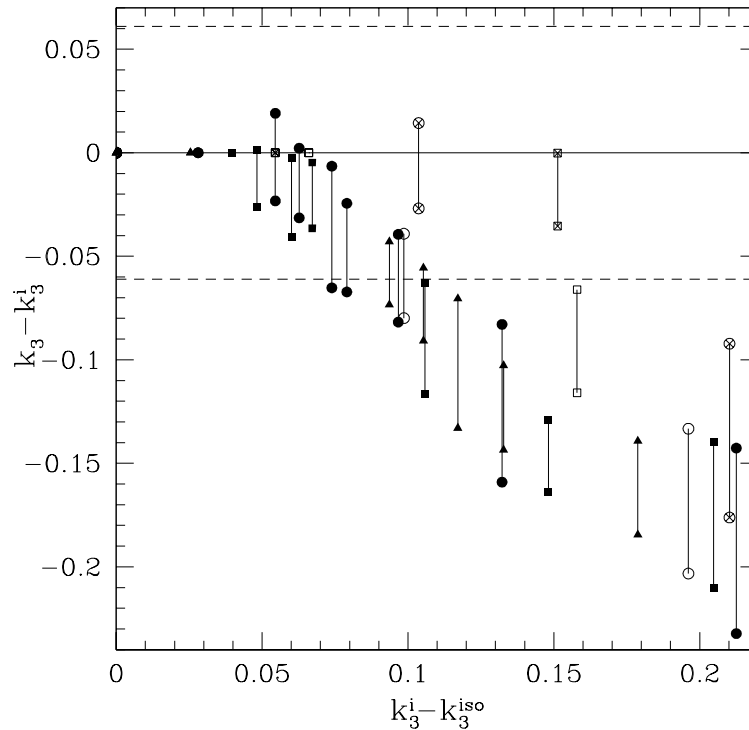


Fig. 13. – End-products of  $N$ -body simulations with anisotropic initial conditions placed on the FP at  $k_3^i - k_3^{iso}$ , where  $k_3^{iso}$  is the coordinate of their isotropic parent galaxy. The FP observed thickness  $\sigma(k_3)$  is marked by the dashed lines (from [231]).

#### 4. – Galaxies and SMBHs: maintenance of Scaling Laws

In this Section two important phenomena, in principle able to *destroy* the galaxy and SMBHs scaling laws, are discussed. The first, galaxy merging, is of *external* origin, while the second, namely the disposal of the huge (compared to the observed mass of the SMBHs) mass return from the passively evolving stellar population in Es, is of *internal* origin.

**4.1. Merging.** – One of the basic problems posed by *dry merging* (i.e. non-dissipative merging of red, old galaxies with no significant amount of gas) as the main channel to form Es was explicitly pointed out and discussed heuristically in [31]. In practice, it is the impossibility to increase the velocity dispersion of the end-products (as requested by the FJ law) while, at the same time, the associated enormous growth of  $R_e$  leads to violate the Kormendy relation. The two facts above are direct consequences of basic physics. In fact, from the virial theorem and conservation of the total energy, in the merging of two galaxies on a parabolic orbit (with masses  $M_1$  and  $M_2$ , virial velocity dispersions  $\sigma_{v,1}$



and  $\sigma_{V,2}$ , virial radii  $r_{V,1}$  and  $r_{V,2}$ ), the virial velocity dispersion and the virial radius<sup>(5)</sup> of the resulting galaxy, in the case of no mass loss and negligible kinetic and interaction energies of the galaxy pair when compared to their internal energies, are given by

$$(33) \quad \sigma_{V,1+2}^2 = \frac{M_1\sigma_{V,1}^2 + M_2\sigma_{V,2}^2}{M_1 + M_2}; \quad \frac{(M_1 + M_2)^2}{r_{V,1+2}} = \frac{M_1^2}{r_{V,1}} + \frac{M_2^2}{r_{V,2}}.$$

It follows that  $\sigma_{V,1+2} \leq \max(\sigma_{V,1}, \sigma_{V,2})$  and  $r_{V,1+2} \geq \min(r_{V,1}, r_{V,2})$ , i.e., *the virial velocity dispersion cannot increase and the virial radius cannot decrease in a merging process of the kind described above*. For example, in a merging hierarchy of identical seed galaxies characterized by  $\sigma_{V,0}$ ,  $r_{V,0}$  and  $M_0$ , we expect  $\sigma_V = \sigma_{V,0}$  and  $r_V = (M/M_0)r_{V,0}$ , independently of the merging sequence: if  $\sigma_o \sim \sigma_V$  and  $R_e \sim r_V$ , then it results that the FJ and Kormendy cannot be consistent with dry merging.

Several high-resolution N-body simulations of dry merging are nowadays available (e.g. [219], [233]-[242]) that can be compared with the expected relations (33). Here I describe in some detail the results obtained in [236] which, by using numerical simulations based on one and two-component isotropic Hernquist galaxy models ([191, 193, 202], see also Sect. 3.2), checked whether the end-products of merging of galaxies, initially lying on the FP, lie on the FP.

In particular, the study explored two extreme situations, namely the case of *major merging*, in which equal mass galaxies are involved at each step of the hierarchy, and the case of *accretion*, in which a massive galaxy increases its mass by incorporating smaller galaxies. In practice, the first generation of the *equal mass merging* hierarchy is obtained by merging a pair of identical, spherically symmetric and isotropic Hernquist models (the “zeroth order” seed galaxies), while the successive generations (in general 5, for a total mass increase of 32) are obtained by merging pairs of identical systems obtained by duplicating the end-product of the previous step. Cases with dark matter halos ( $\mathcal{R} = 5$  and  $\beta = 2$  in the seed galaxies; for the notation, see Sect. 3.2.1) and non-zero orbital angular momentum have also been considered. In the *accretion* hierarchy, instead, the seed test galaxy grows by accretion of smaller systems: the first merging event is identical to that in the equal mass merging case, but in the successive steps the end-product merges again with a seed galaxy, and so on, until the same final mass as in the equal-mass merging case is reached.

The first important result – which is almost independent of the different cases explored – is shown in Fig. 14: while  $\sigma_V$  is almost constant, the linear growth of  $r_V$  (and of the volume hal-mass radius  $r_M$ ) with  $M$  (dotted line) is apparent. The small increase of  $\sigma_V$  with respect to the expectation  $\sigma_V = \text{const.}$  is explained by the modest mass loss during merging. It is found that the *structure* of the end-products is quite sensitive to the different growth assumptions. In fact, from Fig. 15 demonstrates that the Sersic index  $m$  changes with the mass of the merging end-products: while in the equal-mass mergers  $m$  increases with mass and spans the range  $2 \lesssim m \lesssim 11$ , as in real galaxies (see Sect. 2.1.3), in the accretion case  $m$  *decreases* with the galaxy mass at mass ratios  $\gtrsim 4$  for the head-on accretions. Therefore, the explored head-on accretion scenario fails at reproducing the relation between the surface brightness profile shapes and luminosity of

---

<sup>(5)</sup> By definition, in a one-component galaxy  $\sigma_V^2 \equiv 2T/M$  and  $r_V \equiv -GM^2/U$ , where  $T$  and  $U$  are the total kinetic and the gravitational energy of the galaxy, respectively. See beginning of Sect. 3 for the two-component case.

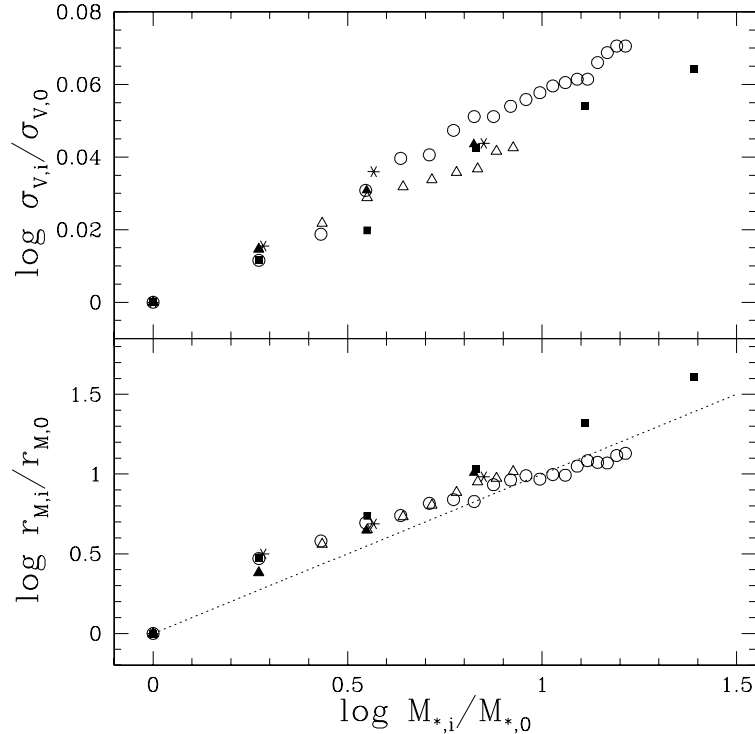


Fig. 14. – *Top panel*: virial velocity dispersion of the stellar component at stage  $i$  of the merging hierarchy vs. the total stellar mass of the merger. *Bottom panel*: angle-averaged half-mass radius  $r_M$  vs. total stellar mass. Equal mass mergers are shown as solid triangles and squares (one-component galaxies), and stars (two-component galaxies); empty triangles and circles represent the accretion hierarchies. Triangles correspond to simulations with non zero orbital angular momentum. The dotted line indicates the relation  $r_M \propto M$ ;  $M_{*,0}$ ,  $r_{M,0}$  and  $\sigma_{v,0}$  are the stellar mass, the virial velocity dispersion and the half-mass radius of the seed galaxy. In the two-component cases,  $\sigma_v$  and  $r_M$  refer to the stellar component only. Note the different range spanned in the ordinate axes in the two panels (from [236]).

real galaxies.

The impact of dry-merging on the FJ and Kormendy relations is summarized in Fig.16: by analogy with the results shown in Fig. 14, the FJ and the Kormendy relations are again shown to be violated at high masses (luminosities). Figure 17 shows the position of the end-products in the edge-on ( $k_1, k_3$ ) and face-on ( $k_1, k_2$ ) projections of the FP. The progenitor of the merging hierarchy (the black dot without bar) is placed exactly on the edge-on FP at  $k_1 \lesssim 3$ . Consistent with the adopted dissipationless scenario, the value of  $\Upsilon_*$  is kept constant during the whole merging hierarchy. Due to the loss of spherical symmetry of the end-products of the merging simulations, their coordinates depend on the line-of-sight direction; however, being the luminosity (mass) of each end-product fixed, variations of  $k_1, k_2, k_3$  due to projection effects are not independent. In fact, the

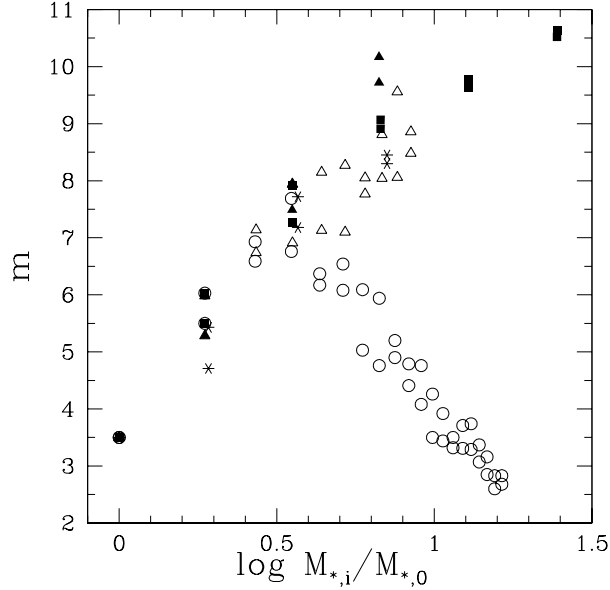


Fig. 15. – Sersic best-fit parameter  $m$  vs. total stellar mass of the end-products at stage  $i$  of the merging hierarchy. Same symbols as in Fig. 14 (from [236]).

$k_1$  and  $k_3$  coordinate of a galaxy of given luminosity are linearly dependent as

$$(34) \quad k_3 = \sqrt{\frac{2}{3}}k_1 + \sqrt{\frac{1}{3}}\log \frac{2\pi}{L_B},$$

corresponding to the segments in the top panel. The main conclusion of this analysis is that one-component (solid squares and triangles) and two-component (stars) equal mass mergers behave almost in the same way: models climb over the edge-on FP and remain well inside the populated zone in the face-on FP, moving along roughly parallel to the line defining the *zone of avoidance* (see also [75]). Thus, equal mass dry merging seems to be surprisingly consistent with the existence of the FP, especially considering its small thickness when seen edge-on. The most striking difference of the end-products of head-on accretion simulations (empty circles) with respect to the equal mass merging hierarchy and also to accretion simulations with angular momentum (empty triangles) shows up in the edge-on FP: after few accretion events, the end-products are characterized by a  $k_3$  decreasing for increasing  $k_1$ , and the models corresponding to an effective mass increase of a factor  $\sim 12$  are found at a distance  $\delta k_3$  larger than the FP scatter. This result is not surprising. In fact, being the coordinate  $k_3$  a measure of non-homology (for galaxies with constant  $\Upsilon_*$ ), the decrease of the Sersic parameter  $m$  with increasing mass reflects directly in the unrealistic trend in the  $(k_1, k_3)$  plane. In contrast, in the face-on  $(k_1, k_2)$  plane, the end-products of accretion (both head-on and with angular momentum) evolve along the same direction followed by equal mass mergers, but with a smaller excursion in  $k_1$  and  $k_2$ . Thus, while in the equal-mass mergers the deviations from the FJ and Kormendy relations curiously compensate to reproduce the edge-on FP, in the accretion

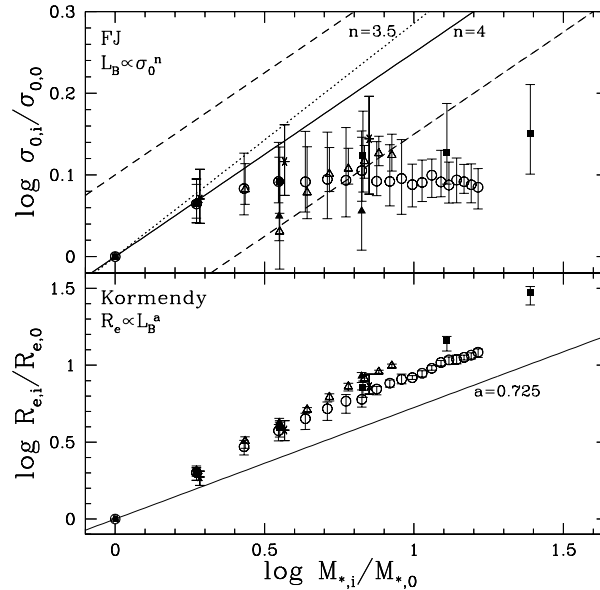


Fig. 16. – *Top panel*: stellar central velocity dispersion (normalized to that of the first progenitor) vs. total stellar mass. Points correspond to angle-averaged values, bars indicate the range spanned by projection effects. The solid and the two dashed lines represent the FJ relation  $L_B \propto \sigma_0^n$  and its scatter, while the dotted line represents  $L_B \propto \sigma_0^{3.5}$ . *Bottom panel*: stellar effective radius (normalized to that of the first progenitor) vs. total stellar mass. Points and bars have the same meaning as in the top panel. The solid line represents the adopted “fiducial” Kormendy relation. Note the different range spanned in the ordinate axes in the two panels (from [236]).

case there is not enough compensation, and the FP tilt is not reproduced.

Finally, we can move to consider the effects of dry merging on the  $M_{\text{BH}}-\sigma_0$  relation<sup>(6)</sup>. It is assumed that each seed galaxy contains a BH of mass  $M_{\text{BH},0}$ , and that each merging end-product contains a BH obtained by the merging of the BHs of the progenitors. Unfortunately, BH merging is still a poorly understood physical process, in particular with respect to the amount of emitted gravitational waves (e.g. [31, 244, 245]), and for this reason we consider two extreme situations: the case of *classical* combination of masses ( $M_{\text{BH},1+2} = M_{\text{BH},1} + M_{\text{BH},2}$ , with no emission of gravitational waves) and the case of *maximally efficient radiative merging* ( $M_{\text{BH},1+2}^2 = M_{\text{BH},1}^2 + M_{\text{BH},2}^2$ , corresponding to entropy conservation in a merging of two non rotating BHs [246, 247]). Figure 18 shows the central velocity dispersion of the mergers versus the mass of their central BH in the case of classical (panel a) and maximally radiative (panel b) BH merging. As expected from the similarity between the FJ and the  $M_{\text{BH}}-\sigma_0$  relations, in the classical case, both equal mass mergers and accretion mergers are unable to reproduce the observed relation. Thus, as for the FJ, the reason of the failure of dissipationless merging at reproducing

<sup>(6)</sup> The simulations of [236] do not consider the central SMBH. However, it has been shown [243] that the formation of a binary BH does not modify significantly  $\sigma_0$ .

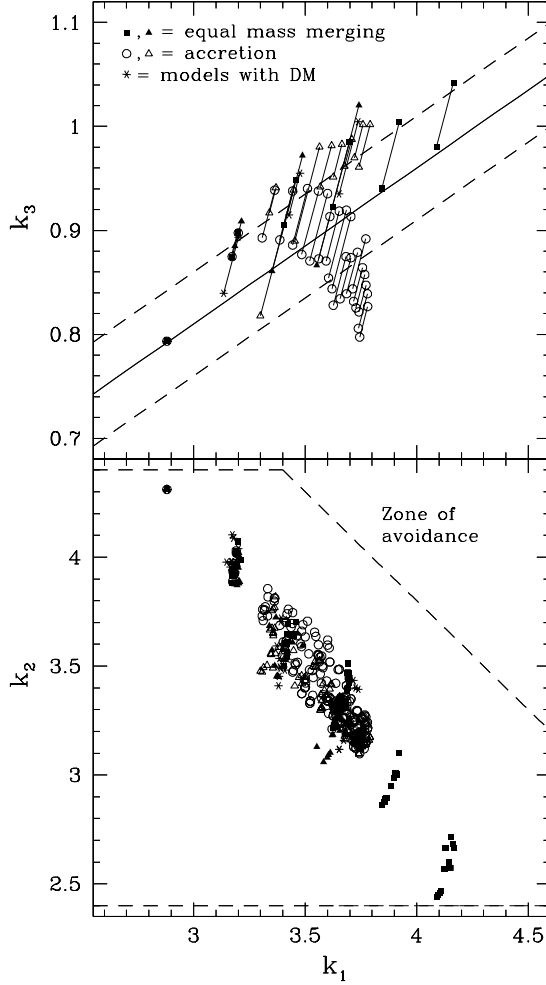


Fig. 17. – *Top panel:* the merging end-products in the  $(k_1, k_3)$  plane, where the solid line represents the FP relation as given by equation (4) with its observed  $1-\sigma$  dispersion (dashed lines). Bars show the amount of projection effects. *Bottom panel:* the merging end-products in the  $(k_1, k_2)$  plane, where the dashed lines define the region populated by real (as given in [75]). Each model is represented by a set of points corresponding to several random projections (from [236]).

the  $M_{\text{BH}}-\sigma_o$  relation is that the end-products are characterized by a too low  $\sigma_o$  for given  $M_{\text{BH}}$ , i.e.,  $M_{\text{BH}}$  is too high for the resulting  $\sigma_o$ . A promising solution to this problem could be the emission of some fraction of  $M_{\text{BH}}$  as gravitational waves. In fact, by assuming maximally efficient radiative BH merging, the points are found remarkably closer to the observed relation, even if it appears that the slope of the  $M_{\text{BH}}-\sigma_o$  relation is not well reproduced by the end-products of head-on accretion (empty circles). While in

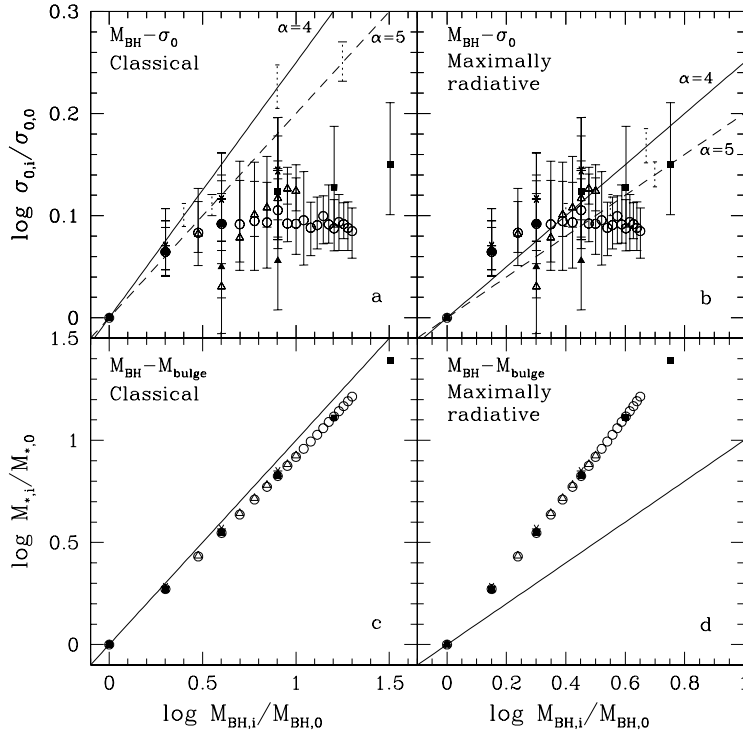


Fig. 18. – *Panel a*: galactic central velocity dispersion vs. BH mass for classical BH merging;  $\sigma_{0,0}$  and  $M_{\text{BH},0}$  are the central velocity dispersion and BH mass of the first progenitor, respectively. The points correspond to the mean value over the solid angle, while the bars indicate the range spanned by projection effects. Solid and dashed lines represent the  $M_{\text{BH}}-\sigma_0$  relation for  $\alpha = 4$  and  $\alpha = 5$ , respectively, while vertical dotted lines show the observed scatter around these best-fit relations. *Panel b*: same data as in panel a, but for maximally radiative BH merging. *Panel c*: stellar mass vs. BH mass for classical BH merging;  $M_{*,0}$  is the stellar mass of the first progenitor and the solid line represents the Magorrian ( $M_{\text{BH}} \propto M_{\text{bulge}}$ ) relation. *Panel d*: same data as in panel c, but for maximally radiative BH merging (from [236]).

the classical scenario the Magorrian relation is (obviously) nicely reproduced, in the case of substantial emission of gravitational waves the relation between BH mass and bulge mass is *not* reproduced. All the results presented hold under the strong assumption that the BHs of the merging galaxies are retained by the end-products, but there are at least two basic mechanisms that could be effective in expelling the central BHs. The first is related to the general instability of three body systems: if a third galaxy is accreted by the end-product of a previous merging before the binary BH at its center merged in a single BH, then the escape of the smallest BH is likely. It is clear that if this process happens more than a few times, then the Magorrian relation will not be preserved at the end (for a detailed discussion of this problem see, e.g. [243], [248]-[250]). A second physical mechanism, which could be even more effective in expelling the resulting BH from the center of a galaxy merger, is related to the possibility of anisotropic emission of gravitational waves. This process, commonly known as the “kick velocity”, is directly

related to the fraction of BH mass emitted anisotropically during BH coalescence. In fact, gravitational waves in fact travel at the speed of light, and so even the anisotropic emission of *a few thousandths* of the mass of the BH binary will produce a recoil (due to linear momentum conservation) of the resulting BH with a characteristic velocity of the order of, or higher than, the escape velocity typical of massive galaxies. In conclusion, it is not obvious that in each galaxy merging the resulting BH will remain at the center of the galaxy.

I illustrate now the results of a Monte-Carlo investigation of merging effects, in which also gas dissipation is heuristically taken into account [251]. This is done with the aid of a simple yet robust approach designed to model the influence of merging on galaxy structure and the consequent effects on the scaling laws followed by Es. In fact, simple physical arguments show that gas dissipation should be able to mitigate the problems posed by dry merging to the explanation of the observed scaling laws (e.g. [31], [252]-[255]). Unfortunately, numerical simulations with gas dissipation are considerably more complex than pure N-body simulations (e.g. [253, 254], [256]-[262]), so that simple arguments as those following can be of help.

For simplicity, each elliptical is modeled as a non rotating, isotropic and spherically symmetric one-component virialized system (i.e., dark matter is distributed proportionally to the visible matter), characterized by stellar mass  $M_*$ , gas mass  $M_{\text{gas}} = \alpha M_*$ , and SMBH mass  $M_{\text{BH}} = \mu M_*$ ; from the observations ([3]) we set  $\mu \simeq 10^{-3}$  in spheroids of the nearby universe ( $z = 0$ ). The total energy of a galaxy is then given by

$$(35) \quad E = K_* + U_g + W,$$

where

$$(36) \quad K_* = \frac{3}{2} \int \rho_* \sigma_*^2 d^3 \mathbf{x}, \quad U_g = \frac{3k_B}{2\langle m \rangle} \int \rho_g T d^3 \mathbf{x}, \quad W = \frac{1}{2} \int (\rho_* + \rho_g)(\Phi_* + \Phi_g) d^3 \mathbf{x}$$

are the stellar kinetic energy, the gas internal energy, and the total gravitational energy of stars and gas. Here  $\sigma_*$ ,  $k_B$ ,  $T$ , and  $\langle m \rangle$  are the stellar 1-dimensional velocity dispersion, the Boltzmann constant, the gas temperature, and the gas mean molecular mass, respectively.

Under the simplifying assumption that the gas is spatially distributed as the stars (i.e.,  $\rho_g = \alpha \rho_*$ ) and that the gas is in equilibrium in the total gravitational field, we have  $\Phi_g = \alpha \Phi_*$ ; from the Jeans and the hydrostatic equations we find  $T = \langle m \rangle \sigma_*^2 / k_B$ , so that

$$(37) \quad W = (1 + \alpha)^2 W_*, \quad U_g = \alpha K_*, \quad E = -(1 + \alpha) K_* = \frac{(1 + \alpha)^2}{2} W_*,$$

where  $W_*$  is the self-gravitational energy of the stellar component. Finally, the characteristic one-dimensional stellar velocity dispersion  $\sigma_V$  and the characteristic radius  $r_V$ , defined as

$$(38) \quad K_* \equiv \frac{3}{2} M_* \sigma_V^2, \quad |W_*| \equiv \frac{G M_*^2}{r_V},$$

are related (in the case of isotropic  $R^{1/m}$  models with  $2 \lesssim m \lesssim 12$ ) to the observables  $R_e$

and  $\sigma_\circ$  (with spectroscopic aperture  $R_e/8$ ):

$$(39) \quad \frac{r_V}{R_e} \simeq \frac{250.26 + 7.15m}{77.73 + m^2}, \quad \frac{\sigma_\circ}{\sigma_V} \simeq \frac{24.31 + 1.91m + m^2}{44.23 + 0.025m + 0.99m^2}.$$

For simplicity, in the following we consider only the case of the parabolic merging of two galaxies, so that the total energy of the system is the sum of the internal potential and kinetic energies of the two progenitor galaxies; we also assume that no mass is lost in the process. During merging, as a consequence of gas dissipation, a fraction  $\eta$  of the available gas mass is converted into stars. The stellar mass balance equation is

$$(40) \quad M_* = M_{*1} + M_{*2} + \eta(M_{g1} + M_{g2}).$$

Furthermore, a new SMBH forms by the coalescence of the two central BHs and a fraction  $f\eta$  of the available gas is accreted on it, leading to a BH of final mass

$$(41) \quad M_{\text{BH}} = (M_{\text{BH}1}^p + M_{\text{BH}2}^p)^{1/p} + f\eta(M_{g1} + M_{g2}).$$

As in [31, 236],  $p = 1$  corresponds to the classical merging case (no gravitational radiation), while  $p = 2$  to the maximally radiative case for non-rotating BHs. In equation (41) it is implicitly assumed that first  $M_{\text{BH},1}$  and  $M_{\text{BH},2}$  merge, and then the gas is accreted on the new BH; the other extreme case would be that of gas accretion followed by merging (e.g. [263]). As a consequence of star formation and BH accretion, the gas mass balance equation is

$$(42) \quad M_{\text{gas}} = (1 - \eta - f\eta)(M_{g1} + M_{g2}),$$

which implies that  $0 \leq \eta \leq 1/(1 + f)$ . Thus, the gas-to-star mass ratio after the merger and the new Magorrian coefficient are given by

$$(43) \quad \alpha \equiv \frac{M_{\text{gas}}}{M_*} = \frac{(1 - \eta - f\eta)(\alpha_1 M_{*1} + \alpha_2 M_{*2})}{(1 + \eta\alpha_1)M_{*1} + (1 + \eta\alpha_2)M_{*2}}$$

and

$$(44) \quad \mu \equiv \frac{M_{\text{BH}}}{M_*} = \frac{(\mu_1^p M_{*1}^p + \mu_2^p M_{*2}^p)^{1/p} + f\eta(\alpha_1 M_{*1} + \alpha_2 M_{*2})}{(1 + \eta\alpha_1)M_{*1} + (1 + \eta\alpha_2)M_{*2}}$$

respectively. In order to describe the effects on  $r_V$  and  $\sigma_V$  of the radiative energy losses associated with gas dissipation, a fraction  $(1 + f)\eta$  of the gas internal energy  $U_g$  of each progenitor is subtracted from the total energy budget of the merger-product, consistent with the previous assumptions. Thus, the final total energy of the remnant is

$$(45) \quad E = E_1 + E_2 - \eta(1 + f)(\alpha_1 K_{*1} + \alpha_2 K_{*2}),$$

and from the identities in eq. (37) one easily obtain

$$(46) \quad \sigma_V^2 = \frac{M_{*1} + M_{g1}}{M_* + M_{\text{gas}}} A_1 \sigma_{V1}^2 + \frac{M_{*2} + M_{g2}}{M_* + M_{\text{gas}}} A_2 \sigma_{V2}^2,$$



and

$$(47) \quad \frac{1}{r_V} = \left( \frac{M_{*1} + M_{g1}}{M_* + M_{\text{gas}}} \right)^2 \frac{A_1}{r_{V1}} + \left( \frac{M_{*2} + M_{g2}}{M_* + M_{\text{gas}}} \right)^2 \frac{A_2}{r_{V2}},$$

where

$$(48) \quad A_1 = 1 + \frac{(1+f)\eta\alpha_1}{1+\alpha_1},$$

and a similar expression holds for  $A_2$ . In a dry ( $\eta = 0$ ) merging  $A_1 = A_2 = 1$ , so that

$$(49) \quad \min(\sigma_{V1}^2, \sigma_{V2}^2) \leq \sigma_V^2 = \frac{(1+\alpha_1)M_{*1}\sigma_{V1}^2 + (1+\alpha_2)M_{*2}\sigma_{V2}^2}{(1+\alpha_1)M_{*1} + (1+\alpha_2)M_{*2}} \leq \max(\sigma_{V1}^2, \sigma_{V2}^2),$$

i.e., the virial velocity dispersion of the merger-product cannot be larger than the maximum velocity dispersion of the progenitors. Instead,  $A > 1$  in the case of “wet” ( $\eta > 0$ ) merging, and the resulting  $\sigma_V$  is larger than in the dry case, possibly larger than the maximum velocity dispersion of the progenitors. A similar argument shows that in the presence of gas dissipation the new  $r_V$  increases less than in the dry case. Note that the above conclusions are obtained under the hypothesis of parabolic merging. If mergers involve galaxies on bound orbits, the additional negative energy term in equation (45) would lead to an increase of  $\sigma_V$  also in equal-mass dry mergers. The analysis of this case, and the question of how much fine-tuned the properties of the progenitor galaxies should be with their binding orbital energy in order to reproduce the SLs, are not discussed further in this review (for additional discussion, see, e.g., [241, 242]).

The previous formulae are now applied to study repeated parabolic merging on a *population* of Es. The merging spheroids are extracted by means of Monte-Carlo simulations from different samples of seed galaxies, the parent galaxies removed from the population and replaced by their end-product, whose properties are determined by using the relations given above. The initial population of seed galaxies is obtained by random extraction of the stellar mass  $M_*$  from the SDSS luminosity function in the Infrared ([265]), under the assumption of constant stellar mass-to-light ratio  $\Upsilon_*$ . For each galaxy mass, the corresponding central velocity dispersion  $\sigma_o$  is fixed according to the FJ, and the effective radius  $R_e$  is assigned from the FP ([74, 79]), while the observational properties of the resulting systems are determined from eq. (39).

In the *first scheme*, the seed galaxies span only a narrow mass range (a factor of  $\sim 5$ ): in this case we then study whether massive ellipticals and the observed scaling relations can be *produced* by repeated mergers of low-mass spheroidal systems. In the *second scheme* the seed Es follow the observed scaling relations over their whole observed mass range ( $\sim 10^3$ ), and so one explores whether repeated merging events *preserve or destroy* these relations. Figure 19 shows the results in the case of dry parabolic merging. The mass interval spanned by the progenitors is indicated by the two vertical ticks, the end-product positions are represented by dots, and the observed SLs are represented by dotted lines. *It results that massive Es cannot be formed by parabolic dry mergers of low-mass spheroids only, because they would be characterized by exceedingly large values of  $R_e$  and almost mass independent values of  $\sigma_o$ , in agreement with the results of [31, 236].* Mergers with gas dissipation (not shown here) produce more realistic objects and the observed SLs are satisfied (even though with large scatter) by the new galaxies, up to a mass increase of a factor of  $10^2$  with respect to the smallest seed galaxies. However, new

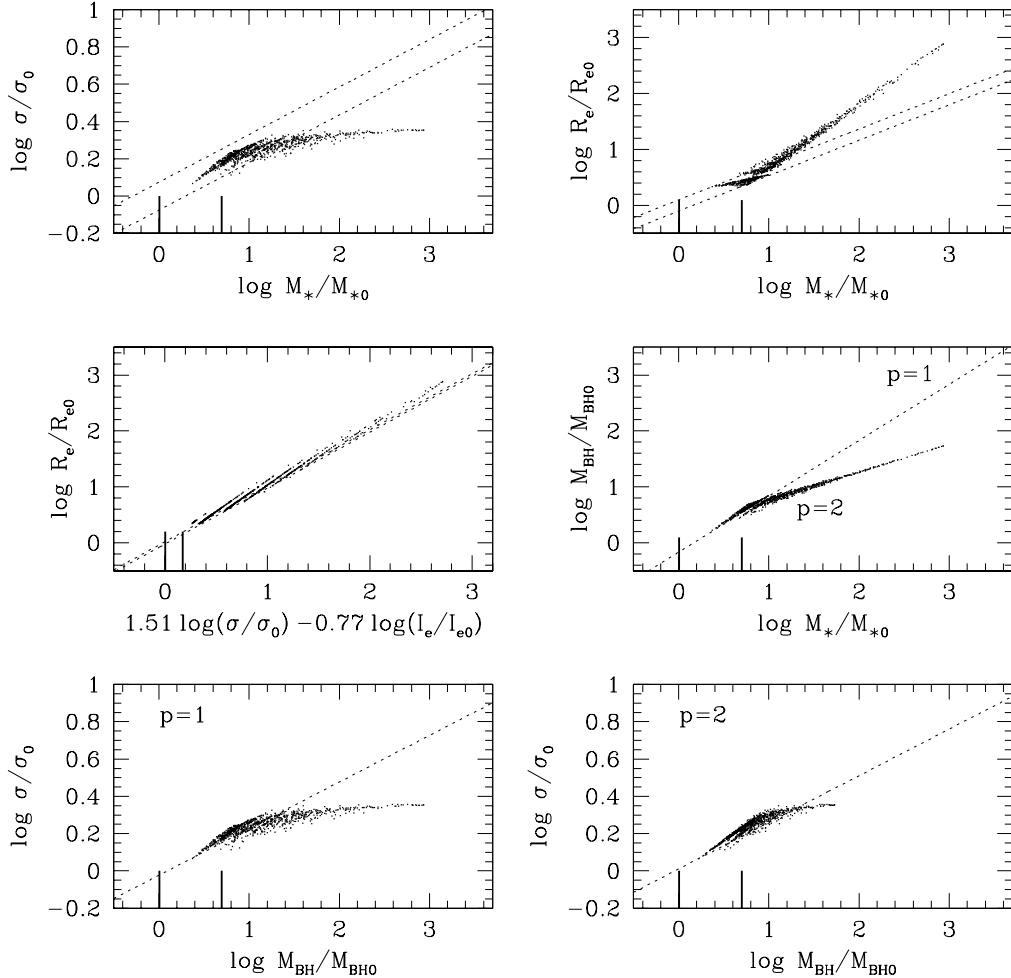


Fig. 19. – Synthetic scaling relations produced by parabolic dry mergers. Seed galaxies span a limited mass range (indicated by the heavy vertical ticks) and random re-merging events are repeated until a factor  $10^3$  increase in mass is reached (see text for details). Dotted lines represent the observed scaling relations. All quantities are normalized to the properties of the lowest mass seed galaxy (from [251]).

galaxies characterized by a mass increase factor  $\gtrsim 10^2$  are mainly formed by mergers of gas poor galaxies that already experienced several mergers, and so they strongly deviate from the observed SLs.

This first exploration therefore reveals that parabolic merging of low mass galaxies only is unable to produce Es obeying the observed scaling laws, even when allowing for structural weak homology in a way consistent with the edge-on FP. However, gas dissipation plays an important role in gas rich merging and, remarkably, the resulting

Es appear to be distributed as the observed SLs, as far as sufficient amounts of gas are available. Quite obviously, the problem of the compatibility of the properties of such merger-products with other key observations, such as the color-magnitude and the metallicity-velocity dispersion relations, and the increasing age of the spheroids with their mass (e.g. [58, 266]) remain opens. In the second scheme, the masses of the seed galaxies span the full range covered by ordinary Es ( $\sim 10^3$ ) and their characteristic size and velocity dispersion follow the observed SLs: in practice, we study the effect of merging (dry and wet) on already established SLs. The main result is that now, at variance with the results of the first scenario, the SLs remain almost unaffected by the merging, both in their slope and scatter. In particular, the  $M_{\text{BH}}-\sigma_{\circ}$  relation (with  $p = 2$ ) is preserved, even though we are in a dry merging regime. The only detectable deviations from the observed SLs, for the same reasons discussed above, are found for Es with masses larger than the most massive galaxies in the original sample (marked by the two vertical ticks in Fig. 20).

Why do mergers preserve so well the scaling relations? The reason is simple: by construction in a population of galaxies spanning the whole mass range observed today and distributed according to the observed SLs, mergers in general involve a “regular” Es, with values of  $R_e$  and  $\sigma_{\circ}$  as observed. These mergings act as a “thermostat”, maintaining values of  $R_e$  in the observed range and increasing the virial velocity dispersion, thus contributing to preserve the SLs at increasing mass. Only when the produced galaxies are so massive that no regular galaxies of comparable mass are available, the new merger products deviate more and more from the SLs. This behavior becomes extreme in the case of repeated mergers in a galaxy population spanning a restricted mass range. Therefore, while Es cannot be produced by the merging of low mass spheroids only (as already pointed out by e.g. [31, 236, 240]) the observed SLs, once established by some other mechanism, are robust against merging.

*4.2. Cooling flows and SMBH feedback.* – Quite often, when discussing the origin of the SLs between SMBHs and their host galaxies, the attention focuses on the galaxy formation mechanism, while almost no attention is payed to the subsequent several Gyrs of evolution (with the exception of possible merging events). This is probably due, quite surprisingly, to the common misconception that Es, once formed, are just “dead and boring red objects”. However, as is well known for the past 30 years by stellar evolutionists and by the “cooling flow” community, this is just wrong (see Sect. 2). In fact, the mass return rate from the passively evolving stellar population sums up to a sizable ( $\gtrsim 10 - 20\%$ ) fraction of the galaxy stellar mass and is the main ingredient of the cooling flow model (and its variants). Clearly, some very efficient feedback mechanism suppressing the cooling flow must be present in Es otherwise, in addition to the problems listed in Sect. 2, the SMBHs would have masses a factor  $\sim 100$  greater than those observed and a luminous QSO should be present at the center of all Es.

A possible (partial) solution to the cooling flow (and indirectly to the SMBHs growth) problems was proposed in [151, 267, 268] by considering the effect of SNIa heating of the galactic gas, and exploring the time evolution of gas flows by using hydrodynamical numerical simulations. It was found that while SNIa input sufficed for low and medium-luminosity Es to produce fast galactic winds, the inner parts of more massive spheroids would nevertheless host inflow solutions similar to cooling flows. This is because, while the number of SNIa per unit optical luminosity is expected to be roughly constant in ellipticals, the gas binding energy per unit mass increases with galaxy luminosity, as dictated by the FJ relation. However, as already recognized by [151], the mass budget

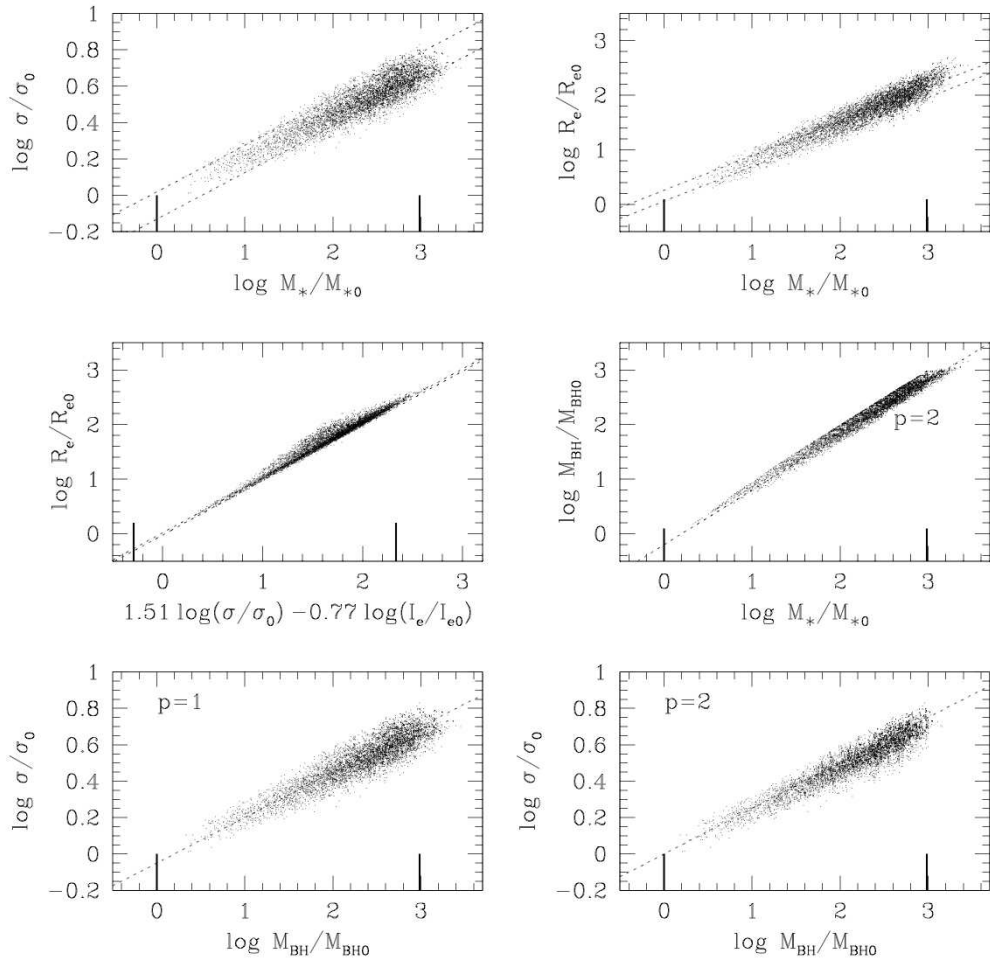


Fig. 20. – Synthetic scaling relations for the merger-products of up to 6 dry major mergers of galaxies extracted from a population that follows the observed scaling laws. Lines are as in Fig. 19 and all quantities are normalized to the properties of the lowest-mass seed galaxy (from [251]).

problem would still affect medium-large galaxies, putative hosts of luminous cooling flows. Thus, a concentrated feedback source is a very promising solution for a variety of problems, and the central SMBH is the natural candidate, by its mass and by its location, through a combination of mechanical and radiative feedback mechanisms. Some calculations have allowed for a physically motivated AGN feedback (e.g. [269]-[275]), and the computed solutions are characterized by relaxation oscillations. Energy output (radiative or mechanical) from the central SMBH pushes matter out, the accretion rate drops and the expanding matter drives shocks into the galactic gas. Then the resulting hot bubble ultimately cools radiatively and the resulting infall leads to renewed accretion. The cycle repeats. Among the computed models that studied the interaction between AGN feedback and galactic cooling flows, those of [270, 271, 275] focused on the effects of *radiative heating* on galactic gas flows. In fact, if one allows the radiation emitted from the accreting SMBH to interact with and heat the galactic gas, one solves the cooling flow problem in Es, and the feedback produces systems that are variable but typically look like normal ellipticals containing hot gas. They sometimes look like incipient cooling flows and rarely, but importantly, appear like quasars. Interestingly, observations seem to support this scenario (e.g. [276]).

In [270, 271], however, a major uncertainty remained about the typical QSO spectrum to adopt, in particular the high energy component of that spectrum, which is most important for heating the ambient gas. Thus, a simple broken power law was adopted for the spectrum with a range of possible values of the Compton temperature – from  $10^{7.2}$  K to  $10^{9.5}$  K – with most of the emphasis of the paper being on the higher temperatures. Subsequent work by Sazonov, Ostriker & Sunyaev ([277], see also [279]), which assessed the full range of observational data of AGNs and computed their Spectral Energy Distribution, concluded that the typical equilibrium radiation temperature was narrowly bounded to values near  $10^{7.3}$  K, i.e., of the order of 2keV. This value is still above the virial temperature of all galaxies and, most importantly, well above the central temperature of the cooling flow gas. As noted in [22], there is a rather large compensating effect also not included in [271]: gas heated by radiation with a characteristic temperature near  $10^7$  K is heated far more effectively by absorption in the atomic lines of the abundant metal species than by the Compton process. In particular, [22] provide a fitting formula for the Compton plus photoionization and line heating/cooling that was implemented into the numerical code developed by Ciotti & Ostriker.

Here I briefly describe the main results of [275]. Consistent with HST observations, which have shown that the central surface brightness profile is described by a power-law (see Sect. 2.1.3) as far in as it can be observed (i.e. to  $\sim 10$  pc for Virgo ellipticals), the stellar component is described by a Hernquist model. In addition, optical (e.g. [214], [280]-[282]), and X-ray (e.g. [283, 284]) based studies typically find that luminous matter dominates the mass distribution inside the effective radius  $R_e$ , while dark matter begins to be dynamically important at  $2 - 3R_e$ , with common values of the total dark-to-luminous mass ratio  $\mathcal{R} \equiv M_h/M_*$  in the range  $1 \lesssim \mathcal{R} \lesssim 6$ . Finally, theoretical (e.g. [206, 187, 209, 285]) and observational (e.g. [286]) arguments support the idea that similarly to the stellar profiles, also the radial density distribution of the dark halos is described by a cuspy profile. Following these empirical indications, in the numerical simulations of [275] the stellar and dark matter distributions are taken to be of the form of eq. (28), with  $M_h = \mathcal{R}M_*$  and  $r_h = \beta r_*$  the halo total mass and scale-length; dynamical and phase-space properties of the resulting two-component Hernquist models are given in [191]. The physical scales of the model are then fixed so that the model satisfies the FJ and the edge-on FP. Once the density profile is fixed, the velocity dispersion profile is

computed by solving the Jeans equations, as this quantity is an important ingredient in the energy budget of the gas flows, namely the thermalization energy of the stellar mass losses. The stellar mass losses are computed following the detailed prescriptions of stellar evolution, while the SNIa rate (the time dependence of which is unfortunately still quite uncertain) is normalized to recent empirical estimates ([287, 288]). Each SNIa event releases  $E_{\text{SN}} = 10^{51}$  erg of energy and  $1.4M_{\odot}$  of material in the Interstellar Medium. The simulations allow for star formation, which cannot be avoided when cool gas accumulates in the central regions of Es. In the new population, described by a Salpeter IMF, the associated total number of Type II Supernovae and the stellar mass return are also computed, together with the radial distribution of the optical and UV luminosity per unit volume of the new stars. The accretion disk around the SMBHs (fed by hydrodynamical processes) is incorporated as a set of ordinary differential equations describing the instantaneous mass of gas and stars (low and high mass, and remnants) in the disk, as well as the disk optical and UV luminosity. Finally the mass accretion on the central SMBH in terms of the so-called  $\alpha$ -viscosity prescription is obtained, leading to the bolometric accretion luminosity

$$(50) \quad L_{\text{BH}}(t) = \epsilon \dot{M}_{\text{BH}}(t) c^2.$$

For the radiative efficiency the standard value  $\epsilon = 0.1$  is assumed (as suggested by observations, e.g. [36, 37, 289]), but a generalization to include an ADAF-like efficiency ([271, 290]) is also explored. The radiative heating and cooling produced by the accretion luminosity are computed from the formulae provided in [22], which describe the net heating/cooling rate per unit volume  $\dot{E}$  of a cosmic plasma in photoionization equilibrium with a radiation field characterized by the average quasar Spectral Energy Distribution given in [277], for which the associated spectral (Compton) temperature is  $T_{\text{X}} \simeq 2$  keV. In particular, Compton heating and cooling, bremsstrahlung losses, line and recombination continuum heating and cooling are taken into account. Radiation pressure on the Interstellar Medium (via electron scattering, dust opacity, photoionization opacity) produced by accretion luminosity and by stellar light (consequence of star formation) is obtained numerically by solving the two lowest spherically symmetric moment equations of radiative transfer in the Eddington approximation (e.g., [291]).

The evolution of the galactic gas flows is obtained by integrating the time-dependent Eulerian equations of hydrodynamics,

$$(51) \quad \frac{\partial \rho}{\partial t} + \nabla \cdot (\rho \mathbf{v}) = \alpha \rho_* + \dot{\rho}_{\text{II}} - \dot{\rho}_*^+,$$

$$(52) \quad \frac{\partial \mathbf{m}}{\partial t} + \nabla \cdot (\mathbf{m} \mathbf{v}) = -(\gamma - 1) \nabla E - \nabla p_{\text{rad}} + \rho \mathbf{g} - \dot{\mathbf{m}}_*^+,$$

$$(53) \quad \frac{\partial E}{\partial t} + \nabla \cdot (E \mathbf{v}) = -(\gamma - 1) E \nabla \cdot \mathbf{v} + H - C + \frac{(\alpha \rho_* + \dot{\rho}_{\text{II}})(v^2 + 3\sigma_*^2)}{2} + \dot{E}_{\text{I}} + \dot{E}_{\text{II}} - \dot{E}_*^+.$$

where  $\rho$ ,  $\mathbf{m}$ , and  $E$  are the gas mass, momentum and internal energy per unit volume, respectively, and  $v$  is the gas velocity (for a complete description of the source and sink

terms, for a discussion of the adopted assumptions, and for an outline of the numerical integration scheme, see [275, 292]). The initial conditions are represented by a very low density gas at the local virial temperature. The establishment of a high-temperature gas phase at early cosmological times is believed to be due to a “phase-transition” when, as a consequence of star formation, the gas-to-stars mass ratio was of the order of 10% and the combined effect of SNIa explosions and AGN feedback became effective in heating the gas and driving galactic winds. Several theoretical arguments and much empirical evidence, such as galaxy evolutionary models and the metal content of the Intrachuster Medium, support this scenario (e.g. [24, 293]).

What are the main phases of the model evolution? As an illustration, Figs. (21)-(25) refer to a model with an initial stellar mass  $M_* = 4.6 \times 10^{11} M_\odot$ , effective radius  $R_e = 6.9$  kpc and  $\sigma_o = 260 \text{ km s}^{-1}$  (chosen to lie on the FP), total dark-to-visible mass ratio  $\mathcal{R} = 5$  and dark-to-visible scale-length ratio  $\beta = 5.22$  (corresponding to an identical amount of stellar and dark matter within the half-light radius). The initial SMBH mass follows the present day Magorrian relation, i.e.,  $M_{\text{BH}} \simeq 10^{-3} M_*$ . After a first evolutionary phase in which a galactic wind is sustained by the combined heating of SNIa and thermalization of stellar velocity dispersion, the central “cooling catastrophe” begins. In the absence of the central SMBH a “mini-inflow” would be then established, with the flow stagnation radius (i.e., the radius at which the flow velocity is zero) of the order of a few hundred pc to a few kpc. These decoupled flows are a specific feature of cuspy galaxy models with moderate SNIa heating ([268]). However, after the central cooling catastrophe, the feedback caused by photoionization and Compton heating strongly affects the subsequent evolution, as can be seen in Fig. 21. The bolometric luminosity (top panel) ranges between roughly 0.001 to 0.1 of the Eddington limit at peaks in the SMBH output but, since obscuration is often significant, the optical accretion luminosity as seen from infinity can be much lower (bottom panel). The major AGN outbursts are separated by increasing intervals of time (set by the cooling time) and present a characteristic temporal substructure, whose origin is due to the cooperative effect of direct and reflected shock waves. At  $t \simeq 8$  Gyrs the SNIa heating, also sustained by a last strong AGN burst, becomes dominant, a global galactic wind takes place, and the nuclear accretion switches to the optically thin regime.

Remarkably, the coronal X-ray luminosity  $L_X$ , due to the hot galactic atmosphere, falls in the range commonly observed in massive Es, with mean values lower than the expected luminosity for a standard cooling flow model. It is also found that a large fraction of the starburst luminosity output occurs during phases when shrouding by dust is significant. An important quantity associated with the time evolution of the various luminosities is their *duty cycle* (for the operational definition see [271, 275]), whose temporal evolution is showed in Fig. 22: of course, the duty-cycles of starburst optical and UV luminosities are larger and less fluctuating than those of the AGN, and overall they are in agreement with the observations (e.g. [294]). Of particular interest for the present discussion is the evolution of the mass budget of the model. In Fig. 23 the time evolution of some of the relevant mass budgets of the model, both as time-integrated properties and instantaneous rates, is shown. At the end of the simulation the total Interstellar Medium mass in the galaxy is  $\sim 5 \times 10^8 M_\odot$ , while the SMBH mass reaches a final mass of  $\sim 7 \times 10^8 M_\odot$ . a model with a smaller initial SMBH mass would accrete less, thus maintaining the Magorrian relation even better. The SMBH mass accretion rate strongly oscillates as a consequence of radiative feedback, with peaks of the order of 10 or (more)  $M_\odot/\text{yr}$ , while during the final, hot-accretion phase the almost stationary accretion rate is  $\lesssim 10^{-4} M_\odot/\text{yr}$ : this value is close to the estimates obtained for the nuclei of nearby galaxies ([165]). Note that in the last 6 Gyrs the SMBH

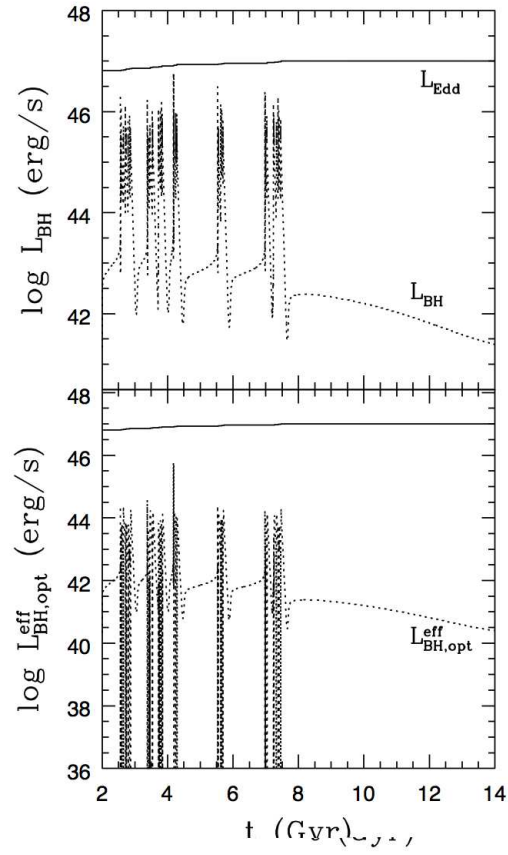


Fig. 21. – Dotted lines are the bolometric accretion luminosity (top panel) and the optical SMBH luminosity corrected for absorption (bottom panel). The almost horizontal solid line is the Eddington luminosity  $L_{\text{Edd}}$  (from [275]).



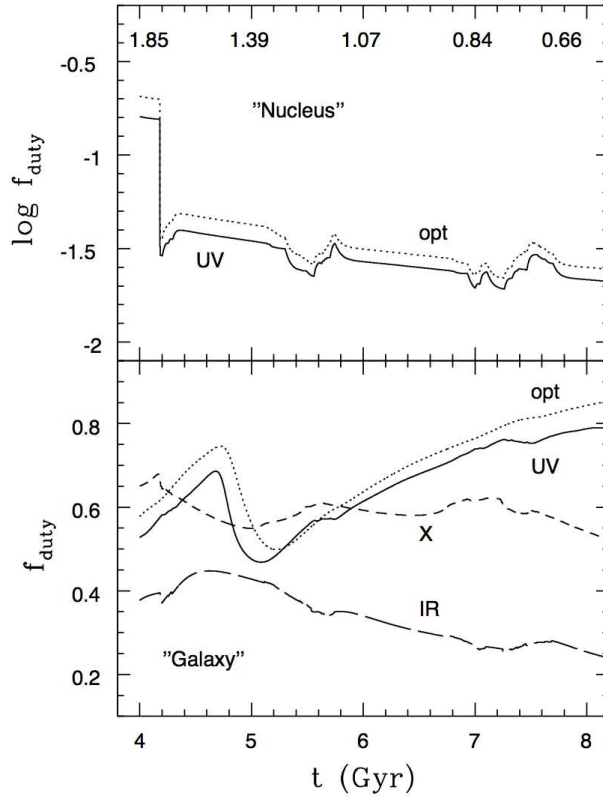


Fig. 22. – Time evolution of duty cycles. *Top panel:* duty-cycle of  $L_{\text{BH,UV}}^{\text{eff}}$  (solid) and  $L_{\text{BH,opt}}^{\text{eff}}$  (dotted); the top axis shows the corresponding redshift. We see that these systems would be observed from afar in the (rest-frame) optical or UV as quasars several percent of the time. *Bottom panel:* duty-cycle of the starburst  $L_{\text{UV}}^{\text{eff}}$  (solid),  $L_{\text{opt}}^{\text{eff}}$  (dotted), of the Interstellar Medium X-ray luminosity (computed in a volume excluding the inner 100 pc), and of the recycled IR luminosity  $L_{\text{IR}}$  (from [275]).

virtually stops its growth, while the Interstellar Medium mass first increases, due to the high mass return rate of the evolving stellar population, and then decreases, due to the global galactic wind induced by SNIa. During the entire model evolution, more than  $10^{10.5} M_{\odot}$  of recycled gas are added to the Interstellar Medium from stellar mass losses. Approximately  $2.1 \times 10^{10} M_{\odot}$  have been expelled as a galactic wind, while  $\sim 1.4 \times 10^{10} M_{\odot}$  are transformed into new stars, so that only 0.7% of the recycled gas is accreted onto the central SMBH. The central paradox of the mass budget is thus resolved. An identical model without SMBH feedback, but with the same star formation treatment of the model described above, would produce a SMBH of final mass  $\gtrsim 10^{10} M_{\odot}$ , while the total mass in new stars would be reduced to  $\sim 3 \times 10^9 M_{\odot}$ . The star formation rate during the periods of feedback dominated accretion oscillates from 0.1 up to several hundreds (with peaks near  $10^3$ )  $M_{\odot} \text{ yr}^{-1}$ , while it drops monotonically from  $10^{-1}$  to  $\lesssim 10^{-3} M_{\odot} \text{ yr}^{-1}$  in the last 6 Gyrs of quiescent accretion. These violent star formation episodes (with SMBH accretion to star formation mass ratios  $\sim 10^{-2}$  or less) are induced by accretion feedback and are spatially limited to the central 10–100 pc; thus, the bulk of gas flowing to the center is consumed in the starburst. These findings are nicely supported by recent observations (e.g [295, 296]). Note that the “age” effect of the new stars on the global stellar population of the galaxy is small, as the new mass is only 3% of the original stellar mass and it is virtually accumulated during the first Gyrs (see Fig. 23).

In Fig. 24 the final spatial density profile of the system is shown, together with its projection and the best-fit obtained with the Sersic law. As expected, the profiles show an increase of the best-fit Sersic parameter  $m$ , due to the mass accumulation in the central regions. Remarkably, the final value of  $m$  is within the range of values commonly observed in ellipticals: however, in the final model we note the presence of a central ( $\sim 30$  pc) nucleus originated by star formation which stays above the best fit profile, similar to the light spikes characterizing “nucleated” galaxies.

Figure 25 shows the temperature and density in the central regions of the model: note how the SMBH bursts heat the central gas, causing the density to drop, and launching gas at positive velocities of the order of thousands  $\text{km s}^{-1}$ . The Compton temperature  $T_X$  is the horizontal dashed line; during the bursts, the local gas is heated above this limit. As was already found in [271], the galaxy cooling catastrophe starts with the formation of a *cold shell* placed around the galaxy core radius: however, in the present models (see also [268]), the cooling catastrophe happens at significantly earlier times, because of the higher central stellar density and of the different time dependence and amount of SNIa explosions. This cycle of shell formation, central burst, and expanding phase, repeats during all the bursting evolution, along the lines described in detail in [271]. Finally, when the SNIa heating per unit gas mass becomes dominant over the decline of fresh mass input from evolving stars, the galaxy hosts a wind, and the accretion becomes stationary without oscillations; the central SMBH radiates at  $\sim 10^{-5} L_{\text{Edd}}$  (e.g. [297]).

**4.3. Summary.** – In this Section I briefly addressed an astrophysical question possibly as important as the origin of the galaxy and SMBH Scaling Laws, i.e. *the robustness of the relevant SLs against physical phenomena (in principle) able to destroy them*. In particular, I focused on galaxy merging and SMBH accretion at the center of cooling flows fed by stellar mass losses, which represents the major contributor to the Interstellar Medium in the life of Es after their formation. The main conclusions can be summarized as follows:

1) Parabolic dry merging in a population of low mass spheroids leads to massive Es that fail the FJ and Kormendy relations, being characterized by low velocity dispersion and very large effective radii. Parabolic wet merging in the same population of low mass

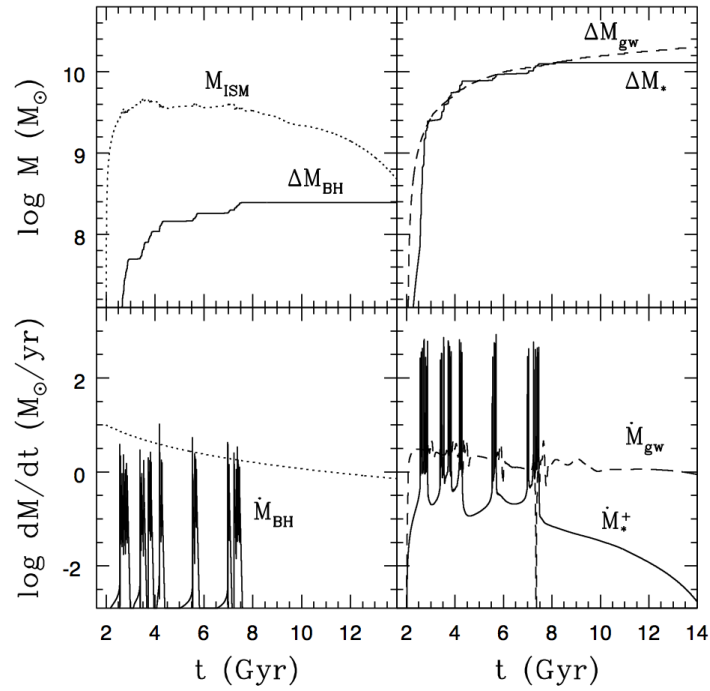


Fig. 23. – Mass budget evolution. *Top left panel:* total hot gas mass in the galaxy (within  $10R_e$ ,  $M_{\text{ISM}}$ , dotted line), and accreted mass on the central SMBH ( $\Delta M_{\text{BH}}$ ). *Top right:* mass lost as a galactic wind at  $10R_e$  ( $\Delta M_{\text{gw}}$ , dashed line), and total mass of new stars ( $\Delta M_*$ ). *Bottom left panel:* global mass return rate from the evolving stellar population and mass accretion rate on the central SMBH ( $\dot{M}_{\text{BH}}$ ). *Bottom right:* galactic wind mass loss rate at  $10R_e$  ( $\dot{M}_{\text{gw}}$ , dashed line) and instantaneous, volume integrated, star formation rate. Note that for  $t > 8$  Gyrs the mass lost as a galactic wind is almost coincident with the mass input from evolving stars (from [275]).

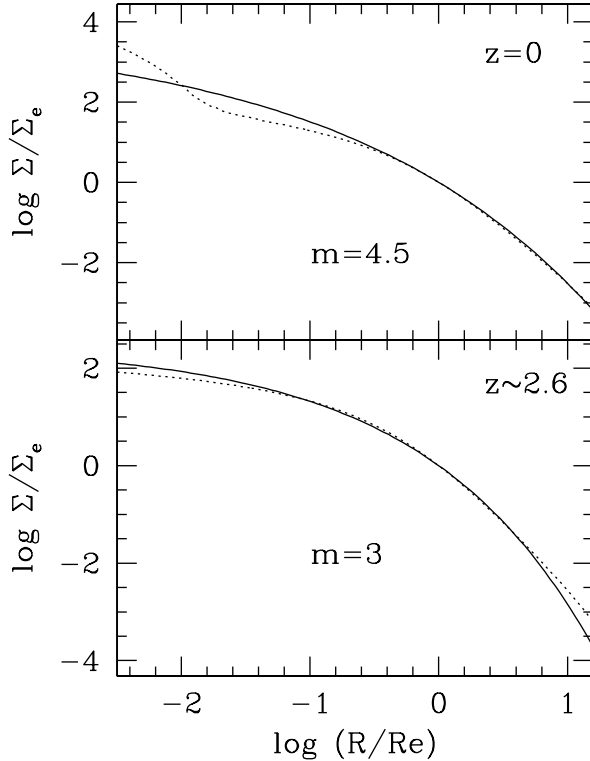


Fig. 24. – Dotted lines are the projected surface density of the model shortly after the beginning of the simulation ( $t = 2.5$  Gyr,  $z \sim 2.6$ , bottom panel) and at  $t = 13.5$  Gyr ( $z = 0$ , top panel), normalized to the surface density at the effective radius. Solid lines are the best-fit Sersic law. The effective radius contracts from  $\sim 9.2$  kpc to  $\sim 8.4$  kpc, while the surface density  $\Sigma_e$  increases from  $\sim 3 \times 10^{22}$  to  $\sim 3.6 \times 10^{22}$  protons per  $\text{cm}^{-2}$  (from [275]).

progenitors leads to galaxies in better agreement with the observed scaling relations, as long as enough gas for dissipation is available.

2) The edge-on structure of the FP is surprisingly preserved (except in the case of numerous minor mergers with galaxies on radial orbits). In fact, in the last case the deviations from the FJ and Kormendy relations do not compensate. Another manifestation of the problem encountered by head-on minor mergers is that the Sersic parameter  $m$  describing the mass profile of the end-products decreases for increasing mass, at variance with observations. In all cases, galaxies remain in the populated region of the face-on FP. Incidentally, points 1) and 2) show that *the FJ and Kormendy relations, despite their larger scatter, are stronger tests for merging than the edge-on FP, thus providing a powerful way to investigate the assembly history of massive elliptical galaxies.*

3) Parabolic dry or wet mergers in a population of galaxies following the observed

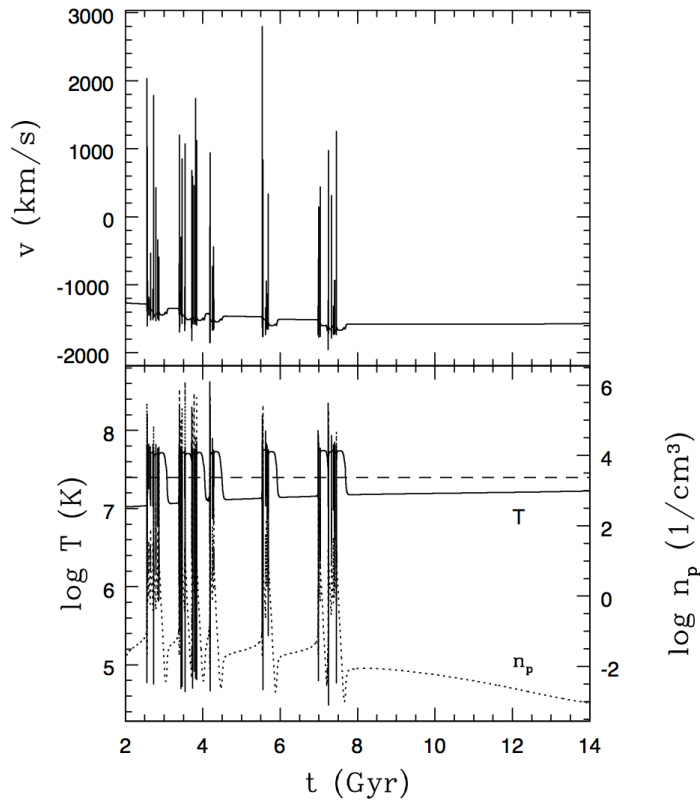


Fig. 25. – *Top panel:* gas velocity at 5 pc from the SMBH. Note how the SMBH growth affects the lower envelope of velocity values. *Bottom panel:* Gas number density (dotted line, scale on the right axis) and temperature at 5 pc from the SMBH (solid line, scale on the left axis). Low-temperature, high-density phases end when accretion luminosity  $L_{\text{BH}}$  increases sharply heating the ambient gas to a high-temperature, low-density state. The horizontal dashed line is the model Compton temperature  $T_{\text{X}} = 2.5 \times 10^7$  K (from [275]).

scaling laws over the full mass range populated today by stellar spheroids, preserve the Kormendy, FJ, and edge-on FP remarkably well. *The reason of this behavior is due to the presence, in the merger population, of galaxies with velocity dispersion increasing with galaxy mass.* Thus, massive Es cannot be formed by (parabolic) merging of low mass spheroidal galaxies, even in presence of substantial gas dissipation. However, the observed scaling laws of Es, once established by galaxy formation, are robust against merging.

4) Under the reasonable hypothesis that the derived values of  $\sigma_0$  are not strongly affected by the dynamical evolution of binary BHs, dissipationless merging, while in accordance with the Magorrian relation, fails to reproduce the  $M_{\text{BH}}-\sigma_0$  relation. Curiously, by allowing for substantial emission of gravitational waves during the BHs coalescence, the  $M_{\text{BH}}-\sigma_0$  relation is reproduced, but the Magorrian relation is not. In the case of gas dissipation, the resulting  $M_{\text{BH}}-\sigma_0$  relation is in better agreement with the observations, also in the case of significant mass loss (via gravitational waves) of the coalescing BHs. However, significant deviations from the observed scaling laws are expected for massive galaxies.

5) The recycled gas from dying stars is an important source of fuel for the central SMBH, *even in the absence of external phenomena such as galaxy merging*, which are often advocated as the way to induce QSO activity. Radiative feedback from a central SMBH has dramatic effects on its mass growth: much of the recycled gas falling towards the galaxy center during the accretion events is consumed in central starbursts with a small fraction (of the order of 1% or less) accreted onto the central SMBH. Thus, the central starburst regulates the amount of gas available to be accreted onto the central SMBH. If we did not allow for the (AGN feedback induced) central star formation, the SMBH would grow to be far more massive than seen in real galaxies.

## 5. – Toward a unified picture?

After discussing how the SLs can be maintained over cosmological times, we have now to address plausible scenarios aimed at explaining how these laws are established. In this Section I discuss three seemingly unrelated arguments, that will be connected in Sect. 6. In particular, in Sect. 5.1 I discuss the growth of SMBHs, in Sect. 5.2 I describe the results of numerical simulations of fast (dissipationless) collapse in pre-existing dark matter halos, and finally in Sect. 5.3 I consider the remarkable SLs imprinted in dark matter halos produced by cosmological simulations.

**5.1. SMBH and spheroid growth.** – It is now universally accepted that the SLs involving the central SMBHs and the global properties of the host spheroids are established at the epoch of galaxy formation. In other words, the Magorrian relation reveals that the bulk of SMBH fueling in AGNs must be associated with star formation in the spheroidal components of their host galaxies (e.g. [18, 29, 30, 37], [316]-[318]). This argument is rich in consequences, as it naturally links galaxy formation to the SMBH growth. A first quantification of this link is provided by the so-called *Soltan argument* ([289]), which in its more recent applications (e.g. [36, 37]) shows that the integrated luminosity emitted by QSOs over the life of the Universe nicely matches the present day total mass of SMBHs at the center of Es, for efficiencies of  $\sim 0.1$ . In particular, the approach in [37] is based on two working hypotheses, i.e. that 1) spheroid star formation and BH fueling are – at any time and in any system – proportional to one another with the proportionality constant independent of time and place, and that 2) the SMBH accretion luminosity always stays

near the Eddington limit when the QSO is in the luminous phase and the BH does not produce any radiation in the “off” state (e.g. because accretion is suppressed). Assumptions 1) and 2) are then coupled with three observational inputs, namely the present-day luminosity function of spheroids, where the number of spheroids per unit volume with rest-frame B-band luminosities in the interval  $(L_B, L_B + dL_B)$  is given by  $\Phi_S dL_B$ , with

$$(54) \quad \Phi_S(L_B) = \sum_{i=1}^4 \frac{\Phi_{S*i}}{L_{S*i}} \times \left( \frac{L_B}{L_{S*i}} \right)^{-\alpha_i} \exp\left(-\frac{L_B}{L_{S*i}}\right),$$

and the different indices correspond to the different galaxy types mentioned in Footnote 1. The second ingredient is the luminosity function of QSO

$$(55) \quad \Phi_Q(L_Q, z) = \frac{\Phi_{Q*}/L_{Q*}(z)}{[L_Q/L_{Q*}(z)]^{\beta_i} + [L_Q/L_{Q*}(z)]^{\beta_h}},$$

where the characteristic luminosity  $L_{Q*}$  in the rest-frame B band is

$$(56) \quad L_{Q*}(z) = L_{Q*}(0)(1+z)^{\alpha_Q-1} \frac{e^{\zeta z}(1+e^{\xi z_*})}{e^{\xi z} + e^{\xi z_*}}$$

(e.g. [33, 34]). Finally, the third ingredient is the Magorrian relation, obtained by combining the FJ with the  $M_{\text{BH}} - \sigma$  relation

$$(57) \quad \frac{M_{\text{BH}}}{M_\odot} \simeq 0.016 \frac{L_B}{L_\odot}.$$

(see also Sect. 2). Note that under assumption 2) it is expected that the redshift evolution of the QSO emissivity and of the star formation history in spheroids should be roughly parallel to each other: indeed, numerical simulations of feedback-modulated accretion flows (radiative, as in [271, 275], or mechanical, as in [269, 319, 320]) show that the accretion luminosity during short episodes of bursts stays near the Eddington value (see Fig. 22).

For illustrative purposes, let us first consider a population of  $N_g$  identical galaxies over the Hubble time  $t_H$ , each of which today (i.e. at  $t = t_H$ ) hosts a spheroid of mass  $M_S$ , and a SMBH of mass  $M_{\text{BH}}$ . Let us further assume that during the entire time elapsed from 0 to  $t_H$ , each SMBH had only two states: it was either “on” or “off”. We identify the “on” state as the active quasar phase, and we define the duty cycle  $f_Q$  as the fraction of the time each BH spends in the “on” state. At any given time, the number of active quasars is then  $N_Q = f_Q N_g$ . In the “on” state, the SMBH grows by accretion at the rate  $\dot{M}_{\text{BH}}$ , and shines at the (bolometric) luminosity  $L_Q$  with radiative efficiency  $\epsilon$ , defined as the fraction of the rest mass energy of the infalling gas converted to radiation. The remaining fraction  $(1 - \epsilon)$  of the rest mass then leads to the growth of the BH mass ([36]). Simple algebra shows that

$$(58) \quad \frac{\epsilon}{1 - \epsilon} = \frac{E_Q^{\text{T}}}{M_{\text{BH}}^{\text{T}} c^2} = \frac{f_Q t_H L_Q N_g}{M_{\text{BH}} N_g c^2} = \frac{t_H L_Q N_Q}{M_{\text{BH}} N_g c^2}.$$

Here  $c$  is the speed of light; the numerator represents the total light emitted by all SMBHs, and the denominator represents the total mass in SMBHs today. In the third

equality, we have used  $N_Q = f_Q N_g$ . Note that the last term involves only quantities that are, in principle, directly observable and that it is *independent* of the duty cycle. Equation (58) describes the entire galaxy population, but a similar equation applies to individual galaxies:  $L_Q f_Q t_H = \epsilon M_{\text{BH}} c^2$ . This last expression does not have a dependence on the duty cycle, which can therefore be written as

$$(59) \quad f_Q = \frac{N_Q}{N_g} = \frac{\epsilon M_{\text{BH}} c^2}{t_H L_Q}.$$

The above argument demonstrates that the radiative efficiency can be obtained independently of the duty cycle and that the duty cycle can be obtained in two different ways, based either on the *number* or on the *characteristic SMBH mass* of quasars. By using bona-fide observed values for the different quantities involved in the above equations, in [37] it is found that  $\epsilon = 0.071$ , in good agreement with the result of [36].

The duty cycle defined in eq. (59) can be generalized to a population of evolving galaxies under the assumption that the duty cycle does not vary with time but it is a function of luminosity. This is done by defining the average duty cycle of all quasars above luminosity  $L_Q(x, 0)$ ,

$$(60) \quad \langle f_{Q,N} \rangle_x \equiv \frac{\int_{M_{\text{BH}}(x)}^{\infty} dM \Phi_{\text{BH}}}{\int_{L_Q(x,0)}^{\infty} dL \Phi_Q},$$

where  $L_Q(x, 0)$  is such that QSOs at redshift  $z = 0$  brighter than  $L_Q(x, 0)$  emit a fraction  $x$  of the total quasar light  $L_Q^T = \int_0^{\infty} dL L \Phi_Q(L, 0)$ . Likewise, if  $M_{\text{BH}}(x)$  is such that all SMBHs more massive than  $M_{\text{BH}}(x)$  sum up to the same fraction  $x$  of the total SMBH mass at  $z = 0$ , then the last term in eq. (59) becomes

$$(61) \quad \langle f_{Q,M} \rangle_x \equiv \frac{\epsilon c^2 M_{\text{BH}}(x)}{\int_0^{\infty} L_Q(x, t) dt}.$$

It is found that  $\langle f_{Q,N} \rangle_{0.1} \simeq 0.008$  and  $\langle f_{Q,N} \rangle_{0.9} \simeq 0.05$ , and that the two methods agree well on the high mass end, while  $\langle f_{Q,M} \rangle$  is systematically lower by a factor of  $\sim$ two towards the low-mass end. These results for the duty cycle are in good agreement with the values reported in [36],[321]-[323], and with theoretical expectations (e.g [270, 271, 275]).

In a complementary approach to the previous phenomenological investigation, it is natural to attempt the modeling of the simultaneous growth of Es and their central SMBHs. While numerical simulations of galaxy formation are becoming richer and richer in the input physics, simple “toy models” are still helpful, because of their specific capability to incorporate in an intuitive way the core physics of the investigated process. As an example, here I describe the results obtained with the model explored in [22, 272] (see also [15, 17], [19]-[21],[30, 250, 321, 318]). The basic idea of [22] is that the UV and high energy radiation from a typical quasar can photoionize and heat a low density gas up to an equilibrium Compton temperature ( $T_c \approx 2 \times 10^7$  K) that exceeds the virial temperatures of giant ellipticals. Note that the radiative output is not the only, nor even necessarily the dominant mechanism whereby feedback from accretion onto central SMBHs can heat gas in Es. For example, [269, 319] have stressed that the mechanical



input from radio jets will also provide a significant source of energy, and much detailed work has been performed to follow up this suggestion.

An empirical indication that radiative feedback from the accreting SMBHs can indeed lead to final masses following the observed scaling with the host system velocity dispersion has been obtained by Sazonov et al. ([22, 277]). In fact, Sazonov et al. ([277]) computed for the observed average quasar Spectral Energy Distribution the equilibrium temperature  $T_{\text{eq}}$  of gas of cosmic chemical composition as a function of the ionization parameter  $\xi = L_{\text{BH}}/(nr^2)$ , showing that

$$(62) \quad T_{\text{eq}}(\xi) \approx \begin{cases} 10^4 \text{ K} & \text{for } \xi \ll 100; \\ 2 \times 10^2 \xi \text{ K}; & \\ 2 \times 10^7 \text{ K} & \text{for } \xi \gg 5 \times 10^4, \end{cases}$$

where  $n$  is the hydrogen number density and  $r$  is the distance from the SMBH. In practice,  $T_{\text{eq}}$  is the temperature at which heating through Compton scattering and photoionization balances Compton cooling and cooling due to continuum and line emission. Suppose now that the gravitational potential experienced by the gas is due to the central SMBH alone. Then the condition

$$(63) \quad \frac{5}{2}kT_{\text{eq}}(\xi) - \frac{GM_{\text{BH}}\mu m_{\text{p}}}{r} > 0$$

( $\mu$  is the mean molecular weight) roughly defines a situation where gas of density  $n$ , located at  $r$ , will be heated to  $T_{\text{eq}}$  by the central radiation and blown out of the SMBH potential. Thus, for given  $M_{\text{BH}}$ ,  $L_{\text{BH}}/L_{\text{Edd}}$  and  $r$ , gas with density below a certain critical value, cannot accrete onto the SMBH. In terms of  $L_{\text{BH}}$ , this means that Bondi accretion ([278]) of gas at temperature  $T$  can be disrupted if  $L_{\text{BH}}$  is sufficiently high that  $T_{\text{eq}}(R_{\text{B}}) \gtrsim T$ , or equivalently  $L_{\text{BH}} > L_{\text{crit}}$ , where

$$(64) \quad L_{\text{crit}}(T) = \xi(T)R_{\text{B}}^2(T)n(R_{\text{B}}),$$

$\xi(T)$  is the ionization parameter corresponding to  $T_{\text{eq}} = T$ , and finally

$$(65) \quad R_{\text{B}} = \frac{GM_{\text{BH}}\mu m_{\text{p}}}{2\gamma kT} = 16 \text{ pc} \frac{1}{\gamma} \frac{M_{\text{BH}}}{10^8 M_{\odot}} \left( \frac{T}{10^6 \text{ K}} \right)^{-1},$$

is the Bondi radius.

The previous argument suggests that, before the SMBH grows to a certain *critical mass*  $M_{\text{BH,crit}}$ , its radiation will be unable to heat efficiently the ambient gas, and accretion onto the SMBH will proceed at a high rate. Once the SMBH has grown to  $M_{\text{BH,crit}}$ , its radiation will heat and expel a substantial amount of gas from the central regions of the galaxy. Feeding of the SMBH will then become self-regulated on the cooling time scale of the low density gas. Subsequent quasar activity will be characterized by a very small duty cycle ( $\sim 0.001$ ), and the SMBH growth will be essentially terminated. On a more quantitative level, suppose that the galaxy density distribution is that of a singular isothermal sphere, with the gas density following the total density profile:

$$(66) \quad \rho_{\text{gas}}(r) = \frac{M_{\text{gas}}}{M_{*}} \frac{\sigma^2}{2\pi G r^2},$$

where  $M_{\text{gas}}$  and  $M_*$  are the gas mass and the stellar mass within some reference radius. Then, simple algebra shows that radiation from the central SMBH can heat the ambient gas up to the temperature

$$(67) \quad T_{\text{eq}} \approx 6.5 \times 10^3 \frac{L_{\text{BH}}}{L_{\text{Edd}}} \frac{M_*}{M_{\text{gas}}} \frac{M_{\text{BH}}}{10^8 M_{\odot}} \left( \frac{200 \text{ km s}^{-1}}{\sigma} \right)^2 \text{ K}.$$

The transition from rapid SMBH growth to slow, feedback limited SMBH growth is expected to meet the critical condition  $T_{\text{eq}} = \eta_{\text{esc}} T_*$  (where  $\eta_{\text{esc}} \gtrsim 1$  and  $T_*$  is the temperature associated with the galaxy velocity dispersion  $\sigma$ ), so that

$$(68) \quad M_{\text{BH,crit}} = 4.6 \times 10^{10} M_{\odot} \eta_{\text{esc}} \left( \frac{\sigma}{200 \text{ km s}^{-1}} \right)^4 \frac{L_{\text{Edd}}}{L_{\text{BH}}} \frac{M_{\text{gas}}}{M_*}.$$

Therefore, for fixed values of  $\eta_{\text{esc}}$ ,  $L_{\text{BH}}/L_{\text{Edd}}$  and  $M_{\text{gas}}/M_*$  one expects  $M_{\text{BH,crit}} \propto \sigma^4$ . It follows that the observed  $M_{\text{BH}}-\sigma$  relation will be established if

$$(69) \quad \frac{M_{\text{gas}}}{M_*} \simeq \frac{3 \times 10^{-3}}{\eta_{\text{esc}}} \frac{L_{\text{BH}}}{L_{\text{Edd}}}$$

To satisfy the observed  $M_{\text{BH}}-\sigma$  relation, the gas-to-stars ratio is thus required to be relatively low and approximately constant for spheroids with different masses at the epoch when the SMBH reaches its critical mass.

The approximately linear  $T_{\text{eq}}(\xi)$  dependence is crucial to the above argument leading to the  $M_{\text{BH,crit}} \propto \sigma^4$  result. However, the  $T_{\text{eq}}(\xi)$  function becomes strongly nonlinear outside the range  $2 \times 10^4 \text{ K} < T_{\text{eq}} < 10^7 \text{ K}$  and a more general result can be obtained if we consider the exact curve  $T_{\text{eq}}(\xi)$  from [277]. The situation is summarized in Fig. 26. It is perhaps interesting that the range of masses shown in Fig. 26 for which  $M_{\text{BH}} \propto \sigma^4$  is obtained from considerations of atomic physics (and the observed AGN spectra) corresponds closely with the range of masses for which this power law provides a good fit to the observations.

Starting from the previous results it is possible to study the SMBH-galaxy co-evolution, by using a physically-motivated one-zone model. The model differential equations for the gas mass budget  $M_{\text{gas}}$  of the galaxy adopted in [22] are

$$(70) \quad \dot{M}_{\text{gas}} = \dot{M}_{\text{inf}} - \dot{M}_* + \dot{M}_{\text{rec}} - \dot{M}_{\text{BH}} - \dot{M}_{\text{esc}},$$

where the quantities on the r.h.s. describe the cosmological infall on the forming galaxy, the amount of gas subtracted by star formation, the gas produced by evolving stars, the gas accreted on the SMBH, and finally the gas lost as a galactic wind when the thermal energy of the Interstellar Medium is high enough to escape from the galaxy potential well, respectively. More in detail,

$$(71) \quad \begin{cases} \dot{M}_{\text{inf}} = \frac{M_{\text{gal}}}{\tau_{\text{inf}}} e^{-t/\tau_{\text{inf}}}, & \dot{M}_* = \frac{\alpha_* M_{\text{gas}}}{\max(\tau_{\text{dyn}}, \tau_{\text{cool}})} - \dot{M}_{\text{rec}}, \\ \dot{M}_{\text{rec}} = \int_0^t \dot{M}_*^+(t') W_*(t-t') dt', \end{cases}$$

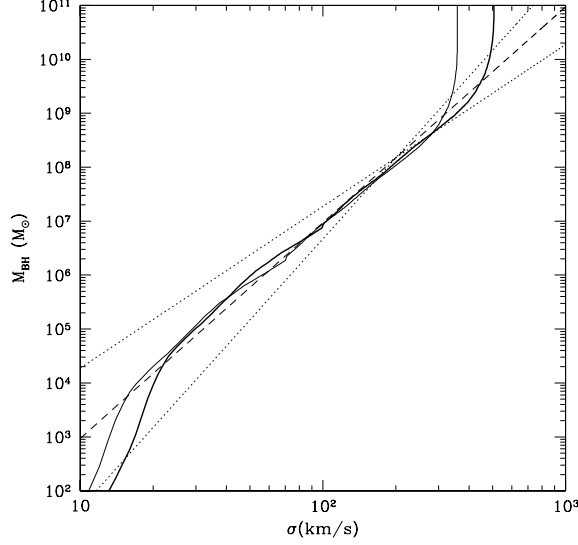


Fig. 26. – Thick solid line shows the predicted  $M_{\text{BH}}-\sigma_0$  relation resulting from the requirement that heating of the interstellar gas by radiation from the central SMBH at the Eddington limit be below the level required to drive the gas from the galaxy ( $T_{\text{eq}} \leq T_*$ ,  $M_{\text{gas}}/M = 0.003$  and  $\eta_{\text{esc}} = 1$ ). The thin solid line corresponds to  $M_{\text{gas}}/M = 0.0015$  and  $\eta_{\text{esc}} = 2$ . The dashed line is the observed  $M_{\text{BH}} \propto \sigma_0^4$  relation in the range  $10^6 < M_{\text{BH}}/M_\odot < 10^9$ . The dotted lines are  $M_{\text{BH}} \propto \sigma_0^3$  and  $M_{\text{BH}} \propto \sigma_0^5$  laws (from [22]).

$$(72) \quad \dot{M}_{\text{BH}} = \dot{M}_{\text{BH,acc}} + \beta_{\text{BH},*} \dot{M}_*^+, \quad \dot{M}_{\text{BH,acc}} = M_{\text{inf}}(f_{\text{Edd}} \dot{M}_{\text{Edd}}, \dot{M}_{\text{B}}),$$

where  $\dot{M}_*^+$  is the stellar mass formation rate, and finally

$$(73) \quad \dot{M}_{\text{esc}} = \begin{cases} \frac{M_{\text{gas}}}{\tau_{\text{esc}}}, & T \geq \eta_{\text{esc}} T_*, \\ 0, & T < \eta_{\text{esc}} T_*. \end{cases}$$

The dynamical time  $\tau_{\text{dyn}}$  is defined as

$$(74) \quad \tau_{\text{dyn}} \equiv \frac{2\pi R_e}{v_c},$$

where  $v_c$  is some characteristic circular velocity of the dark matter halo. For an isothermal halo with 1-dimensional velocity dispersion  $\sigma$

$$(75) \quad T_* = \frac{\mu m_p \sigma^2}{k} = \frac{\mu m_p v_c^2}{2k}.$$

Moreover, the cooling time is evaluated as

$$(76) \quad \tau_{\text{cool}} \equiv \frac{E}{\dot{E}_C}, \quad \dot{E}_C = n_e n_p \Lambda(T),$$

where  $\Lambda(T)$  is the gas cooling function, and  $E$  the gas internal energy per unit volume. The gas recycled by the evolving stellar population is obtained as a convolution between the instantaneous star formation rate and the kernel  $W_*(t)$  derived from stellar evolution ([151, 270, 271, 275]). In eq. (72) the Eddington and Bondi accretion rates are given by

$$(77) \quad \dot{M}_{\text{Edd}} \equiv \frac{L_{\text{Edd}}}{\epsilon c^2}, \quad \dot{M}_B = 4\pi R_B^2 \rho_B c_s,$$

where  $0.001 \leq \epsilon \leq 0.1$ , the Eddington luminosity is given by

$$(78) \quad L_{\text{Edd}} = 1.3 \times 10^{46} \frac{M_{\text{BH}}}{10^8 M_\odot} \text{erg s}^{-1},$$

and  $c_s = \sqrt{kT/\mu m_p}$  is the (isothermal sound velocity).

Finally, the thermal state of the gas is described by the rate at which (internal) energy per unit volume changes with time:

$$(79) \quad \dot{E} = \dot{E}_{\text{H,SN}} + \dot{E}_{\text{H,w}} + \dot{E}_{\text{H,AGN}} - \dot{E}_C + \dot{E}_{\text{inf}}^{\text{esc}}$$

where the terms on the r.h.s. are the heating produced by supernova explosions, the thermalization heating of stellar winds, AGN heating, gas cooling and finally adiabatic heating and cooling due to galactic winds and cosmological accretion.

The time evolution of the quantities shown in Fig. 27 refers to a galaxy model characterized by  $R_e = 4 \text{ kpc}$  and a halo (constant) circular velocity of  $400 \text{ km s}^{-1}$ ; the total mass of the gas infall is  $10^{11} M_\odot$ , and the characteristic infall time is 2 Gyr. The initial black hole mass is assumed to be  $10 M_\odot$ . The complete description of the toy-model behavior for different choices of the input parameters is given in [22]. Here I just recall that after an initial ‘‘cold’’ phase dominated by gas infall, as soon as the gas density becomes sufficiently low, and correspondingly the cooling time becomes longer than the dynamical time, the gas heating dominates, and the galaxy switches to a ‘‘hot’’ solution. The gas mass/stellar mass ratio ( $\sim 0.003$ ) at that moment is remarkably near to the value inferred from the argument leading to the right  $M_{\text{BH}}\text{-}\sigma_*$  relation. Note also how the gas content of the present day galaxy model and the final black hole mass are in nice agreement with observations.

An interesting experiment is obtained by reducing the circular halo velocity and the infall mass in the reference model. In these cases, galactic winds, powered by supernova heating, are favoured, i.e. small galaxies lose their gas content easily, in accordance with the predictions of hydrodynamical simulations and as expected from the  $M_{\text{g}_2}\text{-}\sigma_*$  and the FJ relations. Remarkably, the transition to the hot phase of these models happens for  $M_{\text{gas}}/M_* \sim 0.01$ , similarly to the behavior seen in the case of the more massive spheroid in the reference model. This sort of cooperation between AGN feedback and stellar energy injection, i.e., the fact that *in general substantial galactic winds are due to stellar heating, and are reinforced by the presence of the central AGN*, was already found in numerical simulations.

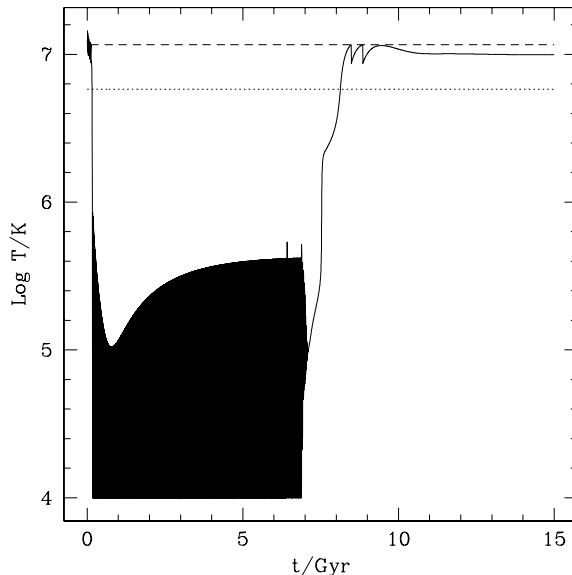


Fig. 27. – Time evolution of the model gas temperature (solid line). The model virial temperature is represented by the dotted line, while the dashed line represents the “escape” temperature (here assumed  $2T_*$ ). Note the strongly fluctuating temperature in the initial “cold” phase (from [22]).

An important and apparently robust conclusion that can be drawn from these simulations is that inevitably stellar heating leads to a transition from cold to hot solution when the gas-to-star mass ratio drops to of order 1 per cent or somewhat less. Now, since a gas fraction of this order is required for the radiative feedback from the central SMBH to limit its growth at the mass obeying the observed  $M_{\text{BH}}-\sigma_*$  relation, it is tempting to suggest that the SMBH reaches its critical mass, determined by radiative feedback, approximately at the epoch of transition from cold to hot galaxy phase. The near coincidence of the gas fraction corresponding to the beginning of the hot galactic phase with that in eq. (69) required by our argument leading to the correct  $M_{\text{BH}}-\sigma_*$  relation offers the possibility of the following evolutionary scenario. At the early stages of galaxy evolution, when the protogalactic gas is dense and cold, active star formation is accompanied by the growth of a central SMBH. However, the black hole is not massive enough to produce a strong heating effect on the ambient, dense gas, even during episodes when it shines near the Eddington limit. This cold phase would be identified observationally with the Lyman Break Galaxies and bright submillimeter galaxies, which are characterized by high star formation rate and moderate AGN activity. The cold phase ends when the gas-to-star mass ratio has been reduced to  $\sim 0.01$ , when the energy input from the evolving stellar population and possibly from the central SMBH heats the gas to a sub-virial temperature. The SMBH continues to grow actively during this transition epoch (that would be identified with the quasar epoch), because there are still sufficient supplies of gas for accretion, and soon reaches the critical mass (obeying the  $M_{\text{BH}}-\sigma_*$  relation), when the SMBH radiative output causes a major gas outflow. The subsequent evolution is passive and characterized by AGN activity with a duty cycle reduced by

a factor of ten to 0.001; this late phase would be identified with the present day Es, discussed in Sect. 4.

Obviously, the results described above should not be overinterpreted. As is common in studies based on a similar approach, the parameter space is huge (even though several input parameters are nicely constrained by theory and/or observations), so that the results of simulations of this kind should be interpreted more as indications of possible evolutionary histories than exact predictions. In particular, the *toy-model cannot directly test the ability of radiative feedback to produce the right final SMBH mass*. In fact, this can be done only using true hydrodynamical simulations. This is not surprising, because the toy-model, by construction, is a *one zone* model, and we already know that feedback mechanisms are strongly scale-dependent, in the sense that central galaxy regions react in a substantially different way with respect to the rest of the system.

**5.2. Collapse.** – It is a well established fact that the end-products of dissipationless collapse reproduces several structural and dynamical properties of Es. For example, the pioneering work of van Albada ([60]) showed that the end-products of cold collapse have projected density profiles well described by the  $R^{1/4}$  de Vaucouleurs law, radially decreasing line-of-sight velocity dispersion profiles, and radially increasing velocity anisotropy, in agreement with observations of Es ([325, 326]). More recently, dissipationless collapse has been studied in greater detail thanks to the advances in N-body simulations (e.g. [327]-[330]). These studies show that a smooth final density distribution with  $R^{1/4}$  projected mass profile is produced when the initial conditions are cold, extended, and clumpy in phase-space. From the astrophysical point of view the dissipationless collapse ([47]) was introduced to describe a complex physical scenario, in which the gas cooling time of the forming galaxy is shorter than its dynamical (free-fall) time, so that stars form “in flight”, and the subsequent dynamical evolution is a dissipationless collapse.

The explanation of the observed weak homology of Es is important to understand galaxy formation. For example, the presence of a core is usually interpreted as the signature of merging of SMBHs, consequence of the merging of the parent galaxies (e.g. [332, 333, 243]), while in N-body simulations of repeated equal-mass dissipationless mergers the best-fit Sersic index  $m$  of the end-products increases with their mass ([236]). However, [31, 236] showed that repeated dissipationless merging events fail to reproduce the FJ, the Kormendy, and the  $M_{\text{BH}}-\sigma_*$  relations, and also that a substantial number of head-on minor mergings make  $m$  decrease, bringing the end-products out of the edge-on FP (see Sect. 4.1). These results, together with other astrophysical pieces of evidence based on stellar population properties such as the  $\text{Mg}_2-\sigma_*$  relation, indicate that dry merging cannot have had a major role in the formation of Es, and gaseous dissipation is needed (e.g. [253, 260]).

In alternative (or as a complement) to the merging scenario, it is then of great theoretical interest to explore if (and if so, under what conditions and to what extent) the dissipationless collapse of the stellar population produced by a fast episode of gaseous dissipation and the consequent burst of star formation is able to reproduce end-products with projected density profiles well described by the Sersic law. In particular, following the current cosmological picture that galaxies form at peaks of the cold dark matter distribution (e.g. [53, 54]), it is natural to investigate dissipationless collapse in two-component systems.

In [331] this process was studied by means of high-resolution two-component N-body simulations, in which the collapse of the stellar distribution and the response of the dark matter halo are followed in detail. As will be shown, dissipationless collapse in pre-

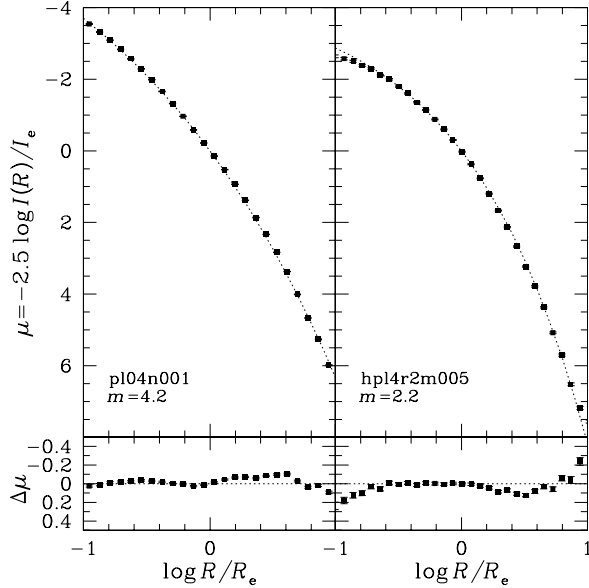


Fig. 28. – Circularized projected stellar density profiles of the end-products of representative one-component (left) and two-component (right) collapse events. The dotted lines are the best-fit  $R^{1/m}$  models (from [331]).

existing dark matter haloes is indeed able to reproduce surprisingly well the observed weak homology of Es. The flat inner surface brightness profiles of core ellipticals arise naturally from dissipationless collapse, with the inner core radius  $R_b$  determined by the coldness of the initial conditions. Two classes of simulations were considered. In the first the virialization of a cold, single-component density distribution was followed. In the second the initial conditions represent a cold component (stars) deemed to collapse in a nearly-virialized live dark matter halo. The initial conditions are the stellar ( $\rho_*$ ) and the halo ( $\rho_h$ ) density distributions, realized by different combinations of “cold” Plummer and  $\gamma$  models (see Sect. 3.2). The corresponding virial ratios  $\beta_*$  and  $\beta_h$  (i.e., the ratio of the total kinetic and gravitational energy of the initial conditions), measure the “coldness” of the distributions: in a virialized system the virial ratio is 1.

For a detailed description of how initial conditions are arranged, of the numerical simulations, and of the dynamical and structural properties of the end-products see [331]. Here it is sufficient to recall that the velocity dispersion tensor of the final states is approximately isotropic in the center and strongly radially anisotropic for  $r \gtrsim r_M$  (where  $r_M$  is the spatial half-mass radius), in agreement with previous results (e.g. [60, 330]).

The projected density profiles of the stellar end-products are fitted over the radial range  $0.1 \lesssim R/R_e \lesssim 10$ , which is comparable with or larger than the typical ranges spanned by observations ([100]). Apparently all the end-products of one-component collapse events do not deviate strongly from the  $R^{1/4}$  law over most of the radial range. The end-products of two-component simulations deviate systematically from the  $R^{1/4}$ , and in most cases the profile remains below it at small and large radii. For these systems the Sersic index is found to be in the range  $1.9 \lesssim m \lesssim 12$ , with average residuals in the

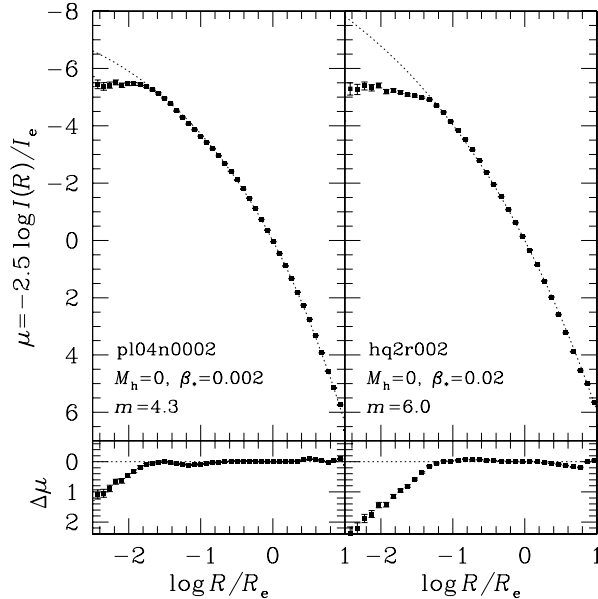


Fig. 29. – Circularized projected density profiles of two representative one-component collapse simulations with different initial virial ratios. The bars are  $1-\sigma$  uncertainties. The dotted lines are the best-fit Sersic models over the radial range  $0.1 < R/R_e < 10$  (from [331]).

same range as those of one-component collapse events. The quality of the fits is apparent in Fig. 28 (left), which plots the surface brightness profile of a projection of one of the end-products, together with the best-fit ( $m = 4.2 \pm 0.07$ ) Sersic law, and the corresponding residuals. The average residuals between data and fits are typically  $0.04 \lesssim \langle \Delta\mu \rangle \lesssim 0.2$ , where  $\mu = -2.5 \log I(R)/\langle I \rangle_e$ . Figure 28 (right) plots the projected profile of a representative two-component simulation with  $\mathcal{R} = 2$  together with the best-fit ( $m = 2.2 \pm 0.03$ ) model and the residuals.

So far we have considered the properties of intrinsic and projected density profiles at radii  $\gtrsim 0.1r_M$  (and  $0.1R_e$ ). We now focus on the behaviour of the profiles at smaller radii. In fact, the higher resolution of the present simulations allows us to investigate regions (down to  $R \sim 0.01R_e$ ) comparable to those explored by high-resolution photometry of real ellipticals. As apparent from Fig. 29 (top), the end-product density profiles of one-component collapse simulations have flat cores at  $r \lesssim 0.1r_M$ , in agreement with previous studies ([60, 325]). Correspondingly, the projected density profiles are characterized by a break radius  $R_b$ , in the sense that for  $R < R_b$  they stay below the best-fit Sersic profiles that matches the profile on the large scale  $0.1 < R/R_e < 10$ , as shown in Fig. 29 (bottom panels), for a case with  $\beta_* = 0.002$  (left) and a case with  $\beta_* = 0.02$  (right). Thus, the initial virial ratio  $\beta_*$  determines the radial range over which the final surface density profile is well fitted by the Sersic law, with colder initial conditions producing smaller cores (see Fig. 30). In particular, the fact that the size of the core is correlated (and the maximum central density anti-correlated) with the initial virial ratio is a direct consequence of the Liouville Theorem (e.g. [325, 340]). Furthermore, the projected density profiles of two-component end-products flatten at small radii and deviate from an inwards extrap-



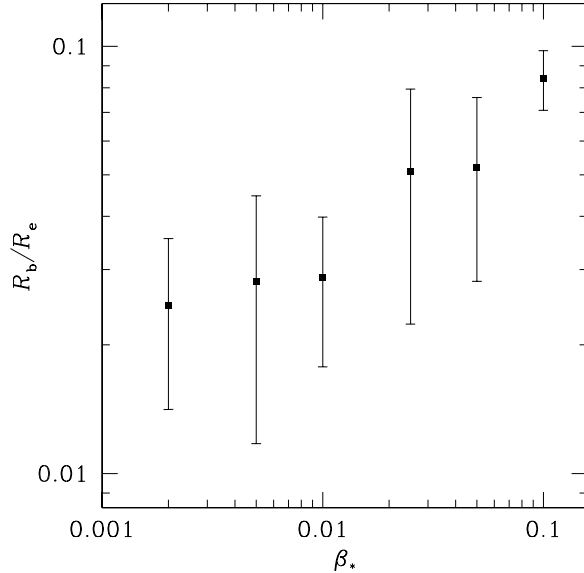


Fig. 30. – Break radius normalized to the effective radius as a function of the initial virial ratio. The symbols refer to the average among the three considered projections values, which span the range represented by the vertical bars (from [331]).

olation of the best-fitting Sersic law. However, the flattening is typically more gradual and the break is not as apparent as in the one-component cases. This is partly due to the fact that the stellar end-products of two-component simulations are characterized, in general, by smaller  $m$ , corresponding to quite shallow profiles. Note that, according to standard interpretations, the central cores observed in several bright ellipticals are a consequence of formation through merging, being produced by the interaction of binary SMBHs with a stellar cusp (e.g. [243, 332, 333]). However, we have seen that a break in the profile at small radii and a flat central core are features produced naturally by dissipationless collapse, and this makes dissipationless collapse a plausible alternative to the binary SMBHs scenario for the origin of the cores.

Overall, these results suggest that dissipationless collapse is able to produce systems with projected density profiles remarkably similar to the observed surface brightness profiles, with high-quality one-parameter Sersic fits even for low  $m$  values when non-negligible amounts of dark matter are present. In particular, the profiles of the end-products of single-component simulations are remarkably similar to those of observed in the so-called “core” ellipticals. For instance, the similarity between the profile plotted in Fig. 29 (bottom, left panel) with that of the core-elliptical NGC 3348, for which the reported best-fit is  $m \simeq 3.8$  and  $R_b/R_e \simeq 0.016$  ([124, 125]), is striking. One can also note that, while for  $m \gtrsim 3$  systems the dark matter mass inside the half mass radius is of the same order as the visible mass, consistent with observations (e.g. [214, 281],[334]-[339]), for very low- $m$  systems dark matter is expected to be dominant.

**5.3. The SLs of dark matter halos.** – As anticipated in Sect. 1, much like early-type galaxies, also nearby clusters of galaxies define their own FP, a luminosity-radius, and

a luminosity-velocity dispersion relations. Understanding similarities and differences of SLs in such diverse physical systems can be of the greatest importance in studies of galaxy formation, because of the (presumably) different physical processes involved.

First of all, we recall that well defined SLs are indeed expected for dark matter halos, on the basis of the simplest model for the formation of structures in an expanding Universe, namely the gravitational collapse of density fluctuations in an otherwise homogeneous distribution of collisionless dark matter (DM). In fact, the spherical top-hat model ([341]) predicts that, at any given epoch, all the existing DM halos have just collapsed and virialized, i.e.,  $M = r_V \sigma_V^2 / G$  (see Footnote 5). In addition, all the halos are characterized by a constant mean density  $\rho_\Delta$ , given by the critical density of the Universe at that redshift times a factor  $\Delta$  depending on  $z$  and on the given cosmological model (e.g. [342, 343]). The radius of the sphere containing such a mean density is indicated as  $r_\Delta$ , so that  $M \propto r_\Delta^3$ . In general,  $r_V \neq r_\Delta$ , but, if for a family of density distributions  $r_V / r_\Delta \simeq \text{const}$ , then the virial theorem can be rewritten as  $M \propto r_\Delta \sigma_V^2$ , and together with  $M \propto r_\Delta^3$ , it brings to  $M \propto \sigma_V^3$ , thus providing three relations that closely resemble the ones observed for luminous matter. Note that these expectations involve the *global three-dimensional* properties of DM halos, while the quantities entering the observed scaling relations are *projected* on the plane of the sky. However, if DM halos are structurally homologous (or weakly homologous) systems and are characterized by similar velocity dispersion profiles, as found in cosmological simulations (e.g. [209, 344]-[346]), their projected properties are also expected to follow well defined SLs (with some scatter due to departures from perfect homology and sphericity).

Of course, the simple above considerations are not sufficient to explain the *observed* SLs of galaxy clusters, at least for two reasons. The first is that a given potential well (as the one associated with the cluster DM distribution) can be filled, in principle, by very different distributions of “tracers” (such as the galaxies in the clusters, from which the SLs are derived). This means that the very existence of the cluster FP implies a remarkable regularity in their formation processes: galaxies must have formed or “fallen” in all clusters in a similar way. The second reason is that any trend of the cluster mass-to-light ratio (necessary to transform masses, involved in the theoretical relations, into luminosities<sup>(7)</sup>, entering the observed ones) must be taken into account for a proper interpretation of the observed SLs.

A distinct but strongly related question about the origin and the meaning of the SLs naturally arises when applying the predictions of cosmological models also at galactic scales. In fact, while scale-invariant relations are predicted, different slopes of the FJ relation are observed for galaxies and for galaxy clusters (see Sect. 2.3). This suggests that different processes have been at work in setting or modifying the correlations at the two mass scales. As discussed in Sect. 3, the theoretical implications of the scaling laws for Es have been extensively explored, and several works have been devoted to their study within the framework of the dissipationless merging scenario in Newtonian dynamics, but surprisingly much less effort has been devoted to the theoretical study of the FP of galaxy clusters (e.g. [233]). In order to get a more complete view of the problems outlined above, here I report the results obtained in [143], where high-resolution N-body simulations have been used to study the scaling relations of very massive DM halos. In particular the analysis employed dissipationless simulations with  $512^3$  particles

---

<sup>(7)</sup> The luminosity of a cluster refers to the sum of the optical luminosities of all its constituent galaxies.

of  $6.86 \times 10^{10} M_\odot/h$  mass each, in a (comoving) box of side  $479 h^{-1}$  Mpc. The adopted cosmological model is a  $\Lambda$ CDM Universe with  $\Omega_m = 0.3$ ,  $\Omega_\Lambda = 0.7$ ,  $h = 0.7$ , spectral shape  $\Gamma = 0.21$ , and normalization to the local cluster abundance,  $\sigma_8 = 0.9$ . From this simulation, a sub-sample of 13 halos at  $z = 0$ , with masses between  $10^{14} M_\odot/h$  and  $2.3 \times 10^{15} M_\odot/h$  was randomly selected. A first check showed that  $M \propto r_\Delta^3$ ,  $M \propto r_\Delta \sigma_V^2$  with a *rms* scatter of 0.03 only, and  $M \propto \sigma_V^{3.1}$ , with *rms*  $\simeq 0.05$ , for all the halos, as expected.

However, *projected* quantities are involved in the observations and the first step of the analysis is the determination of which (if any) scaling relations are satisfied by the DM halos when projected. Therefore the projected radial profiles of the selected halos have been constructed by counting the DM particles within concentric shells around the center of mass for three arbitrary orthogonal directions, and  $R_H$  is defined as the projected radius of the circle containing half of the total number of particles. Then, the velocity dispersion  $\sigma_h$  has been computed from the line-of-sight (barycentric) velocity of all the particles within  $R_H$ . Since the DM halos (as well as real clusters) are not spherical, such a procedure gives different values of  $R_H$  and  $\sigma_h$  for the three line-of-sights (the maximum variations however never exceed 33% and 21% for the two quantities, respectively), so that the adopted sample of simulated clusters contains three orthogonal projections for each halo. With the projected properties  $R_H$  and  $\sigma_h$  now available, we have determined the best fit relations between  $M$  and  $R_H$ , and between  $M$  and  $\sigma_h$  by minimizing the distance of the residuals perpendicular to a straight line, and thus obtaining the DM analogues of the observed FJ, Kormendy, and FP relations:

$$(80) \quad M \propto \sigma_h^{3.02 \pm 0.15}, \quad M \propto R_H^{2.36 \pm 0.14},$$

$$(81) \quad M \propto R_H^{1.1 \pm 0.05} \sigma_h^{1.73 \pm 0.04},$$

in particular, for the last fit it is found that *rms* = 0.04. Compared to the relations among the virial properties, these relations have larger scatter, as expected. The FJ and FP have slopes similar to those obtained for the virial quantities, while the  $M$ - $R_H$  relation appears to be significantly flatter. I stress again that while scaling relations between  $M$ ,  $r_\Delta$  (or  $r_V$ ) and  $\sigma_V$  are expected on theoretical grounds, a tight correlation between projected properties is a much less trivial result. In fact, structural and dynamical non-homology can, in principle, produce significantly different effective radii and projected velocity dispersion profiles for systems characterized by identical  $M$ ,  $r_V$ , and  $\sigma_V$ . It is also known that weak homology, coupled with the virial theorem, does indeed produce well defined SLs (see Sect. 3). Therefore, the SLs presented in eqs. (80)-(81) are a first interesting result. The difference between the values of the exponents appearing in eqs. (80)-(81) and those in the virial relations (under the assumption of homology) is the direct evidence of weak homology of the halos. Note that this finding is in agreement with the results already pointed out by several groups, namely the fact that DM halos obtained from numerical N-body simulations in standard cosmologies are characterized by significant structural and dynamical weak homology (e.g., [209, 344]).

Comparison of eqs. (80)-(81) and eqs. (11)-(12) reveals that at the scale of clusters of galaxies, the FJ, Kormendy and FP relations of simulated DM halos are characterized by different slopes with respect to those derived observationally. What are the implications of these differences? In order to answer this question, it is useful to define the dimensionless quantities  $\Upsilon \equiv M/L$ ,  $\mathcal{Q} \equiv R_H/R_e$ , and  $\mathcal{S} \equiv \sigma_h/\sigma$ , where  $R_e$  and  $\sigma$  are the

quantities related to the optical distribution of galaxies. Focusing first on the edge-on FP, from eqs. (12) and (81) one obtains:

$$(82) \quad \frac{\Upsilon}{\mathcal{Q}^{1.1} \mathcal{S}^{1.73}} \propto R_e^{0.2} \sigma^{0.42}.$$

Thus, in order to satisfy both the FP of DM halos and the FP of observed clusters of galaxies, the product  $\Upsilon \mathcal{Q}^{-1.1} \mathcal{S}^{-1.73}$  must systematically increase as  $R_e^{0.2} \sigma^{0.42}$ , which is approximately proportional to  $L^{0.3}$ . In principle,  $\Upsilon$ ,  $\mathcal{Q}$ , and  $\mathcal{S}$  could all vary in a *combined* and *regular* way from cluster to cluster, so that eq. (82) is satisfied. Of course, given the small scatter around the best fit relation (12), this kind of solution requires a remarkable fine tuning of the variations of the three parameters. Alternatively, it is possible that only one of the three parameters varies significantly, while the other two are approximately constant. This situation is analogous to that faced in the studies of the physical origin of the FP tilt of Es, where the so called ‘‘orthogonal exploration of the parameter space’’ is often adopted (see Sect. 3). In the present context some of this arbitrariness can be removed: in fact, here we assume that 1) the DM distribution in real clusters is described by the simulated DM halos, 2) in addition to the edge-on FP, we also consider the constraints imposed by the FJ and the Kormendy relations. These two points will *allow us to use the orthogonal exploration approach to determine what is the most plausible origin of the tilt between the simulated and the observed cluster FP*.

In order to make the DM halos FP reproduce the observed one within the framework of the orthogonal exploration approach, we have three different possibilities, each corresponding to the choice of  $\Upsilon$ ,  $\mathcal{Q}$ , or  $\mathcal{S}$  as the key parameter, while keeping constant the remaining two in the l.h.s. of eq. (82). The two choices based on variations of  $\mathcal{Q}$  or  $\mathcal{S}$  should be interpreted from an astrophysical point of view as systematic differences in the way galaxies populate the cluster DM potential well as a function of the cluster mass. However, the orthogonal analysis of the FJ and the Kormendy relations strongly argue against these two solutions, since from eqs. (11) and (80) one obtains

$$(83) \quad \frac{\Upsilon}{\mathcal{S}^{3.02}} \propto \sigma^{0.84}, \quad \frac{\Upsilon}{\mathcal{R}^{2.36}} \propto R_e^{0.81}.$$

Thus, it is apparent that any attempt to reproduce equation (82) by a variation of  $\mathcal{Q}$  (or  $\mathcal{S}$ ) alone will fail at reproducing the FJ (or the Kormendy) relation. In fact, the only common parameter appearing in all the eqs. (82) and (83) is the mass-to-light ratio<sup>(8)</sup>  $\Upsilon$ .

Therefore, while a *purely structural* ( $\mathcal{Q}$ ) and a *purely dynamical* ( $\mathcal{S}$ ) origin of the tilt between the DM halos FP and the cluster FP seem to be both ruled out by the above arguments, a systematically varying mass-to-light ratio, for  $\mathcal{Q}$  and  $\mathcal{S}$  constant, could in principle account for all the three considered scaling relations. In particular, from eq. (82),  $\Upsilon \propto L^\alpha$  with  $\alpha \sim 0.3$ . Guided by this indication, one can try to superimpose the points corresponding to the simulated DM halos to the sample of observed clusters

---

<sup>(8)</sup> Note that the constraints imposed by the FJ and the Kormendy relations should not be considered redundant with respect to those imposed by the edge-on FP. These two relations, although with a large scatter, describe how galaxies are distributed on the face-on FP.

by using  $\Upsilon \propto M^\beta$ . It turns out that if

$$(84) \quad \Upsilon = 280 h \left( \frac{M}{10^{14} M_\odot/h} \right)^{0.23} \frac{M_\odot}{L_\odot},$$

*the edge-on FP of DM halos is practically indistinguishable from that of real clusters* (see Fig. 5). It is also noticeable (as a non-necessary consequence) that by adopting eq. (84) *also the face-on FP, the FJ, and the Kormendy relations are very well reproduced*, as is apparent from Fig. 4. Remarkably, the same trend of the mass-to-light ratio with luminosity was found for individual galaxies by the SAURON group (e.g. [281]). It would be very interesting to compare the SLs of dark matter halos obtained from high-resolution numerical simulations with the SLs of Es and to repeat the above investigation in the smaller scale context.

**5.4. Summary.** – In this Section three different issues have been addressed. The first point concerns the possible simultaneous growth of SMBHs and of the host galaxies at the epoch of galaxy formation. The second is about the structural and dynamical properties of galaxies formed in dissipationless collapse (the last stages of monolithic-like collapse) in pre-existing dark matter halos. The third is the problem posed by the existence of SLs of galaxy clusters, which has been discussed in the framework of cosmological simulations of structure formation. The main results can be summarized as follows:

1) At galactic scale, the end-products of one-component simulations of dissipationless collapse typically have projected surface brightness profile close to the de Vaucouleurs model. When fitted with the Sersic law over the radial range  $0.1 \lesssim R/R_e \lesssim 10$ , the resulting profiles are characterized by index  $3.6 \lesssim m \lesssim 8$ ; final states with  $m \gtrsim 5$  are obtained only for rather concentrated initial conditions.

2) The end-products of collapse inside a dark matter halo present significant structural non-homology. The best-fit Sersic indices of the stellar projected surface density profile span the range  $1.9 \lesssim m \lesssim 12$ . Remarkably, the parameter  $m$  correlates with the amount of dark matter present within  $R_e$ , being smaller for larger dark-to-visible mass ratios.

3) The projected stellar density profiles are characterized by a break radius  $0.01 \lesssim R_b/R_e \lesssim 0.1$  within which the profile is flatter than the inner extrapolation of the global best-fit Sersic law. Colder initial conditions lead to end-products with smaller  $R_b/R_e$ ; in general, the resulting “cores” are better detectable in high- $m$  systems.

4) For clusters of galaxies, after verifying that DM halos do follow the predictions of the spherical collapse model for virialized systems, we have found that also their projected properties define a FJ, a Kormendy, and a FP-like relations. However, the slopes of the DM halos scaling laws do not coincide with the observed ones, and we have shown that the two families of SLs can be reconciled by assuming that the cluster mass-to-light ratio  $\Upsilon$  increases as a power law of the luminosity. The required normalization and slope agree well with those estimated observationally for real clusters of galaxies. It appears that *the FJ, Kormendy and FP relations of nearby clusters of galaxies can be explained as the result of the cosmological collapse of density fluctuations at the appropriate scales, plus a systematic trend of the total mass-to-light ratio with the cluster mass.*

## 6. – Conclusions

We are finally in the position to connect the different pieces of information described in the previous Sections, to see if it is possible to form a plausible scenario in which the

existence of the galaxy and central black holes Scaling Laws described in Sect. 2 can be traced back to the process of galaxy formation.

The *first* important clue is that stellar spheroids are a remarkably regular family of stellar systems: the regularity is apparent in terms not only of density profiles, but also of orbit composition and of stellar populations. All these indications point towards a *common* formation mechanism, where the galaxy mass has been a *major* parameter, because many galaxy Scaling Laws involve the galaxy luminosity. In Sect. 3 a review of the different proposed interpretations of the galaxy Scaling Laws has been presented. While a definite answer is not reached yet, it is generally acknowledged that the galaxy SLs are mainly due to a *systematic variation with the galaxy luminosity* of the dark matter amount and distribution, of the light distribution (the so-called weak homology), and finally of the metallicity of the bulk of the stellar mass.

The *second* piece of information about galaxy Scaling Laws is indirect and comes from cosmological simulations: by studying simulations of structure formation on the scale of clusters of galaxies, it is found that well defined Scaling Laws are naturally (i.e., by initial conditions) imprinted in the resulting dark matter halos.

Thus, it is tempting to put the two points above together and to suggest that the formation of stellar spheroids proceeded mainly in a way similar to the *monolithic collapse* scenario. This would explain the galaxy Scaling Laws just as the imprint of the dark matter halos Scaling Laws (at the mass scale of galaxies) on the baryons. Numerical simulations of fast (dissipationless) collapse in pre-existing dark matter halos can reproduce Sersic profiles similar to those observed, from the outer parts of the models down to their central regions. Cold dissipationless collapse is a process which is expected to dominate the late stages of an initially dissipative process, in which the gas cooling time of the forming galaxy is shorter than its dynamical time, so that stars form “in flight”, and the subsequent dynamical evolution is dissipationless. Observational evidence supports this argument. In fact, the observed color-magnitude and  $M_{g_2}-\sigma_0$  relations, and the increase of the  $[\alpha/\text{Fe}]$  ratio with  $\sigma_0$  in the stellar population of Es (e.g. [46],??-[349]), suggest that star formation in massive ellipticals was not only more efficient than in low-mass galaxies, but also that it was faster (i.e., completed before SNIa explosions took place), with the time-scales of gas consumption and ejection shorter or comparable to the galaxy dynamical time (e.g. [350, 351]) and decreasing with increasing galaxy mass.

The *third* piece of information is related to the effects of *dry and wet merging* on the Scaling Laws: in fact we know that ellipticals cannot be originated by parabolic merging of low mass spheroids only, even in the presence of substantial gas dissipation (which, at variance with dry merging, is able to increase the galaxy central velocity dispersion, see also [352]). However, it is also known that SLs such as the FJ, Kormendy, FP, and the  $M_{\text{BH}}-\sigma_0$  relations, when considered over the whole mass range spanned by ellipticals in the local Universe, are robust against merging (see also [353]). Thus the galaxy Scaling Laws, possibly established at high redshift by the fast collapse in pre-existing dark matter halos of gas rich and clumpy stellar distributions (e.g. [354]), can persist even in the presence of a (small) number of dry mergers at lower redshift ([355]). If this is the case, then monolithic-like collapse at early times and subsequent merging could just represent the different phases of galaxy formation (collapse) and evolution (merging, in addition to the aging of the stellar populations and related phenomena).

The possibility that monolithic collapse and successive merging events are just the leading physical processes at different times in galaxy evolution, and that they are both important for galaxy formation, is perhaps indicated also by a “contradictory” and often overlooked peculiarity of massive ellipticals. In fact, while the Kormendy relation dictates

that the mean stellar density of galaxies decreases with increasing galaxy mass (a natural result of parabolic dry merging), the normalized light profiles of Es becomes steeper and their metallicity increases at increasing galaxy mass (as expected in case of significant gas dissipation). Thus, the present-day light profiles of ellipticals could represent the fossil evidence of the impact of both processes.

If the above scenario is correct, then one expects that the star formation history in the Universe and the QSO activity should be roughly parallel. It remains to be clarified if QSO activity brought the process of galaxy formation to an end, or the star formation feedback by ejecting the remaining gas from the galaxy brought the epoch of vigorous QSO activity to a conclusion, or finally if a combination of stellar and AGN feedback was the key factor. My personal view is that we currently have more indications supporting the idea that galaxy formation was stopped more by stellar feedback (i.e., supernova heating) than by the AGN feedback (but see [356]). In any case, after the end of the fast star formation epoch, *necessarily* a new evolutionary phase begins for the galaxies and their SMBHs. This obvious fact is curiously neglected quite often in the current literature, but it is unavoidable. In fact, over a cosmological time in a passively evolving galaxy the *stellar mass losses* amount, over a cosmological time, to a considerable fraction ( $\gtrsim 30\%$ ) of the total stellar mass, i.e.,  $\sim 2$  orders of magnitude larger than the observed SMBHs masses. If only a minor fraction of this recycled gas (the basic ingredient of the galaxy “cooling flow” model!) were accreted on the central SMBH, the SLs involving the BH masses (such as the Magorrian and the  $M_{\text{BH}}-\sigma_*$ ) would be completely different. Thus, the need of an *extremely efficient* feedback from SMBHs is *not* required by complex physical arguments, but just by the *mass budget* of the SMBHs. In addition, this feedback *must* be active over the whole galaxy life, and cannot be temporally concentrated just at the end of the star formation epoch. *However, a moderate accretion from the recycled gas by the evolving stars will not destroy an already established SL, such as the Magorrian relation, as the available “fuel” for accretion is naturally proportional to the stellar mass of the host system.*

I conclude this Review with a brief comment on a recent and very interesting observational finding, i.e. the fact that apparently stellar spheroids were much *denser* than today at redshift  $1 \lesssim z \lesssim 2$  (e.g. [357, 358, 359], and references therein). The obvious question is what mechanism could make a galaxy “expand”. Of course, internal dynamical processes cannot be invoked, as their time-scales are measured *either* by the galaxy dynamical time (very short compared to the age of the system), *or* by the 2-body relaxation time (which is orders of magnitude longer than the age of the Universe). Thus, the only obvious possibility is to postulate that a few events of dry merging are common in the life of early-type galaxies. This would also help to explain the “central density-slope paradox” discussed above. In addition, if dry merging (through a small number of events) is the solution to the problem of superdense galaxies then, in order for present-day galaxies to obey the Magorrian relation, the SMBHs at the center of the superdense progenitors should also follow the same SL, because no significant amount of gas can be accreted on the center in a dry merging. Then, the superdense galaxies cannot follow the  $M_{\text{BH}}-\sigma_*$  relation observed in the local Universe because their velocity dispersion is higher than in local galaxies of the same mass. In practice, if superdense galaxies are the progenitors of the nearby Es, and if their expansion was caused by dry merging, they should obey the Magorrian relation observed in the local Universe, but they should fail the local  $M_{\text{BH}}-\sigma_*$  relation, by exhibiting a systematically lower zero-point. Testing observationally this conjecture would be an interesting goal for the future.

\* \* \*

It is a pleasure to thank Tjeerd van Albada, Giuseppe Bertin, James Binney, Annibale D'Ercole, Barbara Lanzoni, Pasquale Londrillo, Carlo Nipoti, Jerry Ostriker, Silvia Pellegrini, Alvio Renzini, Renzo Sancisi, Massimo Stiavelli and Tommaso Treu for sharing with me along the years their views and ideas (not necessarily coincident with mine) on several arguments described in this paper. Useful comments on the manuscript have been provided by Alister Graham and Alessandro Marconi. Giuseppe Bertin is especially thanked for a very careful and insightful reading of the whole draft.

## REFERENCES

- [1] BINNEY J. and MERRIFIELD M., *Galactic Astronomy*, PRINCETON UNIVERSITY PRESS, 1998
- [2] BERTIN G., *Dynamics of Galaxies* CAMBRIDGE UNIVERSITY PRESS, 2000
- [3] MAGORRIAN J., ET AL., *AJ*, **115** (1998) 2285
- [4] FERRARESE L. and MERRITT D., *ApJ*, **539** (2000) L9
- [5] GEBHARDT K. ET AL., *ApJ*, **539** (2000) L13
- [6] GRAHAM A.W., ERWIN P., CAON N. and TRUJILLO I., *ApJ*, **563** (2001) L11
- [7] TREMAINE S., ET AL., *ApJ*, **574** (2002) 740
- [8] MCLURE R.J. and DUNLOP J.S., *MNRAS*, **331** (2002) 795
- [9] MARCONI A. and HUNT L.K., *ApJ*, **589** (2003) L21
- [10] NOVAK G.S., FABER S.M. and DEKEL A., *ApJ*, **637** (2006) 96
- [11] FERRARESE L. ET AL., *ApJ*, **644** (2006) L21
- [12] KORMENDY J. and RICHSTONE D., *ARA&A*, **33** (1995) 581
- [13] VAN DER MAREL R.P., *AJ*, **117** (1999) 744
- [14] DE ZEEUW P.T., in *Black Holes in Binaries and Galactic Nuclei*, edited by L. KAPER, E.P.J. VAN DEN HEUVEL, and P.A. WOUTD, ESO Astrophysics Symposia (Springer), 2001, 78
- [15] SILK J. and REES M.J., *A&A*, **331** (1998) L1
- [16] FABIAN A.C., *MNRAS*, **308** (1999) L39
- [17] BURKERT A. and SILK J., *ApJ*, **554** (2001) L151
- [18] CAVALIERE A. and VITTORINI V., *ApJ*, **570** (2002) 114
- [19] KING A.R., *ApJ*, **596** (2003) L27
- [20] WYTHE J.S.B. and LOEB A., *ApJ*, **595** (2003) 614
- [21] GRANATO G.L., DE ZOTTI G., SILVA L., BRESSAN A. and DANESE L., *ApJ*, **600** (2004) 580
- [22] SAZONOV S.YU., OSTRIKER J.P., CIOTTI L. and SUNYAEV R.A., *MNRAS*, **358** (2005) 168
- [23] MURRAY N., QUATAERT E., and THOMPSON T.A., *ApJ*, **618** (2005) 569
- [24] DI MATTEO T., SPRINGEL V. and HERNQUIST L., *Nature*, **433** (2005) 604
- [25] BEGELMAN M.C. and NATH B.B., *MNRAS*, **361** (2005) 1387
- [26] HOPKINS P.F., HERNQUIST L., COX T.J., ROBERTSON B., DI MATTEO T. and SPRINGEL V., *ApJ*, **639** (2006) 700
- [27] CROTON D.J. ET AL., *MNRAS*, **365** (2006) 11
- [28] KAUFFMANN G. and HAEHNELT M.G., *MNRAS*, **311** (2000) 576
- [29] MONACO P., SALUCCI P. and DANESE L., *MNRAS*, **311** (2000) 279
- [30] GRANATO G.L., SILVA L., MONACO P., PANUZZO P., SALUCCI P., DE ZOTTI G. and DANESE L., *MNRAS*, **324** (2001) 757
- [31] CIOTTI L. and VAN ALBADA T.S., *ApJ*, **552** (2001) L13
- [32] MENCI N., CAVALIERE A., FONTANA A., GIALLONGO E., POLI F. and VITTORINI V., *ApJ*, **587** (2003) L63
- [33] PEI Y.C., *ApJ*, **438** (1995) 623
- [34] MADAU P., HAARDT F. and REES M.J., *ApJ*, **514** (1999) 648



- [35] WYTHE S. and LOEB A., *ApJ*, **581** (2002) 886
- [36] YU Q. and TREMAINE S., *MNRAS*, **335** (2002) 965
- [37] HAIMAN Z., CIOTTI L. and OSTRIKER J.P., *ApJ*, **606** (2004) 763
- [38] FABER S.M. and JACKSON R.E., *ApJ*, **204** (1976) 668 (FJ)
- [39] KORMENDY J., *ApJ*, **218** (1977) 333
- [40] DJORGOVSKI S. and DAVIS M., *ApJ*, **313** (1987) 59
- [41] DRESSLER A., LYNDEN-BELL D., BURSTEIN D., DAVIES R.L., FABER S.M., TERLEVICH R.J. and WEGNER G., *ApJ*, **313** (1987) 42
- [42] BOWER R.G., LUCEY J.R. and ELLIS R.S., *MNRAS*, **254** (1992) 601
- [43] GUZMAN R., LUCEY J.R., CARTER D. and TERLEVICH R.J., *MNRAS*, **257** (1992) 187
- [44] BURSTEIN D., DAVIES R.L., DRESSLER A., FABER S.M. and LYNDEN-BELL D., in *Towards understanding galaxies at large redshift* PROCEEDINGS OF THE FIFTH WORKSHOP OF THE ADVANCED SCHOOL OF ASTRONOMY, DORDRECHT, KLUWER ACADEMIC PUBLISHERS, p.17, 1988
- [45] BENDER R., BURSTEIN D. and FABER S.M., *ApJ*, **411** (1993) 153
- [46] BERNARDI M., ET AL., *AJ*, **125** (2003) 1882
- [47] EGGEN O.J., LYNDEN-BELL D. and SANDAGE A.R., *ApJ*, **136** (1962) 748
- [48] LARSON R.B., *MNRAS*, **166** (1974) 585
- [49] LARSON R.B., *MNRAS*, **173** (1975) 671
- [50] BINNEY J., *ApJ*, **215** (1977) 483
- [51] REES M.J. and OSTRIKER, J.P., *MNRAS*, **179** (1977) 541
- [52] TOOMRE A., in *Evolution of Galaxies and Stellar Populations* Ed. B.M. TINSLEY & R.B. LARSON (NEW HAVEN: YALE UNIVERSITY OBSERVATORY), 1977, p.401
- [53] WHITE S.D.M. and REES M.J., *MNRAS*, **183** (1978) 341
- [54] WHITE S.D.M. and FRENK C.S., *ApJ*, **379** (1991) 52
- [55] KAUFFMANN G., *MNRAS*, **281** (1996) 487
- [56] COLE S., LACEY C.G., BAUGH C.M. and FRENK C.S., *MNRAS*, **319** (2000) 168
- [57] OSTRIKER J.P., *Comments on Astrophysics*, **VIII.6** (1980) 177
- [58] RENZINI A., *ARA&A*, **44** (2006) 141
- [59] VAN DOKKUM P.G., FRANX M., FABRICANT D., KELSON D.D. and ILLINGWORTH G.D., *ApJ*, **520** (1999) L95
- [60] VAN ALBADA T.S., *MNRAS*, **201** (1982) 939
- [61] BERTIN G. and STIAVELLI M., *A&A*, **137** (1984) 26
- [62] MERRITT D., *Rep.Prog.Phys.*, **69** (2006) 2513
- [63] MERRITT D. and SZELL A., *ApJ*, **648** (2006) 890
- [64] MERRITT D., *ApJ*, **648** (2006) 976
- [65] MERRITT D., BERCIK P. and LAUN F., *AJ*, **133** (2007) 533
- [66] CIPOLLINA M. and BERTIN G., *A&A*, **288** (1994) 43
- [67] JØRGENSEN I., FRANX M. and KJÆRGAARD P., *ApJ*, **411** (1993) 34
- [68] JØRGENSEN I., FRANX M. and KJÆRGAARD P., *MNRAS*, **280** (1996) 167
- [69] BENDER R., SAGLIA R.P., ZIEGLER B., ET AL., *ApJ*, **493** (1988) 529
- [70] PAHRE M.A., DJORGOVSKI S.G. and DE CARVALHO R.R., *AJ*, **116** (1998) 1591
- [71] PAHRE M.A., DE CARVALHO R.R. and DJORGOVSKI S.G., *AJ*, **116** (1998) 1606
- [72] TREU T., *On the formation and evolution of early-type galaxies* PHD THESIS, SCUOLA NORMALE SUPERIORE, PISA (ITALY) 2000
- [73] D'ONOFRIO M., VALENTINUZZI T., SECCO L., CAIMMI R. and BINDONI D., *New Astronomy Rev.*, **50** (2006) 447
- [74] BERNARDI M., ET AL., *AJ*, **125** (2003) 1866
- [75] BENDER R., BURSTEIN D. and FABER S.M., *ApJ*, **399** (1992) 462
- [76] DAVIES R.L., EFSTATHIOU G., FALL S.M., ILLINGWORTH G. and SCHECHTER P.L., *ApJ*, **266** (1983) 41
- [77] DRESSLER A., FABER S.M., BURSTEIN D. DAVIES R.L., LYNDEN-BELL D., TERLEVICH R.J. and WEGNER G., *ApJ*, **313** (1987) 37
- [78] MAKTOVIC A. and GUZMAN R., *MNRAS*, **362** (2005) 289
- [79] BERNARDI M., ET AL., *AJ*, **125** (2003) 1849

- [80] ZIEGLER B.L., SAGLIA R.P., BENDER R., BELLONI P., GREGGIO L. and SEITZ S., *A&A*, **346** (1999) 13
- [81] DE VAUCOULEURS G., *Ann. d'Astroph.*, **11** (1948) 247
- [82] DE VAUCOULEURS G. and CAPACCIOLI M., *ApJ*, **40** (1979) 699
- [83] CAPACCIOLI M., in *Structure and dynamics of elliptical galaxies* ED. P.T. DE ZEEUW, REIDEL, DORDRECHT p.47, 1987
- [84] DE CARVALHO R.R. and DA COSTA L.N., *ApJ*, **68** (1988) 173
- [85] CAPACCIOLI M., in *The World of Galaxies* EDs. H.G. CORWIN and BOTTINELLI, SPRINGER-VERLAG, BERLIN p.208, 1989
- [86] BURKERT A., *A&A*, **278** (1993) 23
- [87] SERSIC J.L., *Atlas de galaxies australes* OBSERVATORIO ASTRONOMICO, CORDOBA, 1968
- [88] DAVIES J.I., PHILLIPS S., CAWSON M.G.M., DISNEY M.J. and KIBBLEWHITE E.J., *MNRAS*, **232** (1988) 239
- [89] MAKINO J., AKIYAMA K. and SUGIMOTO D., *Publ. Astron. Soc. Japan*, **42** (1990) 205
- [90] CAON N., CAPACCIOLI M. and D'ONOFRIO M., *MNRAS*, **265** (1993) 1013
- [91] YOUNG C.K. and CURRIE M.J., MNRAS2681994L11
- [92] D'ONOFRIO M., CAPACCIOLI M. and CAON N., *MNRAS*, **271** (1994) 523
- [93] ANDREDAKIS Y.C., PELETIER R.F. and BALCELLS M., *MNRAS*, **275** (1995) 874
- [94] CIOTTI L., LANZONI B. and RENZINI A., *MNRAS*, **282** (1996) 1
- [95] COURTEAU S., DE JONG R.S. and BROEILS A.H., *ApJ*, **457** (1996) L1
- [96] GRAHAM A. and COLLESS M., *MNRAS*, **287** (1997) 221
- [97] PRUGNIEL P. and SIMIEN F., *A&A*, **321** (1997) 111
- [98] GRAHAM A.W., *MNRAS*, **295** (1998) 933
- [99] WADADEKAR Y., ROBBASON B. and KEMBHAVI A., *AJ*, **117** (1999) 1219
- [100] BERTIN G., CIOTTI L. and DEL PRINCIPE M., *A&A*, **386** (2002) 1491
- [101] CIOTTI L. and BERTIN G., *A&A*, **1999** (352) 447
- [102] CIOTTI L., *A&A*, **249** (1991) 99
- [103] CIOTTI L. and LANZONI B., *A&A*, **321** (1997) 724
- [104] GERBAL D., LIMA-NETO G.B., MARQUEZ I. and VERAGHEN H., *MNRAS*, **285** (1997) L41
- [105] ANDREDAKIS Y.C., *MNRAS*, **295** (1998) 725
- [106] BINNEY J., *MNRAS*, **200** (1982) 951
- [107] MICHARD R., *A&A*, **59** (1985) 205
- [108] SCHOMBERT J.M., *ApJ*, **60** (1986) 603
- [109] GRAHAM A.W., LAUER T.R., COLLESS M. and POSTMAN M., *ApJ*, **465** (1996) 534
- [110] KHOSROSHAHI H.G., WADADEKAR Y., KEMBHAVI A. and MOBASHER B., *ApJ*, **531** (2000) L103
- [111] GRAHAM A.W. and GUZMÁN R., *AJ*, **125** (2003) 2936
- [112] CAON N., CAPACCIOLI M. and RAMPAZZO R., *A&A*, **86** (1990) 429
- [113] CAON N., CAPACCIOLI M. and D'ONOFRIO M., *A&A*, **106** (1994) 199
- [114] MØLLER P., STIAVELLI M. and ZEILINGER W.W., *MNRAS*, **276** (1995) 979
- [115] CRANE P. ET AL., *AJ*, **106** (1993) 1371
- [116] JAFFE W., FORD H.C., O'CONNELL R.W., VAN DEN BOSCH F.C. and FERRARESE L., *AJ*, **108** (1994) 1567
- [117] FERRARESE L., VAN DEN BOSCH F.C., FORD H.C., JAFFE W. and O'CONNELL R.W., *AJ*, **108** (1994) 1598
- [118] LAUER T.R., AJHAR E.A., BYUN Y.I., DRESSLER A., FABER S.M., GRILLMAIR C., KORMENDY J., RICHSTONE D.O., and TREMAINE S.D., *AJ*, **110** (1995) 2622
- [119] KORMENDY J., BYUN Y.I., AJHAR E.A., LAUER T.R., DRESSLER A., FABER S.M., GRILLMAIR C., GEBHART K., RICHSTONE D.O. and TREMAINE S.D., in *IAU Symposium 171: New Light on Galaxy Evolution* EDs. R. BENDER AND R.L. DAVIES, DORDRECHT: KLUWER p.105, 1995
- [120] BYUN Y.I., GRILLMAIR C., FABER S.M., AJHAR E.A., DRESSLER A., KORMENDY J., LAUER T.R., RICHSTONE D.O. and TREMAINE S.D., *AJ*, **111** (1996) 1889

- [121] DE ZEEUW P.T. and CAROLLO C.M., in *IAU Symposium 171: New Light on Galaxy Evolution* EDS. R. BENDER AND R.L. DAVIES, DORDRECHT: KLUWER, p.47, 1996
- [122] PELLEGRINI S., *A&A*, **351** (1999) 487
- [123] PELLEGRINI S., *MNRAS*, **364** (2005) 169
- [124] GRAHAM A.W., ERWIN P., TRUJILLO I. and ASENSIO RAMOS A., *ApJ*, **125** (2003) 2951
- [125] TRUJILLO I., ERWIN P., ASENSIO RAMOS A. and GRAHAM A.W., *AJ*, **127** (2004) 1917
- [126] FERRARESE L. ET AL., *ApJS*, **164** (2006) 334
- [127] COTÉ P. ET AL., *ApJS*, **165** (2006) 57
- [128] BALCELLS M., GRAHAM A.W. and PELETIER R., *ApJ*, **665** (2007) 1084
- [129] FERRARESE L. and FORD H.C., *Space Science Reviews*, **116** (2005) 523
- [130] ALLER M.C. and RICHSTONE D.O., *ApJ*, **665** (2007) 120
- [131] MERRITT D. and FERRARESE L., *ApJ*, **547** (2001) L140
- [132] KORMENDY J. and GEBHARDT K., in *Proc. of the 20th Texas Symposium on relativistic astrophysics* EDS J. C. WHEELER AND H MARTEL, AIP CONF.PROCS. VOL.586, p. 363 (2001)
- [133] HÄRING N. and RIX H.-W., *ApJ*, **604** (2004) L89
- [134] GRAHAM A.W., *MNRAS*, **379** (2007) 711
- [135] BARWAY S. and KEMBHAVI A., *ApJ*, **662** (2007) L67
- [136] GRAHAM A., *preprint*, [arXiv0705.3509](https://arxiv.org/abs/0705.3509) (2007)
- [137] HOPKINS P.F., HERNQUIST L., COX T.J., ROBERTSON B. and KRAUSE E., *ApJ*, **669** (2007) 67
- [138] TRUJILLO I., GRAHAM A.W. and CAON N., *MNRAS*, **326** (2001) 869
- [139] GRAHAM A.W. and DRIVER S.P., *PASA*, **22** (2005) 118
- [140] GRAHAM A.W. and DRIVER S.P., *ApJ*, **655** (2007) 77
- [141] SCHAEFFER R., MAUROGORDATO S., CAPPI A. and BERNARDEAU F., *MNRAS*, **263** (1993) L21
- [142] ADAMI C., MAZURE A., BIVIANO A., KATGERT P. and RHEE G., *A&A*, **331** (1998) 493
- [143] LANZONI B., CIOTTI L., CAPPI A., TORMEN G. and ZAMORANI G., *ApJ*, **600** (2004) 640
- [144] ANNIS J., *AAS*, **26** (1994) 1427
- [145] FUJITA Y. and TAKAHARA F., *ApJ*, **519** (1999) L51
- [146] FRITSCH C. and BUCHERT T., *A&A*, **344** (1999) 749
- [147] MILLER C.J., MELOTT A. and GORMAN P., *ApJ*, **526** (1999) L61
- [148] GIRARDI M., BORGANI S., GIURICIN G., MARDIROSSIAN F. and MEZZETTI M., *ApJ*, **530** (2000) 62
- [149] SCODEGGIO M., GAVAZZI G., BELSOLE E., PIERINI D. and BOSELLI A., *MNRAS*, **301** (1998) 1001
- [150] CANIZARES C., FABBIANO G. and TRINCHIERI G., *ApJ*, **312** (1987) 503
- [151] CIOTTI L., D'ERCOLE A., PELLEGRINI S. and RENZINI A., *ApJ*, **376** (1991) 380
- [152] BINNEY J., in *Particles and Fields in Radio Galaxies Conference* EDS. R.A. LAING AND K.M. BLUNDELL ASP CONFERENCE PROCEEDINGS, VOL.250, p. 481 (2001)
- [153] ROBERTS M.S., HOGG D.E., BREGMAN J.N., FORMAN W.R. and JONES C., *ApJS*, **75** (1991) 751
- [154] O'SULLIVAN E., PONMAN T.J. and COLLINS R.S., *MNRAS*, **340** (2003) 1375
- [155] FORMAN W. ET AL., *ApJ*, **665** (2007) 1057
- [156] JONES C., FORMAN W., VIKHLININ A., MARKEVITCH M., DAVID L., WARMFLASH A., MURRAY S., and NULSEN P.E.J., *ApJ*, **567** (2002) L115
- [157] O'SULLIVAN E., VRTILEK J.M. and KEMPNER J.C., *ApJ*, **624** (2005) L77
- [158] FABBIANO G., BALDI A., PELLEGRINI S., SIEMIGINOWSKA A., ELVIS M., ZEAS A. and McDOWELL J., *ApJ*, **616** (2004) 730
- [159] SORIA R., FABBIANO G., GRAHAM A.W., BALDI A., ELVIS M. JERJEN H., PELLEGRINI S. and SIEMIGINOWSKA A., *ApJ*, **640** (2006) 126
- [160] PELLEGRINI S. *et al.*, *ApJ*, **667** (2007) 749
- [161] RANDALL S.W., SARAZIN C.L. and IRWIN J.A., *ApJ*, **600** (2004) 729
- [162] MACHACEK M.E., JONES C. and FORMAN W.R., *ApJ*, **610** (2004) 183
- [163] O'SULLIVAN E., VRTILEK J.M., HARRIS D.E. and PONMAN T.J., *ApJ*, **658** (2007) 299

- [164] FABIAN A.C. and CANIZARES C.R., *Nature*, **333** (1988) 829
- [165] PELLEGRINI S., *ApJ*, **624** (2005) 155
- [166] SORIA R. *et al.*, *ApJ*, **640** (2006) 143
- [167] HO L., *ARAA*, [arXiv:0803.2268](https://arxiv.org/abs/0803.2268) (2008)
- [168] CIOTTI L., in *3rd ESO-VLT Workshop – Galaxy Scaling Relations: Origins, Evolution and Applications* EDS. L. DA COSTA AND A. RENZINI, KLUWER: DORDRECHT 1997, p.38
- [169] VAN DOKKUM P.G. and FRANX M., *MNRAS*, **281** (1996) 985
- [170] KELSON D.D., VAN DOKKUM P., FRANX M., ET AL., *ApJ*, **478** (1997) L13
- [171] VAN DOKKUM P.G., FRANX M, KELSON D.D., ET AL., *ApJ*, **500** (1998) 714
- [172] VAN DOKKUM P.G., FRANX M, KELSON D.D., ET AL., *ApJ*, **504** (1998) L17
- [173] JØRGENSEN I., FRANX M., HJORTH J., ET AL., *MNRAS*, **308** (1999) 833
- [174] TREU T., STIAVELLI M., CASERTANO S., MØLLER P. and BERTIN G., *MNRAS*, **308** (1999) 1037
- [175] KELSON D.D., ILLINGWORTH G.D., VAN DOKKUM P., ET AL., *ApJ*, **531** (2000) 137
- [176] KELSON D.D., ILLINGWORTH G.D., VAN DOKKUM P., ET AL., *ApJ*, **531** (2000) 159
- [177] KELSON D.D., ILLINGWORTH G.D., VAN DOKKUM P., ET AL., *ApJ*, **531** (2000) 184
- [178] TREU T., STIAVELLI M., MØLLER P., ET AL., *MNRAS*, **326** (2001) 221
- [179] TREU T., STIAVELLI M., BERTIN G., ET AL., *MNRAS*, **326** (2001) 237
- [180] FABER S.M., DRESSLER A., DAVIES R.L., ET AL., in *Nearly normal galaxies* ED. S.M. FABER, SPRINGER, NEW YORK, p.175, 1987
- [181] VAN ALBADA T.S., BERTIN G. and STIAVELLI M., *MNRAS*, **276** (1995) 1255
- [182] LYNDEN-BELL, D., *MNRAS*, **136** (1967) 101
- [183] SPITZER L., *ApJ*, **158** (1969) L139
- [184] DEHNEN W., *MNRAS*, **265** (1993) 250
- [185] CIOTTI L., *Cel. Mech. & Dyn. Astron.*, **60** (1994) 401
- [186] RENZINI A. and CIOTTI L., *ApJ*, **416** (1993) L49
- [187] CIOTTI L. and PELLEGRINI S., *MNRAS*, **255** (1992) 561
- [188] DJORGOVSKI S., *ApJ*, **438** (1995) L29
- [189] HJORTH J. and MADSEN J., *ApJ*, **445** (1995) 55
- [190] DJORGOVSKI S. and SANTIAGO B.X., in *Structure, Dynamics and Chemical Evolution of Elliptical Galaxies* EDS. DANZIGER I.J., ZEILINGER W.W., KJÅR K., ESO, GARCHING 1993, p.59
- [191] CIOTTI L., *ApJ*, **471** (1996) 68
- [192] KRITSUK A.G., *MNRAS*, **284** (1997) 327
- [193] CIOTTI L., *ApJ*, **520** (1999) 574
- [194] LANZONI B. and CIOTTI L., *A&A*, **404** (2003) 819
- [195] RICIPUTI A., LANZONI B., BONOLI S. and CIOTTI L., *A&A*, **443** (2005) 133
- [196] CIOTTI L., *Lecture Notes on Stellar Dynamics* ED. SCUOLA NORMALE SUPERIORE (PISA, ITALY) 2000
- [197] BINNEY J. and TREMAINE S., *Galactic Dynamics* PRINCETON UNIVERSITY PRESS, 2ND Ed. 2008
- [198] OSIPKOV L.P., *Soviet Astron. Lett.*, **5** (1979) 42
- [199] MERRITT D., *AJ*, **90** (1985) 1027
- [200] MERRITT D., *MNRAS*, **214** (1985) 25P
- [201] TREMAINE S., RICHSTONE D.O., YONG-IK B., DRESSLER A., FABER S.M., GRILLMAIR C., KORMENDY J. and LAUER T.R., *AJ*, **107** (1994) 634
- [202] HERNQUIST L., *ApJ*, **356** (1990) 359
- [203] JAFFE W., *MNRAS*, **202** (1983) 995
- [204] PLUMMER H.C., *MNRAS*, **71** (1911) 460
- [205] KING I.R., *ApJ*, **174** (1972) L123
- [206] DUBINSKI J. and CARLBERG R.G., *ApJ*, **378** (1991) 496
- [207] KOCHANEK C.S., *ApJ*, **419** (1993) 12
- [208] KOCHANEK C.S., *ApJ*, **436** (1994) 56
- [209] NAVARRO J.F., FRENK C.S. and WHITE S.D.M., *ApJ*, **462** (1996) 563

- [210] GAVAZZI R., TREU T., RHODES J.D., KOOPMANS L.V.E., BOLTON A.S., BURLES S., MASSEY R.J. and MOUSTAKAS L.A., *ApJ*, **667** (2007) 176
- [211] CZOSKE O., BARNABE M., KOOPMANS L.V.E., TREU T. and BOLTON A.S., *MNRAS*, **384** (2008) 987
- [212] BINNEY J., *MNRAS*, **190** (1980) 873
- [213] SAGLIA R.P., BERTIN G. and STIAVELLI M., *ApJ*, **384** (1992) 433
- [214] BERTIN G., BERTOLA F., BUSON L.M., DANZIGER I.J., DEJONGHE H., SADLER E.M., SAGLIA R.P., DE ZEEUW P.T. and ZEILINGER W.W., *A&A*, **292** (1994) 381
- [215] CAROLLO C.M. and DANZIGER I.J., *MNRAS*, **270** (1994) 523
- [216] CAROLLO C.M. and DANZIGER I.J., *MNRAS*, **270** (1994) 743
- [217] CAROLLO C.M., DE ZEEUW P.T., VAN DER MAREL R.P., DANZIGER I.J. and QIAN E.E., *ApJ*, **441** (1995) L25
- [218] BERTIN G. and STIAVELLI M., *Rep. Prog. Phys.*, **56** (1993) 493
- [219] CAPELATO H.V., DE CARVALHO R.R. and CARLBERG R.G., *ApJ*, **451** (1995) 525
- [220] PAHRE M.A. and DJORGOVSKI S.G., in *The Nature of Elliptical Galaxies* Eds. M. ARNABOLDI, G.S. DA COSTA AND P. SAHA, ASP CONF. SER. 1997, vol. 116, p. 154
- [221] DE ZEEUW T. and FRANX M., *ARAA*, **29** (1991) 239
- [222] FRIDMAN A.M. and POLYACHENKO V.L., *Physics of Gravitating Systems* SPRINGER, NEW YORK 1984
- [223] CAROLLO C.M., DE ZEEUW P.T. and VAN DER MAREL R.P., *MNRAS*, **276** (1995) 1131
- [224] MERRITT D. and AGUILAR L.A., *MNRAS*, **217** (1985) 787
- [225] BERTIN G. and STIAVELLI M., *ApJ*, **338** (1989) 723
- [226] SAHA P., *MNRAS*, **248** (1991) 494
- [227] SAHA P., *MNRAS*, **254** (1992) 132
- [228] BERTIN G., PEGORARO F., RUBINI F. and VESPERINI E., *ApJ*, **434** (1994) 94
- [229] MEZA A. and ZAMORANO N., *AJ*, **490** (1997) 136
- [230] TRENTI M. and BERTIN G., *ApJ*, **637** (2006) 717
- [231] NIPOTI C., LONDRILLO P. and CIOTTI L., *MNRAS*, **332** (2002) 901
- [232] TRUJILLO I., BURKERT A. and BELL E.F., *ApJ*, **600** (2004) L39
- [233] PENTERICCI L., CIOTTI L. and RENZINI A., *Astrophysical Letters and Communications*, **33** (1996) 33
- [234] BEKKI K., *ApJ*, **496** (1998) 713
- [235] EVSTIGNEEVA E.A., RESHETNIKOV V.P. and SOTNIKOVA N.Y., *A&A*, **381** (2002) 6
- [236] NIPOTI C., LONDRILLO P. and CIOTTI L., *MNRAS*, **342** (2003) 501
- [237] NIPOTI C., LONDRILLO P. and CIOTTI L., in *The mass of galaxies at low and high redshift* Eds. R. BENDER AND A. RENZINI, ESO ASTROPHYSICS SYMPOSIA (SPRINGER-VERLAG) 2003, p.70
- [238] GONZALEZ-GARCIA A.C. and VAN ALBADA T.S., *MNRAS*, **342** (2003) 36
- [239] DANTAS C.C., CAPELATO H.V., RIBEIRO A.L.B. and DE CARVALHO R.R., *MNRAS*, **340** (2003) 398
- [240] EVSTIGNEEVA E.A., DE CARVALHO R.R., RIBEIRO A.L. and CAPELATO H.V., *MNRAS*, **349** (2004) 1052
- [241] BOYLAN-KOLCHIN M., MA C.-P. and QUATAERT E., *MNRAS*, **362** (2005) 184
- [242] BOYLAN-KOLCHIN M., MA C.-P. and QUATAERT E., *MNRAS*, **369** (2006) 1081
- [243] MILOSAVLJEVIC M. and MERRITT D., *ApJ*, **563** (2001) 34
- [244] FLANAGAN E.E. and HUGHES S.A., *Phys. Rev. D.*, **57** (1998) 4535
- [245] CENTRELLA J.M., in *Proceedings of the Conference on Stellar Collisions* ED. M. SHARA, ASP CONFERENCE SERIES, 2000
- [246] HAWKING S.W., *Phys. Rev. D.*, **13** (1976) 191
- [247] PEACOCK J.A., *Cosmological Physics*, Cambridge University Press 1999
- [248] YU Q., *MNRAS*, **331** (2002) 953
- [249] HAEHNELT M.G. and KAUFFMANN G., *MNRAS*, **336** (2002) 61
- [250] VOLONTERI M., HAARDT F. and MADAU P., *ApJ*, **582** (2003) 559
- [251] CIOTTI L., LANZONI B. and VOLONTERI M., *ApJ*, **658** (2007) 65

- [252] KAZANTZIDIS S., MAYER L., COLPI M., MADAU P., DEBATTISTA V.P., WADSLEY J., STADEL J., QUINN T. and MOORE B, *ApJ*, **623** (2005) L67
- [253] ROBERTSON B., COX T.J., HERNQUIST L., FRANX M., HOPKINS P.F., MARTINI P. and SPRINGEL V., *ApJ*, **641** (2006) 21
- [254] ROBERTSON B., HERNQUIST L., COX T.J., DI MATTEO T., HOPKINS P.F., MARTINI P. and SPRINGEL V., *ApJ*, **641** (2006) 90
- [255] DEKEL A. and COX T.J., *MNRAS*, **370** (2006) 1445
- [256] SÁIZ A., DOMÍNGUEZ-TENREIRO R. and SERNA A., *ApJ*, **601** (2004) L131
- [257] OÑORBE J., DOMÍNGUEZ-TENREIRO R., SÁIZ A., SERNA A. and ARTAL H., *ApJ*, **632** (2005) L57
- [258] OÑORBE J., DOMÍNGUEZ-TENREIRO R., SÁIZ A., ARTAL H. and SERNA A., *MNRAS*, **373** (2006) 503
- [259] JOHANSSON P.H., NAAB T., and BURKERT A., *ApJ*, **arXiv:0802.0210v1** (2008) submitted
- [260] NAAB T., JOHANSSON P.H., OSTRIKER J.P. and EFSTATHIOU G., *ApJ*, **658** (2007) 710
- [261] HOPKINS P.F., HERNQUIST, L., COX, T.J., DUTTA, S.N., and ROTHBERG, B., *ApJ*, **679** (2008) 156
- [262] HOPKINS P.F., COX, T.J., and HERNQUIST, L., *ApJ*, **arXiv0806.3974v1** (2008) submitted
- [263] HUGHES S.A. and BLANDFORD R.D., *ApJ*, **585** (2003) L101
- [264] ALMEIDA C., BAUGH C.M. and LACEY C.G., *MNRAS*, **376** (2007) 1711
- [265] BLANTON M.R., DALCANTON J., EISENSTEIN D., ET AL., *AJ*, **121** (2001) 2358
- [266] GALLAZZI A., CHARLOT S., BRINCHMANN J. and WHITE S.D.M., *MNRAS*, **370** (2006) 1106
- [267] D'ERCOLE A., RENZINI A., CIOTTI L. and PELLEGRINI S., *ApJ*, **341** (1989) L9
- [268] PELLEGRINI S. and CIOTTI L., *A&A*, **333** (1998) 433
- [269] BINNEY J. and TABOR G., *MNRAS*, **276** (1995) 663
- [270] CIOTTI L. and OSTRIKER J.P., *ApJ*, **487** (1997) L105
- [271] CIOTTI L. and OSTRIKER J.P., *ApJ*, **551** (2001) 131
- [272] OSTRIKER J.P. and CIOTTI L., *Phil. Trans. of Roy.Soc.*, **363** (2005) 667
- [273] OMMA H., BINNEY J., BRYAN G. and SLYZ A., *MNRAS*, **348** (2004) 1105
- [274] CHURAZOV E., SAZONOV S., SUNYAEV R., FORMAN W., JONES C. and BÖHRINGER H., *MNRAS*, **363** (2005) L91
- [275] CIOTTI L. and OSTRIKER J.P., *ApJ*, **665** (2007) 1038
- [276] RUSSELL P.A., PONMAN T.J. and SANDERSON A.J.R., *MNRAS*, **378** (2007) 1217
- [277] SAZONOV S.YU., OSTRIKER J.P. and SUNYAEV R.A., *MNRAS*, **347** (2004) 144
- [278] BONDI H., *MNRAS*, **112** (1952) 195
- [279] SAZONOV S.YU., REVNIVTSEV M., KRIVONOS R., CHURAZOV E. and SUNYAEV R.A., *A&A*, **462** (2007) 57
- [280] SAGLIA R.P., BERTIN G., BERTOLA F., DANZIGER I.J., DEJONGHE H., SADLER E.M., STIAVELLI M., DE ZEEUW P.T. and ZEILINGER W.W., *ApJ*, **403** (1993) 567
- [281] CAPPELLARI M. ET AL., *MNRAS*, **366** (2006) 1126
- [282] DOUGLAS N.G. ET AL., *ApJ*, **664** (2007) 257
- [283] FABIAN A.C., THOMAS P.A., FALL S.M. and WHITE III R.E., *MNRAS*, **221** (1986) 1049
- [284] HUMPHREY P.J., BUOTE D.A., GASTALDELLO F., ZAPPACOSTA L., BULLOCK J.S., BRIGHENTI F. and MATHEWS W.G., *ApJ*, **646** (2006) 899
- [285] FUKUSHIGE T. and MAKINO J., *ApJ*, **477** (1997) L9
- [286] TREU T., KOOPMANS L.V., BOLTON A.S., BURLES S. and MOUSTAKAS L.A., *ApJ*, **640** (2006) 662
- [287] CAPPELLARO E., EVANS R. and TURATTO M., *A&A*, **351** (1999) 459
- [288] MANNUCCI F., DELLA VALLE M., PANAGIA N., CAPPELLARO E., CRESCI G., MAIOLINO R., PETROSIAN A. and TURATTO M., *A&A*, **433** (2005) 807
- [289] SOLTAN A., *MNRAS*, **200** (1982) 115
- [290] NARAYAN R. and YI Z., *ApJ*, **428** (1994) L13
- [291] CHANDRASEKHAR S., *Radiative Transfer*, (Dover, New York) 1960

- [292] RECCHI S., D'ERCOLE A. and CIOTTI L., *ApJ*, **533** (2000) 799
- [293] RENZINI A., CIOTTI L., D'ERCOLE A. and PELLEGRINI S., *ApJ*, **419** (1993) 52
- [294] CIMATTI A., ET AL., *A&A*, **381** (2002) L68
- [295] LAUER T.R. ET AL., *AJ*, **129** (2005) 2138
- [296] DAVIES R.I., MUELLER SÁNCHEZ F., GENZEL R., TACCONI L., HICKS E., FRIEDRICH S. and STERNBERG A., *ApJ*, **671** (2007) 1388
- [297] HOPKINS P.F., NARAYAN R. and HERNQUIST L., *ApJ*, **643** (2006) 641
- [298] HAEHNELT M.G., NATARAJAN P. and REES M.J., *MNRAS*, **300** (1998) 827
- [299] HAIMAN Z. and HUI L., *ApJ*, **547** (2001) 27
- [300] MARTINI P. and WEINBERG D.H., *ApJ*, **547** (2001) 12
- [301] BLANDFORD R.D., in *Galaxy Dynamics* ASP CONF. SER. VOL. 182, Eds.D.R. MERRITT, M. VALLURI AND J.A. SELLWOOD, (SAN FRANCISCO: ASP) 1999, p.87
- [302] MAY A. and VAN ALBADA T.S., *MNRAS*, **209** (1984) 15
- [303] MCGLYNN T.A., *ApJ*, **281** (1984) 13
- [304] AGUILAR L.A. and MERRITT D., *ApJ*, **354** (1990) 33
- [305] LONDRILLO P., MESSINA A. and STIAVELLI M., *MNRAS*, **250** (1991) 54
- [306] UDRY S., *A&A*, **268** (1993) 35
- [307] TRENTI M., BERTIN G. and VAN ALBADA T.S., *A&A*, **433** (2005) 57
- [308] NIPOTI C., LONDRILLO P. and CIOTTI L., *MNRAS*, **370** (2006) 681
- [309] MAKINO J. and EBISUZAKI T., *ApJ*, **465** (1996) 527
- [310] FABER S.M., ET AL., *AJ*, **114** (1997) 1771
- [311] GERHARD O., KRONAWITTER A., SAGLIA R.P. and BENDER R., *AJ*, **121** (2001) 1936
- [312] MAGORRIAN J. and BALLANTYNE D., *MNRAS*, **322** (2001) 702
- [313] ROMANOWSKY A.J., DOUGLAS N.G., ARNABOLDI M., KUIJKEN K., MERRIFIELD M.R., NAPOLITANO N.R., CAPACCIOLI M., and FREEMAN K.C., *Science*, **301** (2003) 1696
- [314] TREU T. and KOOPMANS L.V., *ApJ*, **611** (2004) 739
- [315] PIERCE C.M. ET AL., *ApJ*, **660** (2007) L19
- [316] FRANCESCHINI A., HASINGER G., MIYAJI T. and MALQUORI D., *MNRAS*, **310** (1999) 5
- [317] PAGE M.J., STEVENS J.A., MITTAZ J.P.D. and CARRERA F.J., *Science*, **294** (2001) 2516
- [318] GRANATO G.L., DE ZOTTI G., SILVA L., DANESE L. and MAGLIOCCHETTI M., *Ap&SS*, **281** (2002) 497
- [319] TABOR G. and BINNEY J., *MNRAS*, **263** (1993) 323
- [320] BINNEY J., in *The radio galaxy Messier 87* Eds. H.J. RŠER AND K. MEISENHEIMER (NEW YORK:SPRINGER) 1999, p.116
- [321] HAEHNELT M.G., NATARAJAN P. and REES M.J., *MNRAS*, **300** (1998) 827
- [322] HAIMAN Z. and HUI L., *ApJ*, **547** (2001) 27
- [323] MARTINI P. and WEINBERG D.H., *ApJ*, **547** (2001) 12
- [324] BLANDFORD R.D., in *Galaxy Dynamics* ASP CONF. SER. VOL. 182, Eds.D.R. MERRITT, M. VALLURI AND J.A. SELLWOOD, (SAN FRANCISCO: ASP) 1999, p.87
- [325] MAY A. and VAN ALBADA T.S., *MNRAS*, **209** (1984) 15
- [326] MCGLYNN T.A., *ApJ*, **281** (1984) 13
- [327] AGUILAR L.A. and MERRITT D., *ApJ*, **354** (1990) 33
- [328] LONDRILLO P., MESSINA A. and STIAVELLI M., *MNRAS*, **250** (1991) 54
- [329] UDRY S., *A&A*, **268** (1993) 35
- [330] TRENTI M., BERTIN G. and VAN ALBADA T.S., *A&A*, **433** (2005) 57
- [331] NIPOTI C., LONDRILLO P. and CIOTTI L., *MNRAS*, **370** (2006) 681
- [332] MAKINO J. and EBISUZAKI T., *ApJ*, **465** (1996) 527
- [333] FABER S.M., ET AL., *AJ*, **114** (1997) 1771
- [334] GERHARD O., KRONAWITTER A., SAGLIA R.P. and BENDER R., *AJ*, **121** (2001) 1936
- [335] MAGORRIAN J. and BALLANTYNE D., *MNRAS*, **322** (2001) 702
- [336] ROMANOWSKY A.J., DOUGLAS N.G., ARNABOLDI M., KUIJKEN K., MERRIFIELD M.R., NAPOLITANO N.R., CAPACCIOLI M., and FREEMAN K.C., *Science*, **301** (2003) 1696
- [337] TREU T. and KOOPMANS L.V., *ApJ*, **611** (2004) 739
- [338] DEKEL A., STOEHR F., MAMON G.A., COX T.J., NOVAK G.S. and PRIMACK J.R., *Nature*, **437** (2005) 707

- [339] SAMUROVIĆ S. and DANZIGER I.J., *MNRAS*, **363** (2005) 769
- [340] HOZUMI S., BURKERT A. and FUJIWARA T., *MNRAS*, **311** (2000) 377
- [341] GUNN J.E. and GOTT J.R., *ApJ*, **176** (1972) 1
- [342] PEEBLES P.J.E., *The Large-Scale Structure of the Universe* PRINCETON: PRINCETON UNIV. PRESS 1980
- [343] EKE V.R., COLE S. and FRENK C.S., *MNRAS*, **282** (1996) 263
- [344] GRAHAM A.W., MERRITT D., MOORE B., DIEMAND J. and TERZIC B., *AJ*, **132** (2006) 2701
- [345] COLE S. and LACEY C., *MNRAS*, **281** (1996) 716
- [346] SUBRAMANIAN K., CEN R. and OSTRICKER J.P., *ApJ*, **538** (2000) 528
- [347] THOMAS D., GREGGIO L. and BENDER R., *MNRAS*, **302** (1999) 537
- [348] JØRGENSEN I., *MNRAS*, **306** (1999) 607
- [349] SAGLIA R., MARASTON C., GREGGIO L., BENDER R. and ZIEGLER B., *A&A*, **360** (2000) 911
- [350] MATTEUCCI F., *A&A*, **288** (1994) 55
- [351] PIPINO, A. and MATTEUCCI F., *A&A*, **347** (2004) 968
- [352] BURKERT A., NAAB T. and JOHANSSON P.H., *ApJ*, **arXiv:07010.0663v1** (in press)
- [353] PENG C.P., *ApJ*, **671** (2007) 1098
- [354] MCGRATH E.J., STOCKTON A. and CANALIZO G., *ApJ*, **669** (2007) 241
- [355] MASJEDI M., HOGG D.W. and BLANTON M.R., *ApJ*, **679** (2008) 260
- [356] SCHAWINSKI K. *et al.*, *MNRAS*, **382** (2007) 1415
- [357] DI SEREGO ALIGHIERI S. *et al.*, *A&A*, **442** (2005) 125
- [358] TRUJILLO I., CONSELICE J.C., BUNDY K., COOPER M.C., EISENHARDT P., ELLIS R.S., *MNRAS*, **382** (2007) 109
- [359] CIMATTI A. *et al.*, *A&A*, **482** (2008) 21